DOT/FAA/AR-02/129

Side Load Factor Statistics From Commercial Aircraft Ground Operations

January 2003

Final Report

This document is available to the U.S. public
through the National Technical Information
Service (NTIS), Springfield, Virginia 22161.

U.S. Department of Transportation
Federal Aviation Administration

20030523 041

NOTICE

This document is disseminated under the sponsorship of the U.S. Department of Transportation in the interest of information exchange. The United States Government assumes no liability for the contents or use thereof. The United States Government does not endorse products or manufacturers. Trade or manufacturer's names appear herein solely because they are considered essential to the objective of this report. This document does not constitute FAA certification policy. Consult your local FAA aircraft certification office as to its use.

This report is available at the Federal Aviation Administration William J. Hughes Technical Center's Full-Text Technical Reports page: actlibrary.tc.faa.gov in Adobe Acrobat portable document format (PDF).

1. Report No. DOT/FAA/AR-02/129	2. Government Accession No.	3. Recipient's Catalog No.	
4. Title and Subtitle SIDE LOAD FACTOR STATISTICS FROM COMMERCIAL AIRCRAFT GROUND OPERATIONS		5. Report Date January 2003	
		6. Performing Organization Code	
7. Author(s) Daniel O. Tipps, John Rustenburg, Donald Skinn, University of Dayton Thomas DeFiore, Federal Aviation Administration		8. Performing Organization Report No. UDR-TR 2002-00119	
9. Performing Organization Name and Address University of Dayton Research Institute Structural Integrity Division 300 College Park Dayton, OH 45469-0120		10. Work Unit No. (TRAIS) 065110, RPD-510	
		11. Contract or Grant No. 2001-G-005	
12. Sponsoring Agency Name and Address U.S. Department of Transportation Federal Aviation Administration Office of Aviation Research Washington, DC 20591		13. Type of Report and Period Covered Final Report	
		14. Sponsoring Agency Code ANM-110	

15. Supplementary Notes

The Federal Aviation Administration William J. Hughes Technical Center COTR was Thomas DeFiore.

16. Abstract

The University of Dayton is supporting Federal Aviation Administration (FAA) research on the loads and structural integrity requirements for the U.S. commercial transport airplane fleet. The primary objective of this research is to support the FAA's Operational Loads Monitoring Research by developing new and improved methods and criteria for processing and presenting commercial transport airplane flight and ground loads usage data. The scope of activities performed involve but are not limited to (1) defining the service-related factors that affect the operational life of commercial aircraft; (2) designing an efficient software system to reduce, store, and process large quantities of optical quick access recorder data; and (3) providing processed data in formats that will enable the FAA to reassess existing certification criteria. Presented herein are analyses and statistical summaries of landing and ground operations data to provide the FAA with a technical basis for assessing the suitability of the 0.5-g lateral acceleration criteria specified in Federal Aviation Regulation (FAR) 25.495 for turning. The data represent 1037 flights, 1039 flights, and 1361 flights of B-737-400, B-767-200ER, and B-747-400 aircraft, respectively. Included are statistical information on vertical and lateral accelerations, yaw angles, ground speeds, and gross weights experienced during touchdown and ground operations. Ground-turning lateral acceleration data were used in the development of a normalization procedure to allow prediction of lateral load factors due to ground turning on other aircraft. While the data contained in this report might indicate that the FAR 25.495 may be conservative at the 0.5-g level when one considers that FAR 25.495 takes into consideration asymmetric gear loading for both dry and highly slippery conditions, the retention of the traditional 0.5-g value may well be appropriate. The results of this study clearly indicate, however, that the lateral loads experienced by the larger/heavier transport jets during ground turns are substantially less than those of smaller jet transports.

17. Key Words Optical quick access recorder, Flight profiles, Flight loads, Ground loads, Miscellaneous loads, Statistical loads data		18. Distribution Statement This document is available to the public through the National Technical Information Service (NTIS), Springfield, Virginia 22161.	
19. Security Classif. (of this report) Unclassified	20. Security Classif. (of this page) Unclassified	21. No. of Pages 122	22. Price N/A

Form DOT F1700.7 (8-72)   Reproduction of completed page authorized

PREFACE

The Flight Systems Integrity Group of the Structural Integrity Division of the University of Dayton Research Institute (URDI) performed this study under the Federal Aviation Administration (FAA) Research Grant No. 2001-G-005 entitled "Assessment of Actual Operational Usage on Large Widebody Transport Aircraft." Mr. Thomas DeFiore of the FAA William J. Hughes Technical Center at Atlantic City International Airport, New Jersey, was the Program Manager for the FAA and also a major contributor to the report. For UDRI, Mr. Daniel Tipps was the Principal Investigator, Mr. John Rustenburg was the Senior Research Engineer, Mr. Donald Skinn was the Research Programmer, and Mrs. Kathie Smith was the data technician. All five individuals worked together to develop the data reduction algorithms, establish the data reduction criteria, perform the data processing, develop the statistical data formats, perform the data analysis, create the graphical and tabular presentations, and prepare the final study report.

TABLE OF CONTENTS

LIST OF FIGURES

LIST OF TABLES

EXECUTIVE SUMMARY

The University of Dayton is supporting Federal Aviation Administration (FAA) research on the loads and structural integrity requirements for the US commercial transport airplane fleet. The primary objective of this research is to support the FAA's Operational Loads Monitoring Research by developing new and improved methods and criteria for processing and presenting commercial transport airplane flight and ground loads usage data. The scope of activities performed involve but are not limited to (1) defining the service-related factors that affect the operational life of commercial aircraft; (2) designing an efficient software system to reduce, store, and process large quantities of optical quick access recorder data; and (3) providing processed data in formats that will enable the FAA to reassess existing certification criteria. Presented herein are analyses and statistical summaries of landing and ground operations data to provide the FAA with a technical basis for assessing the suitability of the 0.5-g lateral acceleration criteria specified in Federal Aviation Regulation (FAR) 25.495 for turning. The data represent 1037 flights, 1039 flights, and 1361 flights of B-737-400, B-767-200ER, and B-747-400 aircraft, respectively. Included are statistical information on vertical and lateral accelerations, yaw angles, ground speeds, and gross weights experienced during touchdown and ground operations. Ground-turning lateral acceleration data were used in the development of a normalization procedure to allow prediction of lateral load factors due to ground turning on other aircraft. While the data contained in this report might indicate that the FAR 25.495 may be conservative at the 0.5-g level when one considers that FAR 25.495 takes into consideration asymmetric gear loading for both dry and highly slippery conditions, the retention of the traditional 0.5-g value may well be appropriate. The results of this study clearly indicate, however, that the lateral loads experienced by the larger/heavier transport jets during ground turns are substantially less than those of smaller jet transports.

1. INTRODUCTION.

Based on data from the Federal Aviation Administration (FAA) operational loads monitoring research on runway ground friction testing and research conducted in Europe by Messier/Dowty, aircraft and landing gear manufacturers believe that the current 0.5-g lateral load factor requirement, as specified in the Federal Aviation Regulations (FAR) 25.495 for turning, is too stringent, especially for heavy widebody transports. However, little is known about the origin of this loading condition and under what operational situations this might occur. Therefore, regulatory authorities are extremely reluctant to modify FAR requirements without appropriate technical substantiation. Consequently, a joint Federal Aviation Administration/Civil Aviation Authority (FAA/CAA) research program has been initiated to acquire and analyze available ground usage data to either substantiate the current 0.5-g lateral load certification requirement or provide engineering data to support a lower limit load.

The FAA is funding an ongoing Operational Loads Monitoring Program with the University of Dayton Research Institute (UDRI). A significant quantity of flight and ground loads data has been collected from both large transport and commuter aircraft. Aircraft models involved in this program include the B-737-400, B-767-200ER, MD-82/83, BE-1900D, A-320, CRJ200, and B-747-400.

The Operational Loads Monitoring Program is a fundamental element of the FAA's regulatory and certification process because it provides essential input for confirming the continued safety of the current civil transport fleet and provides essential data for updated airframe certification requirements. Research conducted as part of this program provides the opportunity to identify, in a proactive manner, conditions where aircraft usage deviates from assumptions in the original design criteria.

To assess the suitability of the 0.5-g turning requirement specified in FAR/JAR 25.495, UDRI conducted a study to determine the magnitudes and distributions of side load factor (Ny) experienced by B-737, B-767, and B-747 commercial transport aircraft during normal ground operations. An in-depth analysis of lateral, longitudinal, and vertical load operational conditions were characterized for various segments, phases, and events of ground operations. These included:

- During taxi-out
- On the runway prior to liftoff
- During touchdown
- On the runway after touchdown
- During thrust reverser usage
- On the runway after thrust reverser stowage
- During runway turnoff
- During taxi-in

The results of this study, presented herein, should begin to provide the FAA with the technical basis for assessing the suitability of the 0.5-g lateral acceleration criteria specified in FAR/JAR 25.495.

1

2. DATA REDUCTION CRITERIA.

2.1 PHASES OF FLIGHT AND SPECIFIC EVENTS CRITERIA.

UDRI separated the ground portion of each flight from the time it departed the gate area to its return to the gate into phases called taxi-out, takeoff roll, landing roll, and taxi-in. Specific data reduction criteria were developed by UDRI and used to identify the beginning and end of each of these phases. In addition, unique criteria were also developed in order to identify occurrences of maximum side load factor that resulted from specific events within these phases, such as the landing touchdown, thrust reverser deployment and stowage, and during the time when the aircraft started and completed its turnoff from the active runway after landing. Figure 1 shows a sketch depicting these phases and events.
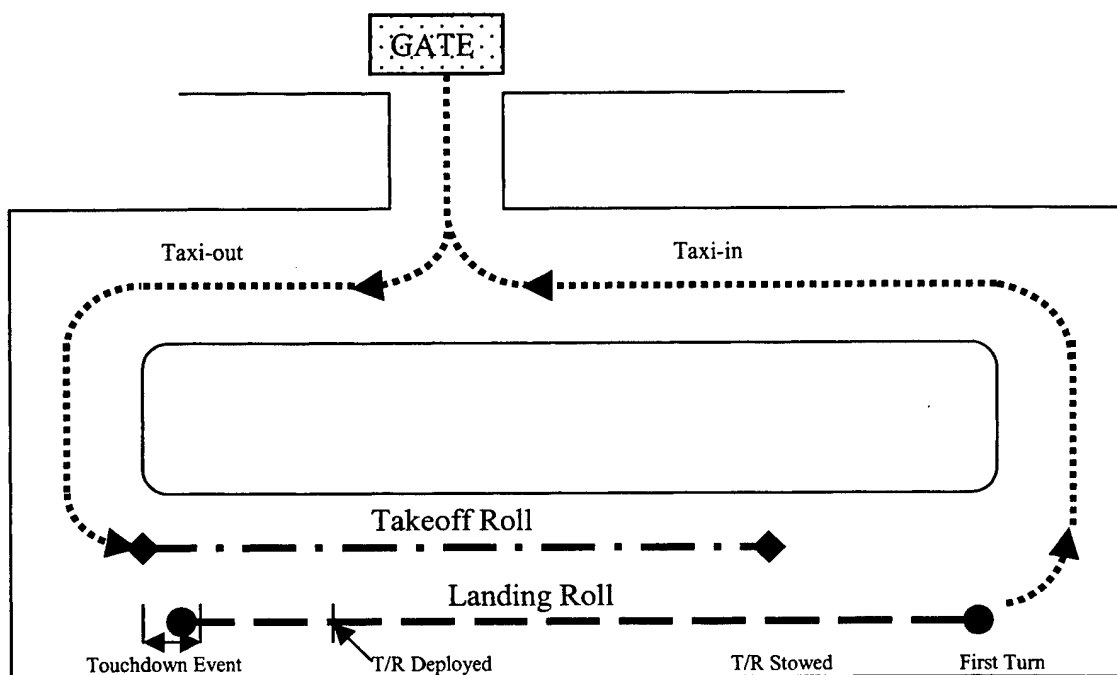
FIGURE 1. SKETCH OF GROUND PHASES AND EVENTS

The criteria used to define each of these phases and specific events are summarized in table 1 and discussed in more detail in sections 2.1.1 to 2.1.5.

2.1.1 Taxi-Out and Taxi-In.

UDRI defined all aircraft movement from engine start-up until the aircraft begins its takeoff roll as being taxi-out. Taxi-in was defined as beginning from the point where the aircraft completed its turnoff from the active runway after its landing roll to when the aircraft was parked at the gate or recorder shut down.

2

TABLE 1. SUMMARY OF PHASES OF FLIGHT AND
SPECIFIC EVENTS CRITERIA

Phase/Event	Defining Conditions
Taxi-Out	From engine start to beginning of takeoff roll
Taxi-In	After runway turnoff to hate or recorder shutdown
Takeoff Roll	From first rate of change of ground speed > 2kts/sec in a 20-second duration sequence to liftoff (squat switch off)
Landing Touchdown	A window varying in duration from 3 to 0.75 seconds prior to squat switch on to 1 second afterwards
Landing Roll	From 1 second after squat switch on to beginning of runway turnoff
Thrust Reverser Deployment/Stowage	From thrust reverser switch on until thrust reverser switch off
Runway Turnoff	From first sequential magnetic heading change >2 degrees in same direction from runway centerline and subsequent heading changes >13.5 or lateral direction dimension from runway centerline >100 feet then return to a straight line heading or turn in opposite direction

2.1.2 Takeoff and Landing Roll.

UDRI identified the beginning of the takeoff roll by searching for ground speeds that accelerated at rates greater than 2 kts/sec for a minimum duration of 20 seconds. When these values were found, the beginning of the takeoff roll was assigned as being the time slice where the first ground speed rate change greater than 2 kts/sec for that sequence occurred. The takeoff roll ends at liftoff with the squat switch off signal.

The landing roll phase was defined as beginning 1 second after the squat switch signaled that the landing touchdown had occurred and ending when the aircraft began its turnoff from the active runway.

2.1.3 Landing Touchdown.

UDRI normally defines touchdown as the time when the landing gear squat switch closes. However, studies have shown that the squat switch is not always a reliable indicator of the actual moment of touchdown, and depending on aircraft type, landing could occur up to almost 3 seconds before the squat switch would be activated. Therefore, in order to ensure that the maximum side load factor associated with touchdown was identified for this study, the actual touchdown event was assumed to occur within a time frame from 3 to 0.75 seconds (depending on aircraft type) prior to the squat switch on signal until 1 second following squat switch on. The 1-second time after squat switch was chosen somewhat arbitrarily, but was intended to ensure that sufficient time was allowed for the aircraft to respond to the touchdown and for the side load acceleration to build to its maximum value.

2.1.4 Thrust Reverser Deployment/Stowage.

An on/off switch identifies when deployment or stowage of the thrust reverser occurs. Thus, side load factor occurrences can be obtained during the time of thrust reverser usage. However, in order to capture the maximum side load factor while the thrust reverser was actually being deployed, UDRI selected an interval from when the thrust reverser on signal indicated deployment until 2 seconds afterwards.

2.1.5 Runway Turnoff.

UDRI used changes in magnetic heading to identify the beginning and end of the aircraft's turnoff from the active runway. After the aircraft touched down and was on the ground for 4 seconds, the subsequent average magnetic heading readings were used to define the aircraft's landing centerline. UDRI then searched for magnetic heading changes that continuously moved in the same direction away from this centerline. When the aircraft's sequential magnetic heading change exceeded 13.5 degrees from the direction of the landing centerline, or the integrated distance from the centerline exceeded 100 feet, the time slice associated with the first sequential heading change greater than 2 degrees from the landing centerline in the direction of the turn was defined as the beginning of the aircraft's turnoff from the runway.

UDRI developed the 100-foot deviation method as an alternate method of identifying flights involving shallow turns from the runway that did not exceed the 13.5-degree turn criteria. This method used aircraft ground speed and magnetic heading to calculate the aircraft's position relative to the runway centerline. Then, as above, the time slice associated with the first aircraft movement away from the landing centerline in the direction of the turn was defined as the beginning of the aircraft's turnoff from the runway.

The end point of this turnoff from the runway was also identified using magnetic heading readings. UDRI developed an algorithm that used the changes in magnetic heading, while the aircraft was in its turn, to identify when the aircraft had either returned to taxiing in a straight line or was turning in the opposite direction. The first point that provided this indication was then defined as the end point of the turnoff from the runway. This point is also the beginning of the taxi-in phase.

3. DATA REDUCTION.

UDRI currently receives and processes recorded flight loads parameters from a number of aircraft operated by U.S. carriers. These data, which are recorded by the airline during normal operations, have been processed through their ground station, desensitized, and provided to UDRI as time history files. UDRI processes and reports on these data as part of its ongoing FAA Operational Loads Monitoring Program. References 1 and 2 are examples of these reports. For this side load factor study, UDRI elected to use the recorded loads parameters listed in table 2 because they either contribute to or influence the magnitude of the side load on an aircraft during its ground operations and provide other valuable supporting information.

4

TABLE 2. LIST OF PARAMETERS

Parameter
Normal acceleration (Nz)
Lateral acceleration (Ny)
Longitudinal acceleration (Nx)
Magnetic heading
Gross weight
Ground speed
Squat switch (main gear)
Thrust reverser

3.1 ACCELEROMETER MEAN AND BIAS CORRECTION.

In order to correct for any drift in the recorded Ny, Nx, and Nz accelerometer readings, UDRI calculated a 1-g mean for Nz and a 0-g mean for Ny and Nx for each flight. Each mean was calculated using data obtained during taxi at very low speeds. If these calculated mean values differed from the respective recorded 1-g or 0-g values, the differences were identified as biases, which were used to correct the recorded acceleration values throughout the flight. A graph showing this procedure is shown in figure 2 for recorded values of Nz.
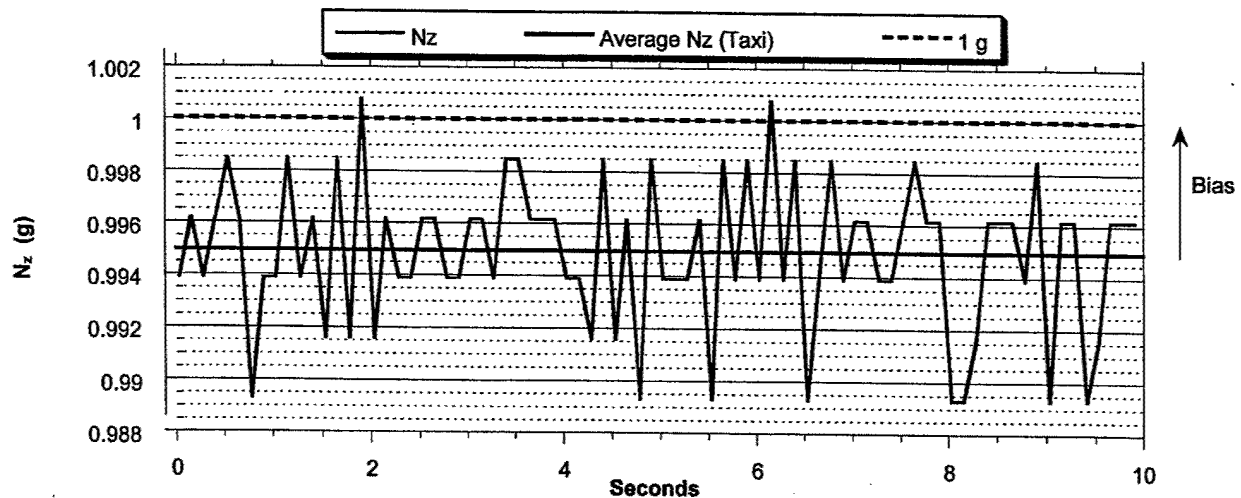
FIGURE 2. BIAS CALCULATION EXAMPLE

3.2 PEAK COUNTING METHOD.

The peak-between-means method was used to count all Ny acceleration peaks occurring during the various ground phases and events involved in this study. This method identifies a cycle and counts a peak value when the accelerometer trace reaches its highest or lowest point outside of a given threshold, then returns to touch or cross the 0-g mean line for Ny. A threshold or dead band area of ±0.005g on either side of the Ny mean was used to avoid counting the smallest

5

peaks/noise levels. A description of the peak-between-means counting method is discussed in reference 6 and illustrated in figure 3.
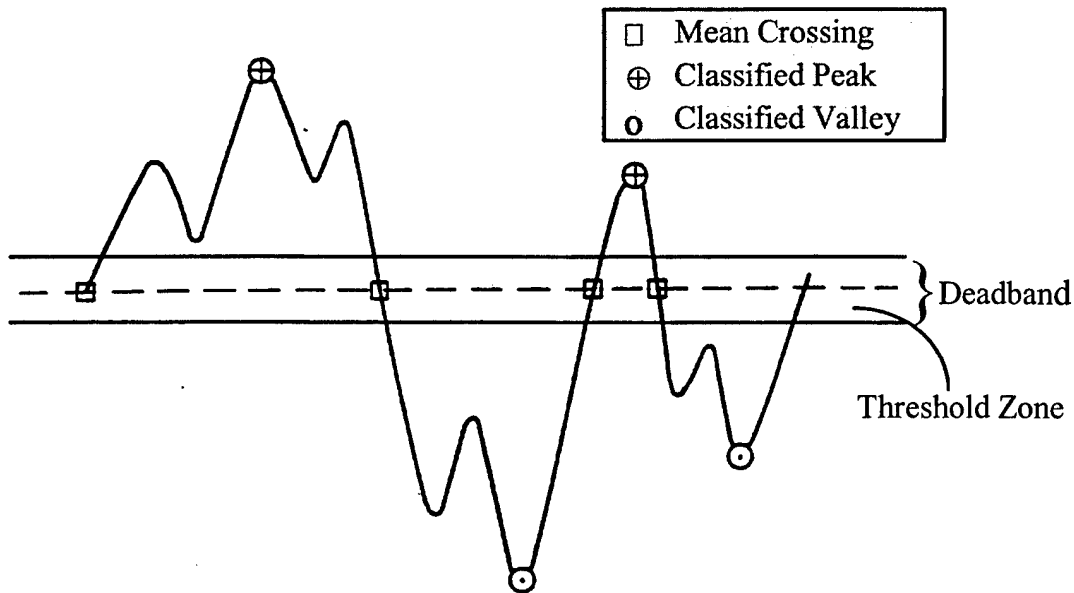
FIGURE 3. PEAK-BETWEEN-MEANS COUNTING PROCEDURE

4. DATA PROCESSING.

B-767-200ER, B-737-400, and B-747-400 flights containing the ground loads parameters (listed in table 1) were processed in accordance with the data reduction criteria and procedures previously defined in sections 2 and 3.

Figure 4 shows typical time history traces of an aircraft's (B-767) ground operations after landing touchdown and while taxiing into the gate area. The time history traces provide an overall look at some of the important parameters that influence the side loads during ground operations and their relative magnitudes. The traces show how the coincident values of magnetic heading; incremental side, vertical, and longitudinal load factor; and ground speed interact during ground operations following landing. The vertical dashed lines indicate the time at thrust reverser deployment and stowage, while the solid line indicates where the runway turnoff begins.

6
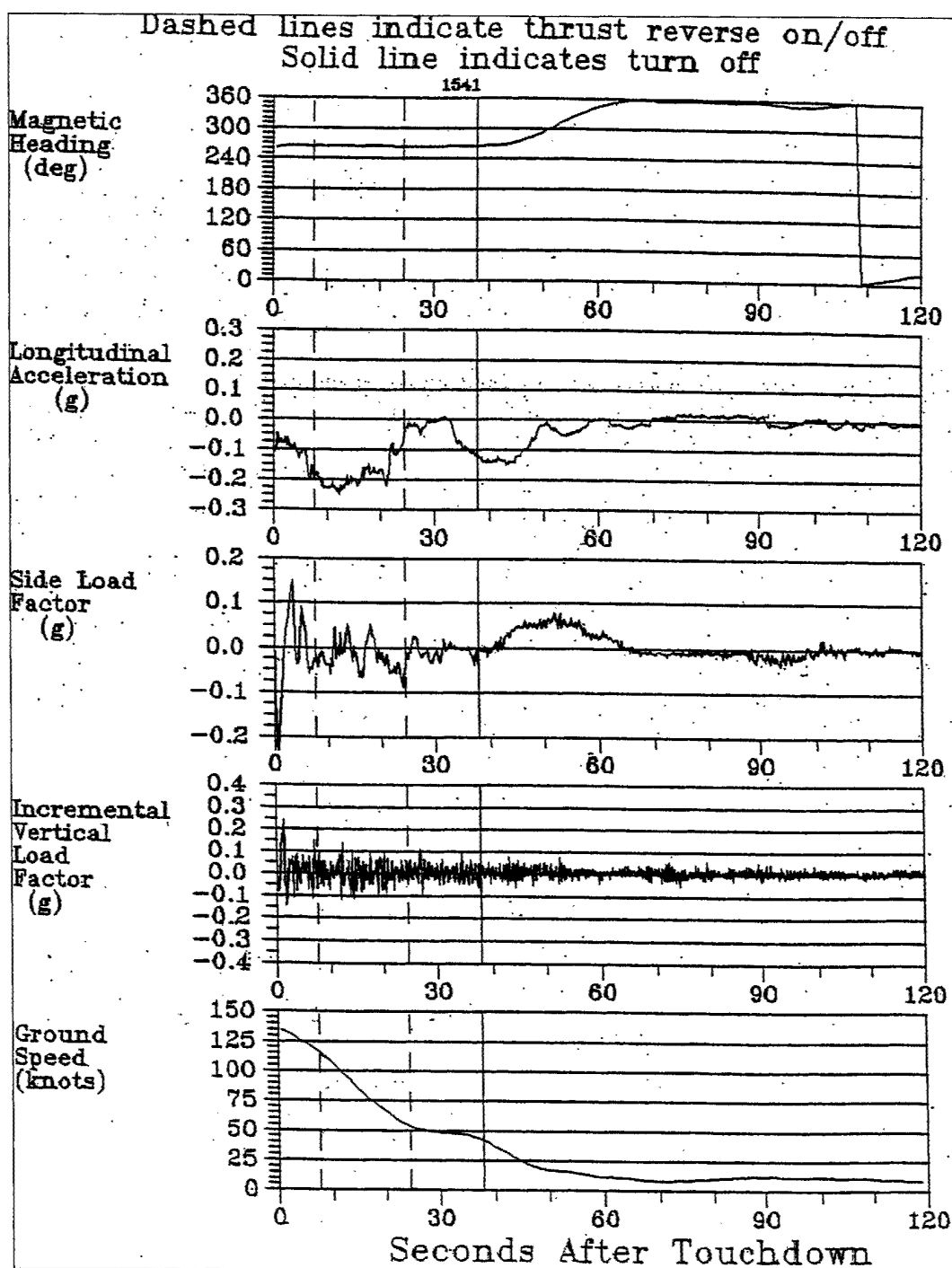
FIGURE 4. TYPICAL TIME HISTORY TRACES OF GROUND OPERATIONS AFTER
TOUCHDOWN

Table 3 presents information about the number of flights, thrust reverser usage, and left or right turns from the active runway for each aircraft type.

TABLE 3. GROUND OPERATIONS DATABASE

Aircraft Type	Number of Flights	Number of Left Turns	Number of Right Turns	Number of Thrust Reverser Cycles	Flights with Thrust Reverser Stowed During Landing Roll	Flights with Thrust Reverser Stowed After Turnoff
B-737-400	1037	476	561	1036	637	399
B-767-200ER	1039	428	611	1028	587	441
B-747-400	1361	832	529	1330	785	545

5. DATA PRESENTATION.

The processed ground loads data were used to develop statistical data formats by aircraft type, showing the magnitudes and frequency distributions of side load factor peaks during each ground phase of operation, touchdown, thrust reverser usage, and during the runway turnoff. UDRI also used the processed ground loads data to generate scatter plots showing various coincident parameters such as ground speed, gross weight, and longitudinal and vertical acceleration with the maximum side load factor peaks. Where appropriate, comparisons of statistical data between the aircraft types were developed.

Table 4 lists all the statistical data formats that were developed during this study and identifies the appendix and figure number where the individual aircraft and comparison between aircraft data formats can be found.

TABLE 4. STATISTICAL DATA FORMATS

Appendix A, B, and C	Figure		
Aircraft Ground Operations Data Plots	B-737	B-767	B-747
Cumulative frequency of side load factor during taxi	A-1	B-1	C-1
Cumulative frequency of side load factor during takeoff and landing roll	A-2	B-2	C-2
Cumulative frequency of maximum side load factor during runway turnoff	A-3	B-3	C-3
Cumulative frequency of side load factor during taxi-in, taxi-out, and runway turnoff	A-4	B-4	C-4
Cumulative frequency of maximum side load factor at touchdown	A-5	B-5	C-5
Cumulative frequency of side load factor after touchdown and before thrust reverser deployment	A-6	B-6	C-6
Cumulative frequency of maximum side load factor at thrust reverser deployment	A-7	B-7	C-7

8

TABLE 4. STATISTICAL DATA FORMATS (Continued)

Appendix A, B, and C	Figure		
Aircraft Ground Operations Data Plots	B-737	B-767	B-747
Cumulative frequency of side load factor while thrust reverser is deployed	A-8	B-8	C-8
Cumulative frequency of side load factor after thrust reverser stowed during landing roll	A-9	B-9	C-9
Cumulative frequency of side load factor at touchdown and during landing roll	A-10	B-10	C-10
Coincident longitudinal load factor at maximum side load factor during takeoff roll	A-11	B-11	C-11
Coincident incremental vertical load factor at maximum side load factor at touchdown	A-12	B-12	C-12
Coincident gross weight at maximum side load factor at touchdown	A-13	B-13	C-13
Yaw angle and maximum side load factor at touchdown	A-14	B-14	C-14
Coincident longitudinal load factor at maximum side load factor before thrust reverser deployment	A-15	B-15	C-15
Coincident longitudinal load factor at maximum side load factor while thrust reverser is deployed	A-16	B-16	C-16
Coincident longitudinal load factor at maximum side load factor after thrust reverser stowage during landing roll	A-17	B-17	C-17
Coincident incremental vertical load factor at maximum side load factor during landing roll	A-18	B-18	C-18
Coincident incremental vertical load factor at maximum side load factor during runway turnoff after landing	A-19	B-19	C-19
Coincident ground speed at maximum side load factor during runway turnoff after landing	A-20	B-20	C-20

Appendix D	
B-737, B-767, and B-747 Aircraft Ground Operations Data Comparisons	Figure
Comparison of cumulative frequency of side load factor during taxi-out	D-1a
Comparison of cumulative frequency of side load factor during taxi-in	D-1b
Comparison of cumulative frequency of side load factor during takeoff roll	D-2a
Comparison of cumulative frequency of side load factor during landing roll	D-2b
Comparison of cumulative frequency of maximum side load factor during runway turnoff	D-3
Comparison of cumulative frequency of maximum side load factor at touchdown	D-4
Comparison of cumulative frequency of side load factor after touchdown and before thrust reverser deployment	D-5
Comparison of cumulative frequency of maximum side load factor at thrust reverser deployment	D-6
Comparison of cumulative frequency of side load factor while thrust reverser is deployed	D-7

TABLE 4. STATISTICAL DATA FORMATS (Continued)

Appendix D	
B-737, B-767, and B-747 Aircraft Ground Operations Data Comparisons	Figure
Comparison of cumulative frequency of side load factor after thrust reverser stowed during landing roll	D-8
Comparison of 95 percentile of coincident longitudinal load factor at maximum side load factor during landing roll	D-9
Comparison of 95 percentile of coincident incremental vertical load factor at maximum side load factor at touchdown	D-10
Comparison of 95 percent bounds of yaw angle and maximum side load factor at touchdown	D-11
Comparison of 95 percentile of coincident longitudinal load factor at maximum side load factor before thrust reverser deployment	D-12
Comparison of 95 percentile of coincident longitudinal load factor at maximum side load factor while thrust reverser is deployed	D-13
Comparison of 95 percentile of coincident longitudinal load factor at maximum side load factor after thrust reverser stowage during landing roll	D-14
Comparison of 95 percentile of coincident incremental vertical load factor at maximum side load factor during landing roll	D-15
Comparison of 95 percentile of coincident incremental vertical load factor at maximum side load factor during turnoff after landing	D-16
Comparison of 95 percentile of coincident ground speed at maximum side load factor during runway turnoff after landing	D-17

Appendices A, B, and C present the statistical ground operations data for individual aircraft. Appendix A contains the B-737 data plots, appendix B the data plots for the B-767 aircraft, and appendix C the data plots for the B-747 aircraft. The sequence of the data plots and titles between appendices are identical and have been arranged to coincide with the phase breakdown presented in table 1.

Appendix D contains comparisons of the statistical ground operations data in appendices A, B, and C for the B-737, B-767, and B-747. These data are presented in the same sequence as the data presented in appendices A, B, and C and the ground phases presented in table 1.

5.1 APPENDICES A, B, AND C—INDIVIDUAL AIRCRAFT GROUND OPERATIONS DATA PRESENTATION.

The data in appendices A, B, and C are presented as line plots and scatter plots for the B-737, B-767, and B-747 aircraft.

The line plots present the cumulative frequency of side load factor during different phases of taxi and landing operations, as shown in figure A-1. The reader should be aware that some plots present the cumulative frequency of all side load factor peaks measured during a given phase, while others present the cumulative frequency of only the maximum side load factor measured during a phase. Figures A-3, A-5, A-7, B-3, B-5, B-7, C-3, C-5, and C-7 present the cumulative

frequencies of the maximum measured side load factor peaks during runway turnoff, at touchdown, and at thrust reverser deployment, respectively. Except for figures A-4, A-10, B-4, B-10, C-4, and C-10 all other line plots show the cumulative frequencies of all measured side load factor peaks. Figures A-4, A-10, B-4, B-10, C-4, and C-10 show comparisons of cumulative frequencies of side load factor that include either all peaks or only maximum peaks, depending on the specific phase. In these comparisons, the line plots for the runway turnoff and for the touchdown, as identified in the legend of the figures, are based on maximum peaks.

Scatter plots are normally used to present data that are thought to be related. Review of the scatter plots shows that, except for the data plotted in figures A-14, B-14, and C-14, no clear correlation exists. For comparison purposes these three figures have been provided with 95% and 99% confidence bounds on the individual points. In order to provide a means of comparing the different relationships in the bivariate load data presented in all other scatter plots, 95 and 99 percentile oval bounds of constant probability were plotted on top of scatter plots of the raw data. The ovals were constructed by first determining the 0.5 and 99.5 percentiles of each variable independently. The center of the oval was picked to be 0 for the maximum load variable and the median of the coincident variable. Then, using axes through the center point, an ellipse was fit separately in each quadrant based on the appropriate maximum and minimum values. The maximum and minimum values chosen for these plots contain 99 percent or 95 percent of the data. However, it must be kept in mind that because of lack of knowledge regarding the exact distribution function of the scatter data, the constant probability ovals must be considered an approximation only.

5.2 APPENDIX D—GROUND OPERATIONS DATA COMPARISON PLOTS, B-737, B-767, AND B-747 AIRCRAFT.

The data in appendix D are presented as comparisons of B-737, B-767, and B-747 line plots, and 95 percentile ovals are presented in appendices A, B, and C.

Figures D-1a and D-1b show the cumulative occurrences of side load factor per 1000 flights during the taxi-in and taxi-out phases of ground operations, respectively. The magnitudes of side load factor and the number of occurrences are slightly higher for the taxi-in phase. This may be due to the higher speeds observed in association with taxi-in as compared to lower speeds during taxi-out. Also, the side load factors experienced become lower as aircraft size increases. It could be postulated, based on limited research on a number of aircraft, that this may be due to differences in gear geometry, such as the main gear track dimension and the distance between the nose and main gear. It is possible that these dimensions could affect the pilot's turning option relative to a fixed taxiway width.

Figures D-2a and D-2b show the cumulative occurrences of side load factor per 1000 flights during the takeoff roll and landing roll phases of ground operations, respectively. The landing roll phase excludes the maximum side load factor associated with landing touchdown and any other Ny that occurs within the touchdown event. Some differences between airplanes are evident, particularly with respect to the landing roll, where the side load factor experienced increases with aircraft size.

Figure D-3 includes only the cumulative occurrences of side load factor per 1000 flights that occurred during the turnoff from the active runway. These occurrences are not included in the taxi-in data presented in figures D-1a and D-1b. When figures D-1a, D-1b, and D-3 are compared, it can be seen that the highest values of side load factor are being contributed by the turnoff. Again, as for taxi-in, side load factors experienced during the turnoff from the active runway decrease with increasing aircraft size. This again may be due to the gear geometry differences discussed previously. Table 3 provided information on the actual left and right turns from the active runway performed by each airplane. Whereas the B-737 and B-767 show more right turns than left turns, the B-747 in contrast shows more left turns than right turns.

Figure D-4 shows the cumulative occurrences per 1000 flights of the maximum side load factor associated with the touchdown event during landing. While use of a short-time interval for the touchdown event probably ensured that the associated maximum value of side load factor was found, in all likelihood, these criteria also probably biased the maximum side load factor during touchdown toward the high side. Not every touchdown results in an Ny peak, so the number of peaks does not necessarily equate to the number of flights.

Figure D-5 presents the cumulative frequency of side load factor occurrences from touchdown (squat switch on plus 1 second) until the time the thrust reversers are deployed. While the reasons for the differences in side load factor magnitude between the aircraft are not known, by comparing figure D-5 with figure D-2b, it can be seen that for the B-767 and B-747, the higher Ny peaks during the landing roll are occurring prior to thrust reverser deployment. This observation is further supported by the data in figures D-6 through D-8. For the B-737, the maximum side load factors occur, while the thrust reversers are deployed. Because of the concern that the plot of side load factor at touchdown plus 1 second might pull some of the higher values of side load factor from this phase, side load factor data were also generated starting from the squat switch on point. When the two plots were compared, this concern proved to be invalid because the higher side load factor values were the same in both plots and there was only a minimal difference between the plots overall. Thus, figure D-5 is plotted using data following touchdown plus 1 second.

Figure D-6 shows the cumulative occurrences of the maximum side load factor at the time the thrust reverser is deployed. The largest side load factor peak that occurred within 2 seconds following thrust reverser deployment was used to develop the statistical data for this figure. This event was investigated because the deployment of the thrust reverser often causes a noticeable vertical load factor peak to occur, and it was suspected that there could also be some effect on Ny. The figure shows that magnitude of the side load factors encountered increases as aircraft size or gross weight increases.

Figure D-7 presents the cumulative frequency of side load factor from the time that the thrust reversers are deployed until they are stowed, or if not stowed, during the landing roll, until the beginning of the runway turnoff. Side load factors experienced while the thrust reversers are deployed are almost identical for the B-737 and the B-767; however, the magnitudes are higher for the B-747, although there are fewer total occurrences per 1000 flights. Thrust reversers are not always used on each flight. Table 3 provides information on the actual thrust reverser cycles.

12

Although thrust reversers are usually used on each flight, the percentage of flights that thrust reversers are not used, while small, increases as the aircraft size or gross weight increases.

Figure D-8 presents the cumulative frequency of side load factor from the time the thrust reversers are stowed until the start of the turnoff from the active runway. Again, side load factor data for these flights were only included in this figure until the aircraft turned off from the active runway.

Figures D-9 to D-17 compare the 95 percentile ovals from the scatter plots for the B-767, B-737, and B-747 as shown in figures A-11 through A-20, B-11 through B-20, and C-11 through C-20. However, a comparison of the percentiles for the gross weight of figures A-13, B-13, and C-13 was not considered to provide worthwhile information and is not included.

Figure D-9 presents a comparison of the 95 percentile ovals of scatter points representing the coincident longitudinal load factor at the maximum side load factor measured during the takeoff roll. The plot shows a generally reduced magnitude of side load factors for the B-747.

Figure D-10 presents the 95 percentile ovals of coincident incremental vertical load factor that occurs in conjunction with the maximum side load factor measured during the touchdown event, as defined in paragraph 2.1.3. In contrast to the comparison of side load factors in figure D-9, the comparisons in figure D-10 show a generally increased magnitude of vertical load factors for the B-747.

Figure D-11 presents a comparison of the 95 percent confidence bounds for the yaw angle and the maximum side load factor that occur at touchdown. Since yaw angle is not a recorded parameter for any of the aircraft, UDRI derived the yaw angle for each landing using values of magnetic heading. UDRI assumed that the last magnetic heading reading prior to touchdown was the final direction of flight prior to touchdown. Then, using the average magnetic heading after touchdown, UDRI calculated the difference in heading prior to touchdown with the heading on the runway after landing and called this the yaw angle.

Figures D-12 through D-14 present comparisons of the envelope of coincident longitudinal load factor at the maximum side load factor measured during the landing roll after touchdown. Figure D-12 compares data from 1 second after touchdown until thrust reverser deployment, figure D-13 compares data during the time the thrust reversers are deployed, and figure D-14 compares data after the thrust reversers have been stowed until the turnoff from the runway.

Figure D-15 compares the 95 percentile ovals of the coincident incremental vertical load factor that occurs at the maximum side load factor during the landing roll phase. This covers the period from 1 second after touchdown until start of turnoff from the runway. The spread for the longitudinal load factor is considerably larger for the B-767 than for either the B-737 or the B-747.

Figure D-16 compares the 95 percentile ovals of the coincident incremental vertical load factor that occurs at the maximum side load factor during runway turnoff after landing. The B-737

envelope shows higher load factor values for both Nx and Ny, which may be attributable to inertia effects associated with aircraft size differences.

Figure D-17 compares the 95 percentile ovals of the coincident ground speeds that occur in conjunction with the maximum side load factor during the runway turnoff after landing. The B-737 envelope is shown to be larger than either the B-767 or B-747 aircraft. Higher side load factors for the B-737 at the same ground speeds as the B-767 may be attributable to sharper turns for the smaller B-737 aircraft.

5.3 APPENDIX E—DEVELOPMENT OF A NORMALIZATION PROCEDURE FOR LATERAL LOAD FACTORS DUE TO GROUND TURNING.

Appendix E presents the development of a data normalization procedure that provides a means to consolidate available ground turning lateral load factor statistical data from B-737-400, MD-82/83, A-320, B-767-200ER, and B-747-400 aircraft into a single relationship. The relationship uses landing gear track and landing gear base dimensional data as input to represent the measured lateral load factor statistics for ground turning operations of the B-737-400, MD-82/83, A-320, B-767-200ER, and B-747-400 aircraft. The relationship provides a means for estimating expected lateral load factor distributions due to ground turning on other aircraft. The relationship is primarily useful for the definition of repeated load criteria. However, it can be used for the definition of discrete static design criteria for ground turning of other aircraft by establishing a common exceedance rate or probability of failure.

6. CONCLUSIONS.

The FAA's Airborne Data Monitoring Program has provided valuable statistical flight and ground loads information for a number of aircraft in commercial operations. These aircraft include the B-767-200ER, the A-320, the B-737-400, and the MD-82/83. The information for these aircraft, as published in references 1-4, cover general flight usage data, ground loads data, flight loads data, and systems operational data in formats primarily useful for the definition of repeated loads criteria. For this study, data available from the FAA program was used to evaluate the realism of existing fixed static design requirement for ground loads in light of the operational experience of aircraft of different size.

The results presented in appendices A, B, C, and D show that the longitudinal, lateral, and vertical load factors measured during landing and ground operations vary by airplane. How these variations are affected by differences in landing gear characteristics for the vertical accelerations or by braking and thrust reverser usage for longitudinal accelerations as opposed to aircraft size is not clear. Lateral load factors are not likely to be influenced much by landing gear characteristics and braking or thrust reversal operations. The data in reference 5 show good correlation between lateral load factor and bank angle at touchdown for the landing condition. Review of the results suggest that asymmetric landings involving bank angle are a normal part of operational experience and are affecting the input of side loads to the gear at touchdown.

As shown in appendix E, for ground turning operations measured, lateral load factors are decidedly a function of airplane size. It was postulated that the differences in gear geometry, such as main gear track dimension and the distance between main and nose gears, could affect the pilot's

turning input options relative to the fixed widths of runways or taxiways. Because no simple theoretical formulation could be derived to account for these differences, the study described in appendix E developed an empirical relationship that accounts for the effect of gear geometry differences on the side load factor experienced during ground turning. This relationship allowed consolidation of the different spectra into a single equation applicable to all aircraft. Using the empirical relationship, a lateral load factor spectra for ground turning can be estimated for other airplanes. The relationship can also be used to estimate the lateral load factor for different airplanes at a fixed probability level. Theoretically, this would allow the establishment of a static design criterion for lateral load factor during ground turning based on aircraft size considerations.

The data in the appendices show that the measured load factors are well within the static design levels specified for ground operations in FAR Part 25.

7. REFERENCES.

1. Tipps, D.O., Rustenburg, J.W., and Skinn, D.A., "Statistical Loads Data for B-767-200ER Aircraft in Commercial Operations," DOT/FAA/AR-00/10, March 2000.

2. Rustenburg, J.W., Skinn, D.A., and Tipps, D.O., "Statistical Loads Data for the Airbus A-320 Aircraft in Commercial Operations," DOT/FAA/AR-02/35, April 2002.

3. Rustenburg, J.W., Skinn, D.A., and Tipps, D.O., "Statistical Loads Data for a Boeing 737-400 in Commercial Operation," DOT/FAA/AR-98/28, August 1998.

4. Skinn, D.A., Tipps, D.O., and Rustenburg, J.W., "Statistical Loads Data for a MD-82/83 in Commercial Operation," DOT/FAA/AR-98/65, February 1999.

5. "Statistical Loads Data for the CRJ200 Aircraft in Commercial Operation," University of Dayton Research Institute, Report UDR-TR-2002-00108, to be published winter 2003.

6. de Jonge, B., "Reduction of Incremental Load Factor Acceleration Data to Gust Statistics," DOT/FAA/CT-94/57, August 1994.
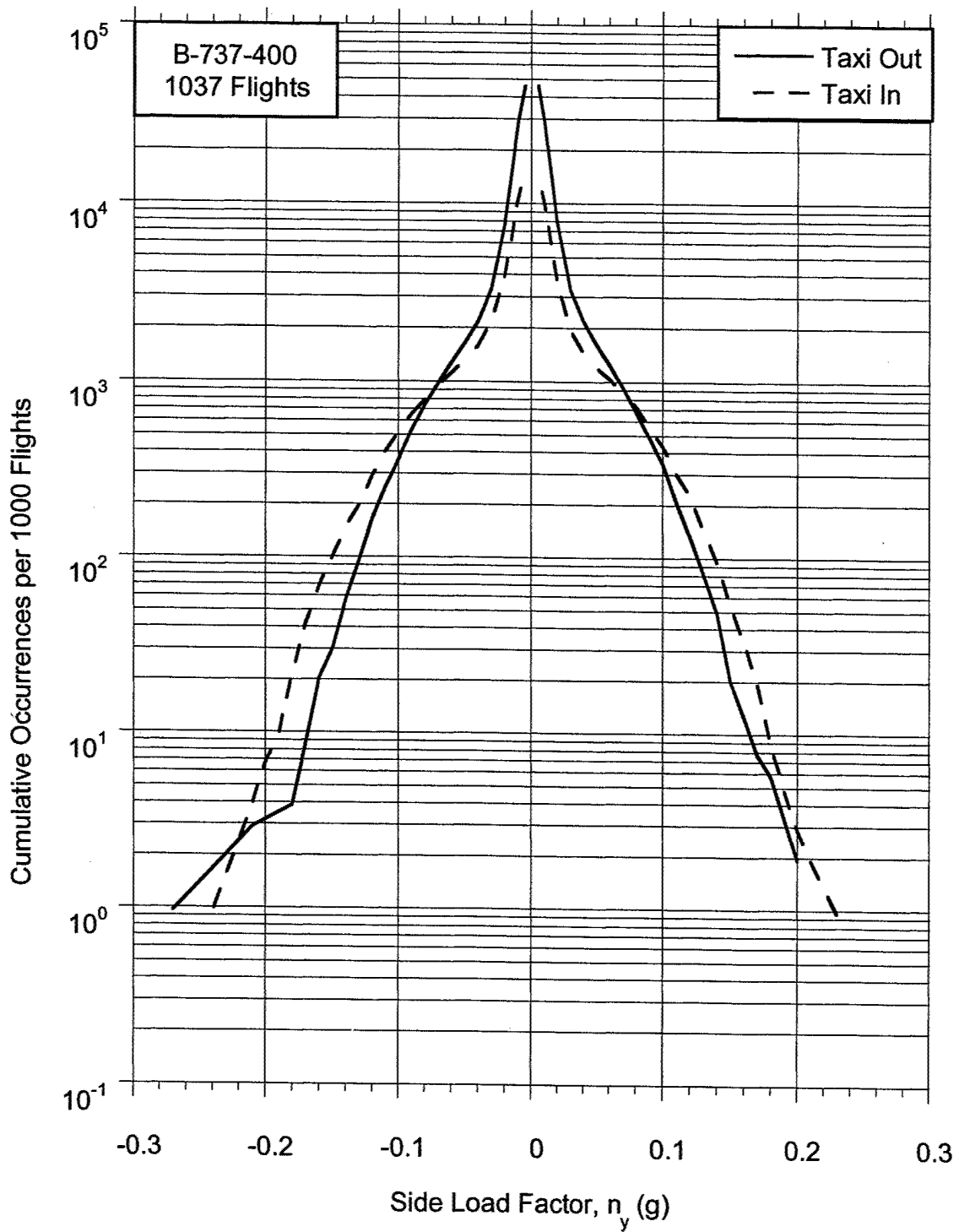
FIGURE A-1. CUMULATIVE FREQUENCY OF SIDE LOAD FACTOR DURING TAXI
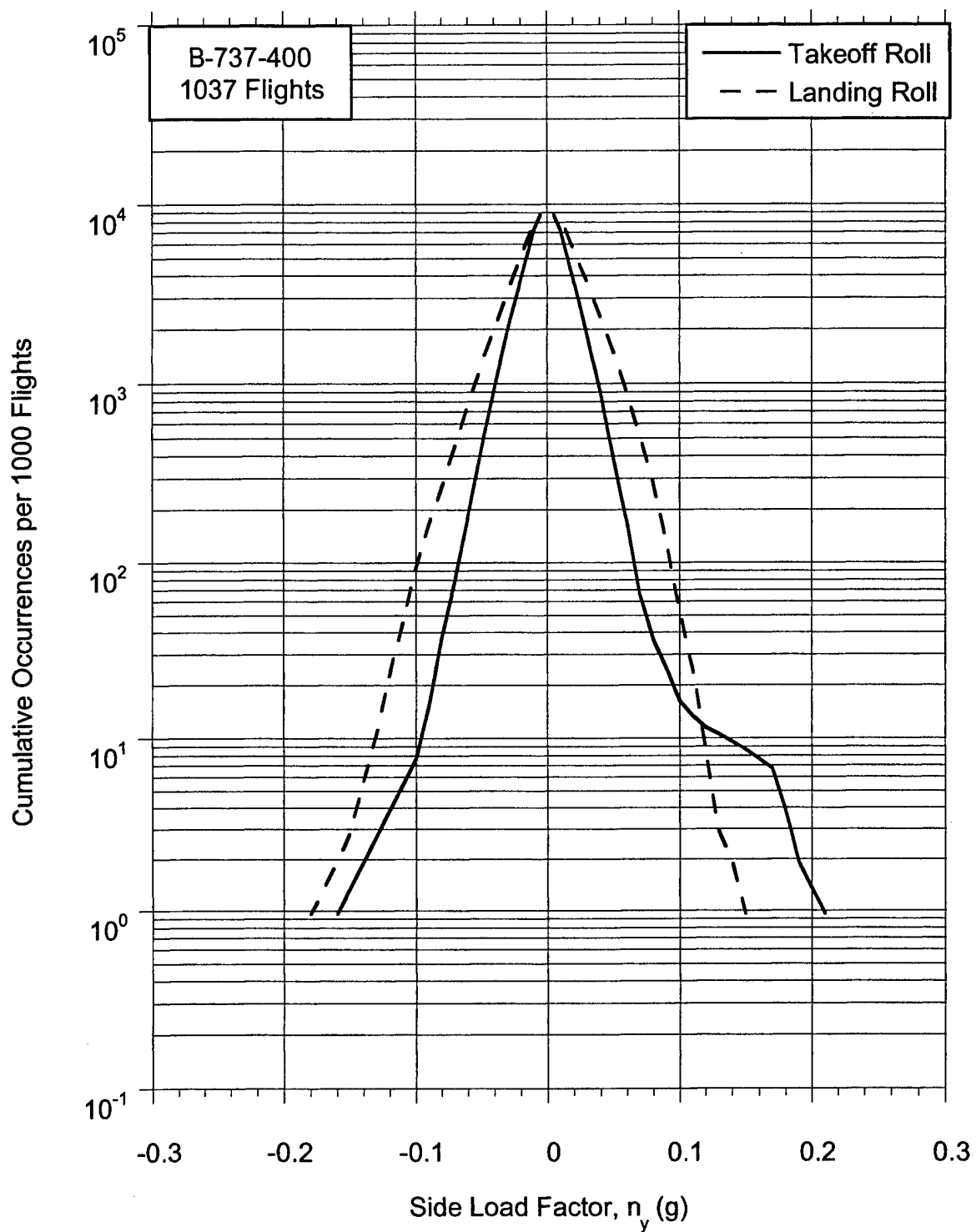
FIGURE A-2. CUMULATIVE FREQUENCY OF SIDE LOAD FACTOR DURING
TAKEOFF AND LANDING ROLL
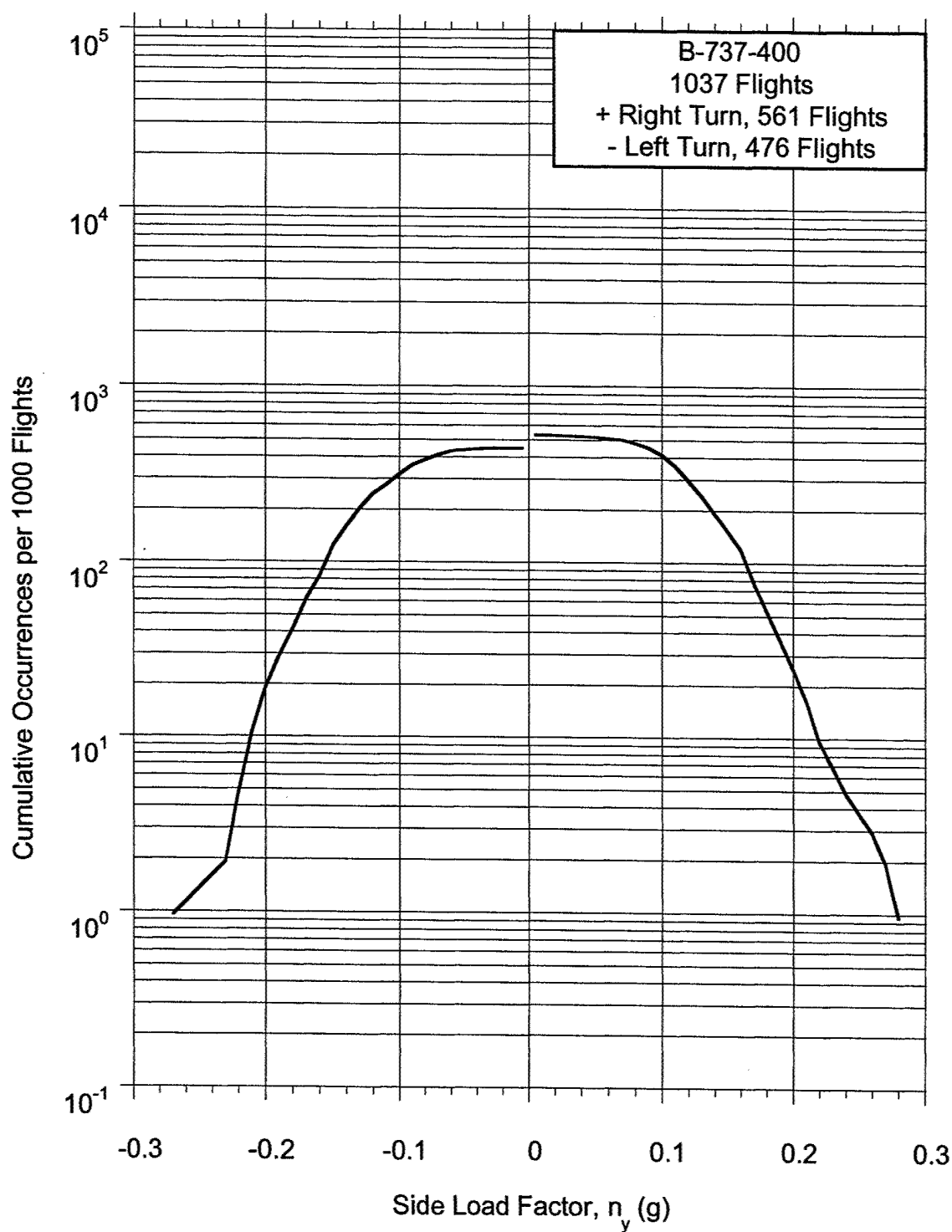
FIGURE A-3. CUMULATIVE FREQUENCY OF MAXIMUM SIDE LOAD FACTOR
DURING RUNWAY TURNOFF
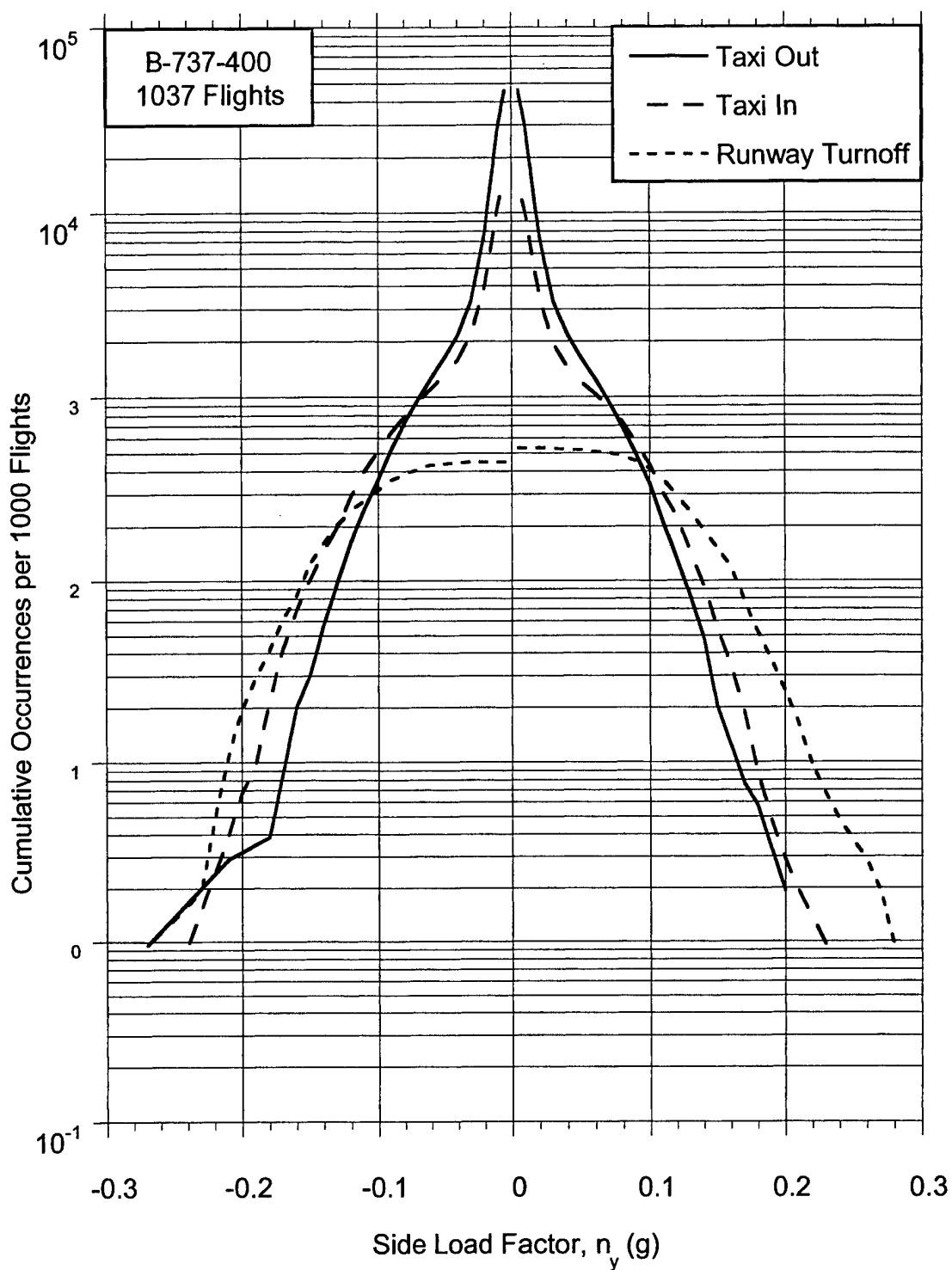
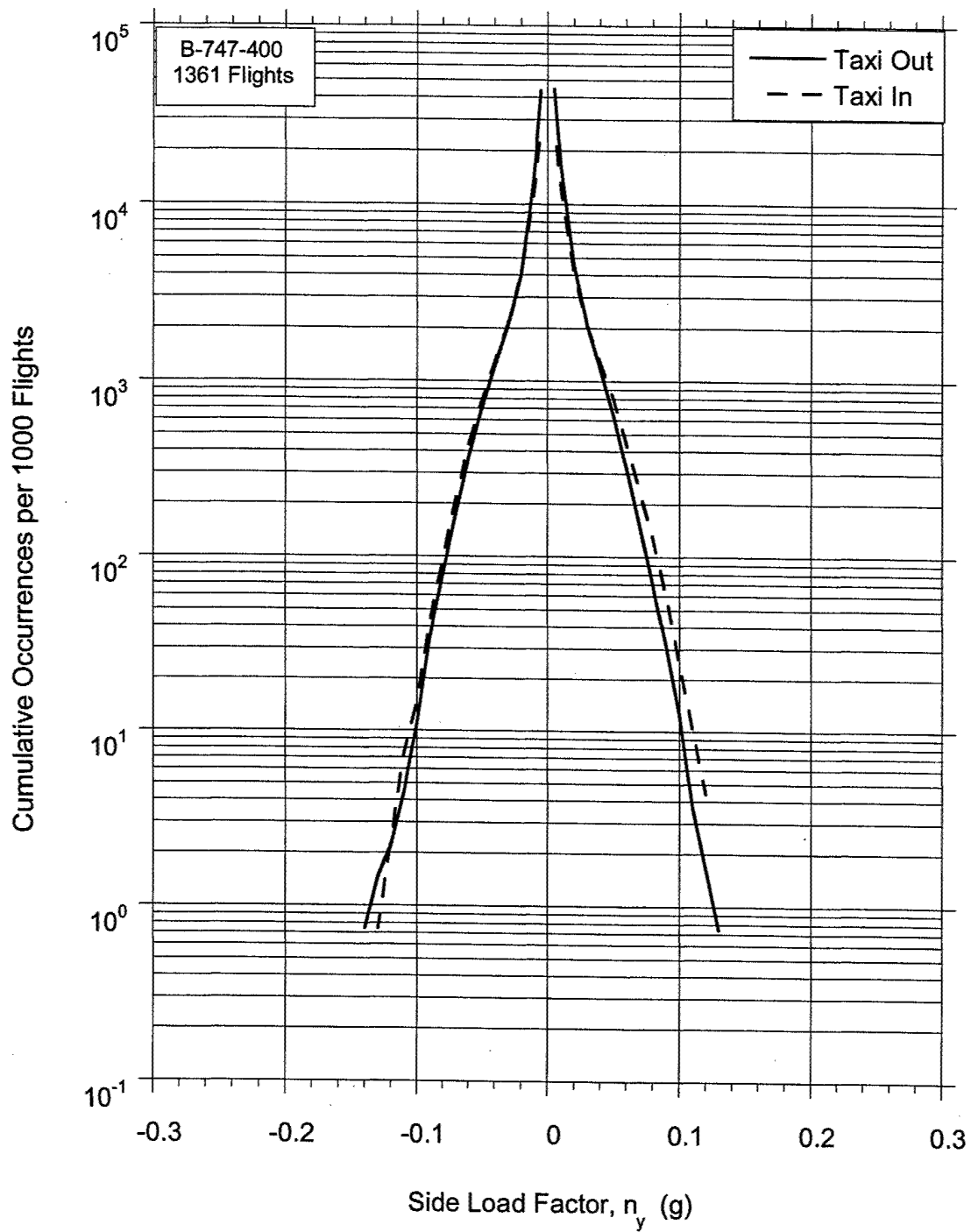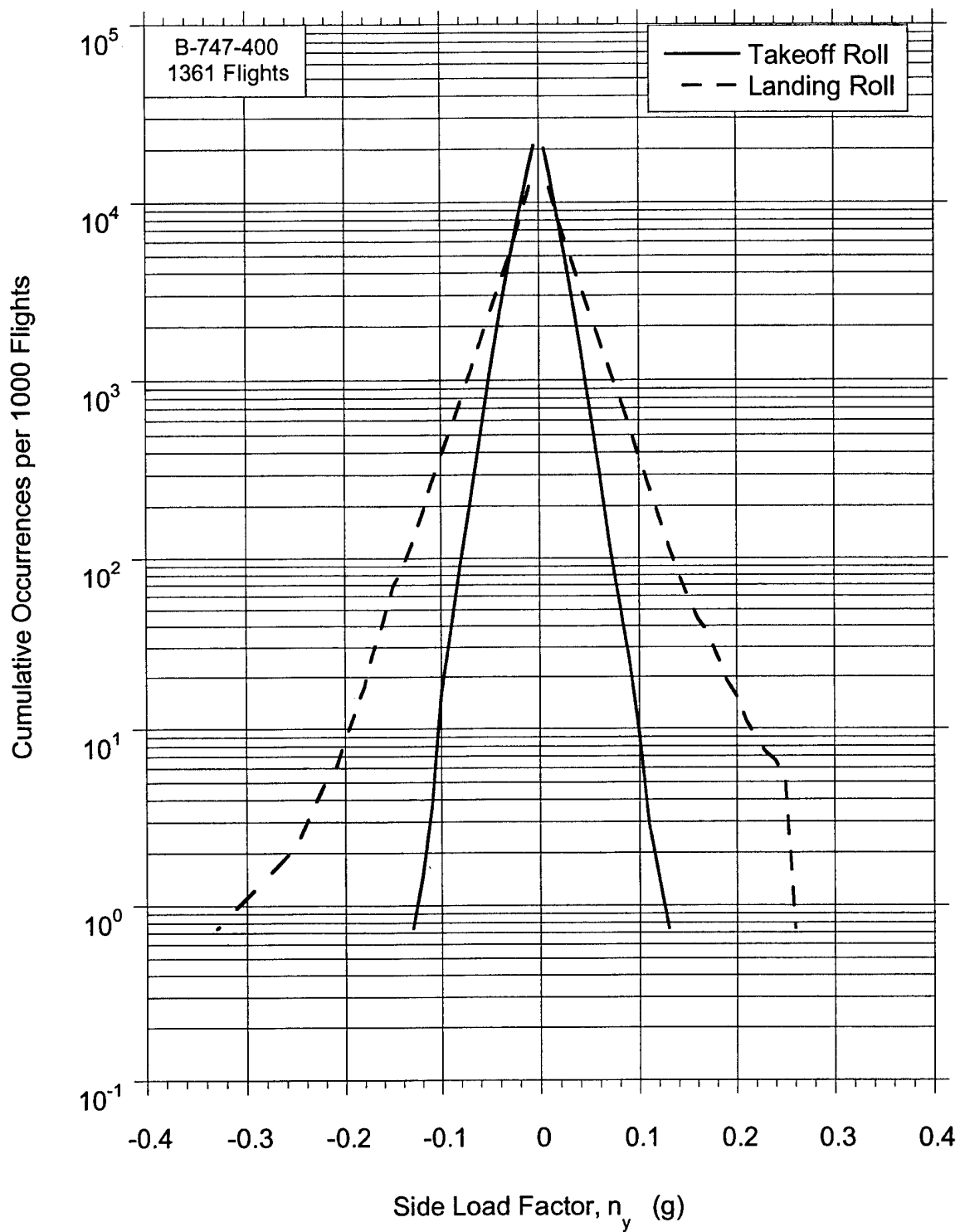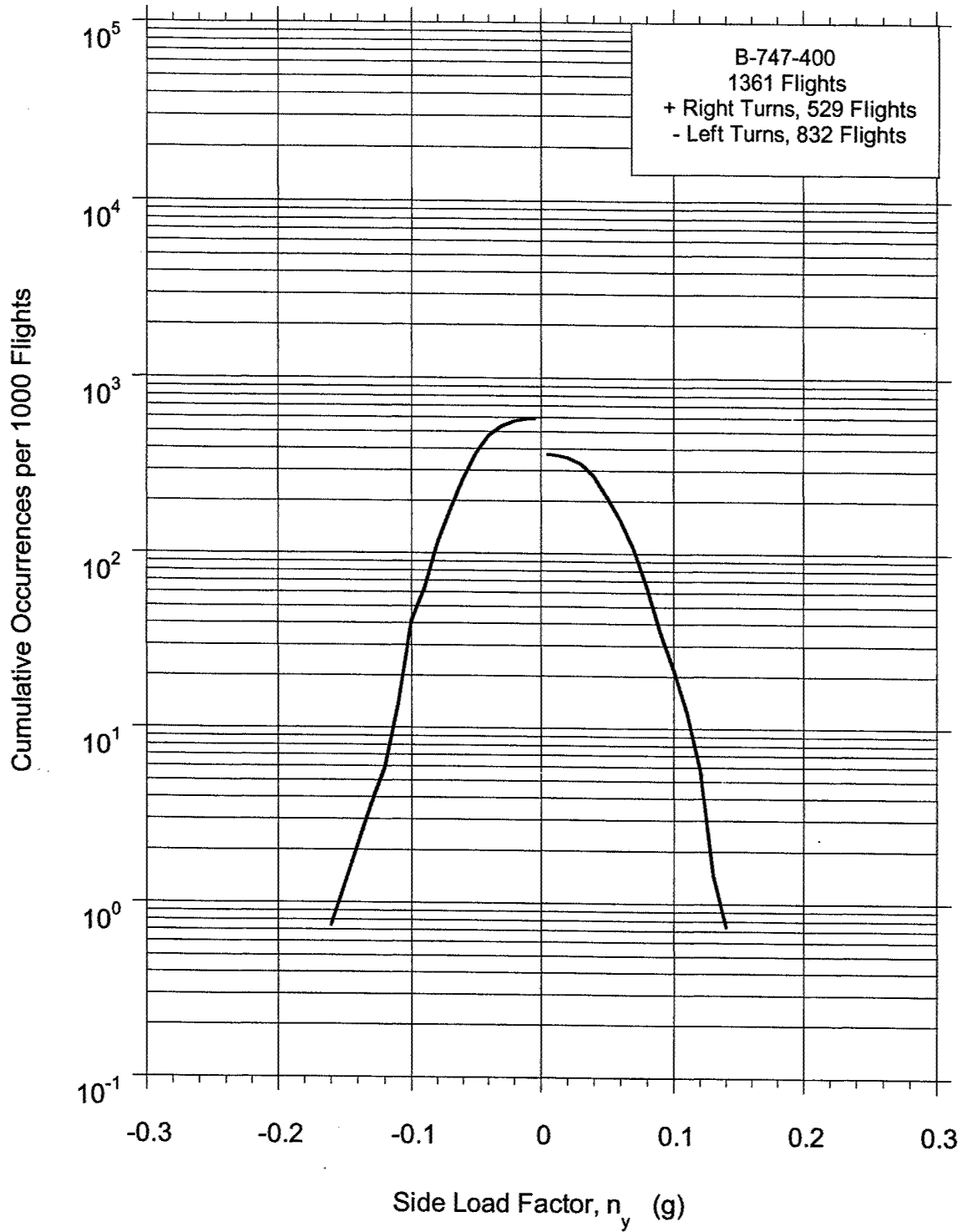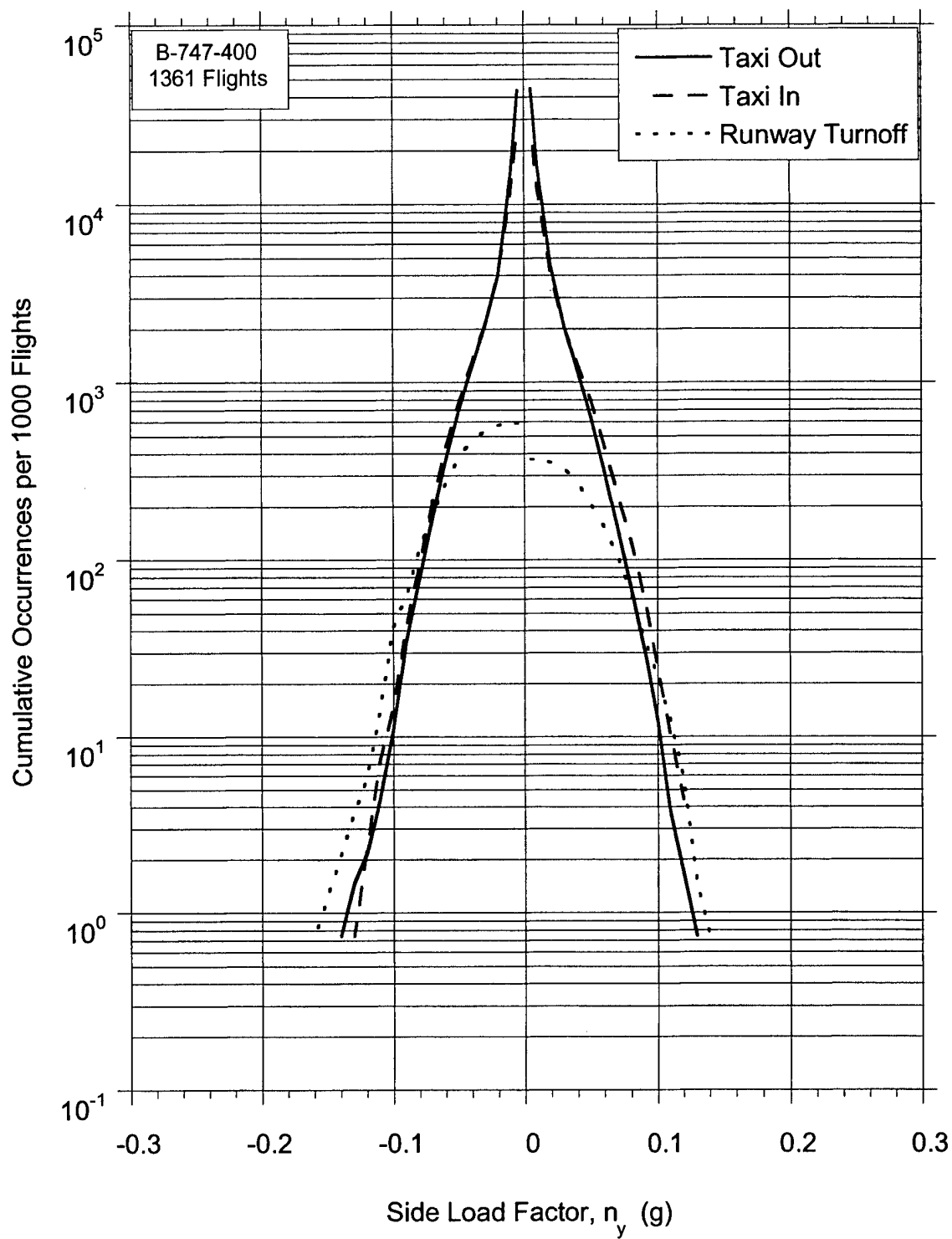FIGURE A-4. CUMULATIVE FREQUENCY OF SIDE LOAD FACTOR DURING TAXI-IN, TAXI-OUT, AND RUNWAY TURNOFF
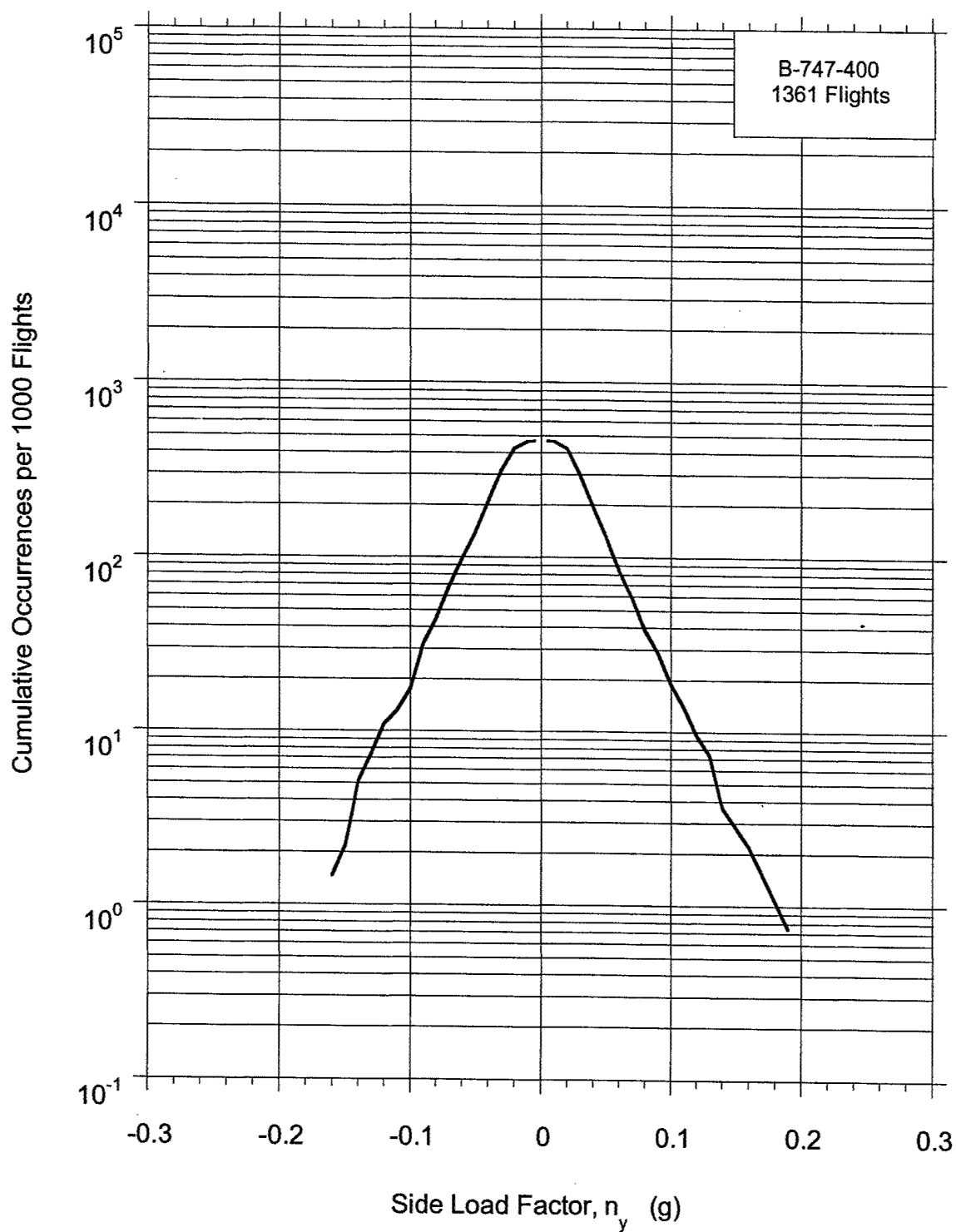
A-4
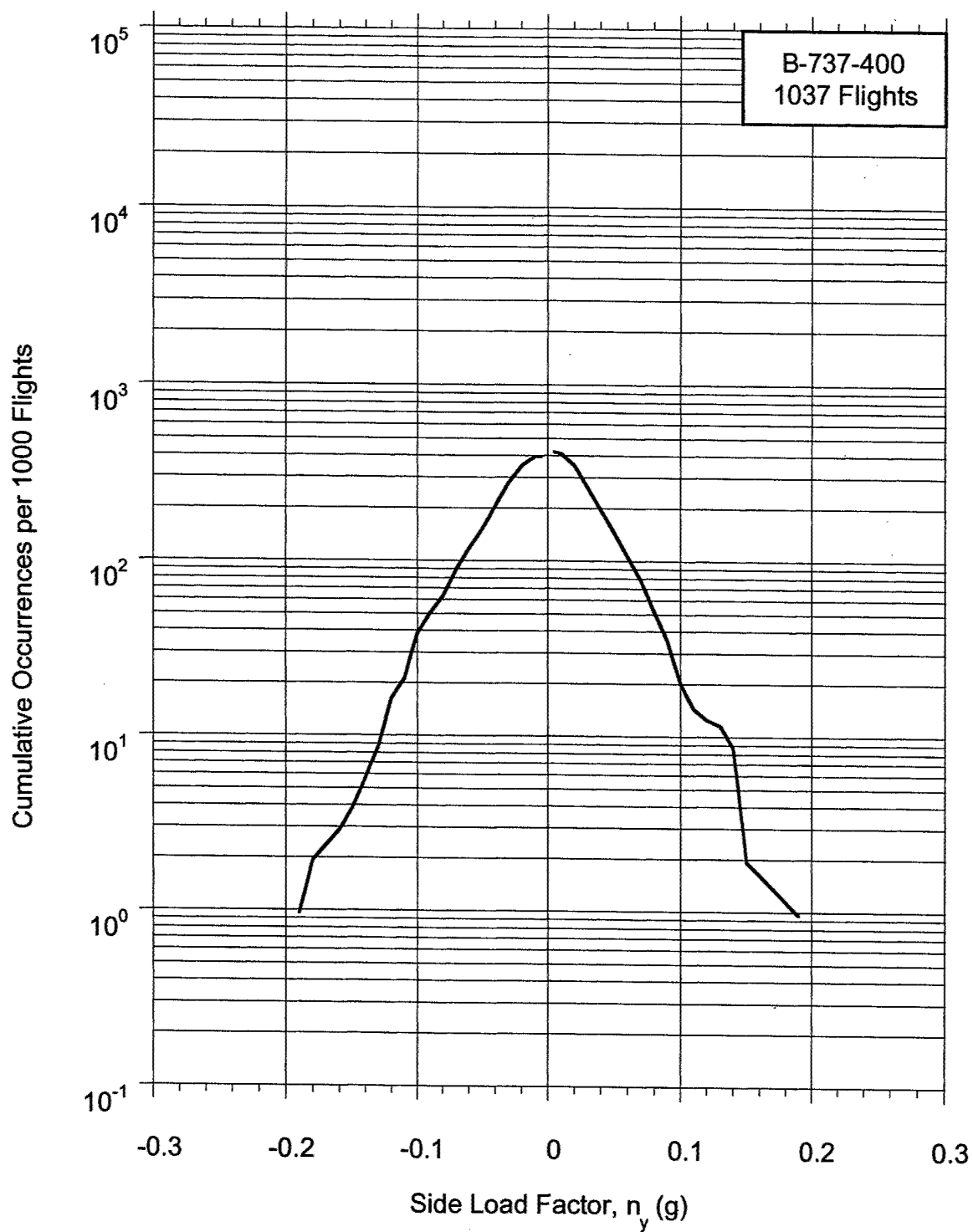
FIGURE A-5. CUMULATIVE FREQUENCY OF MAXIMUM SIDE LOAD FACTOR AT TOUCHDOWN
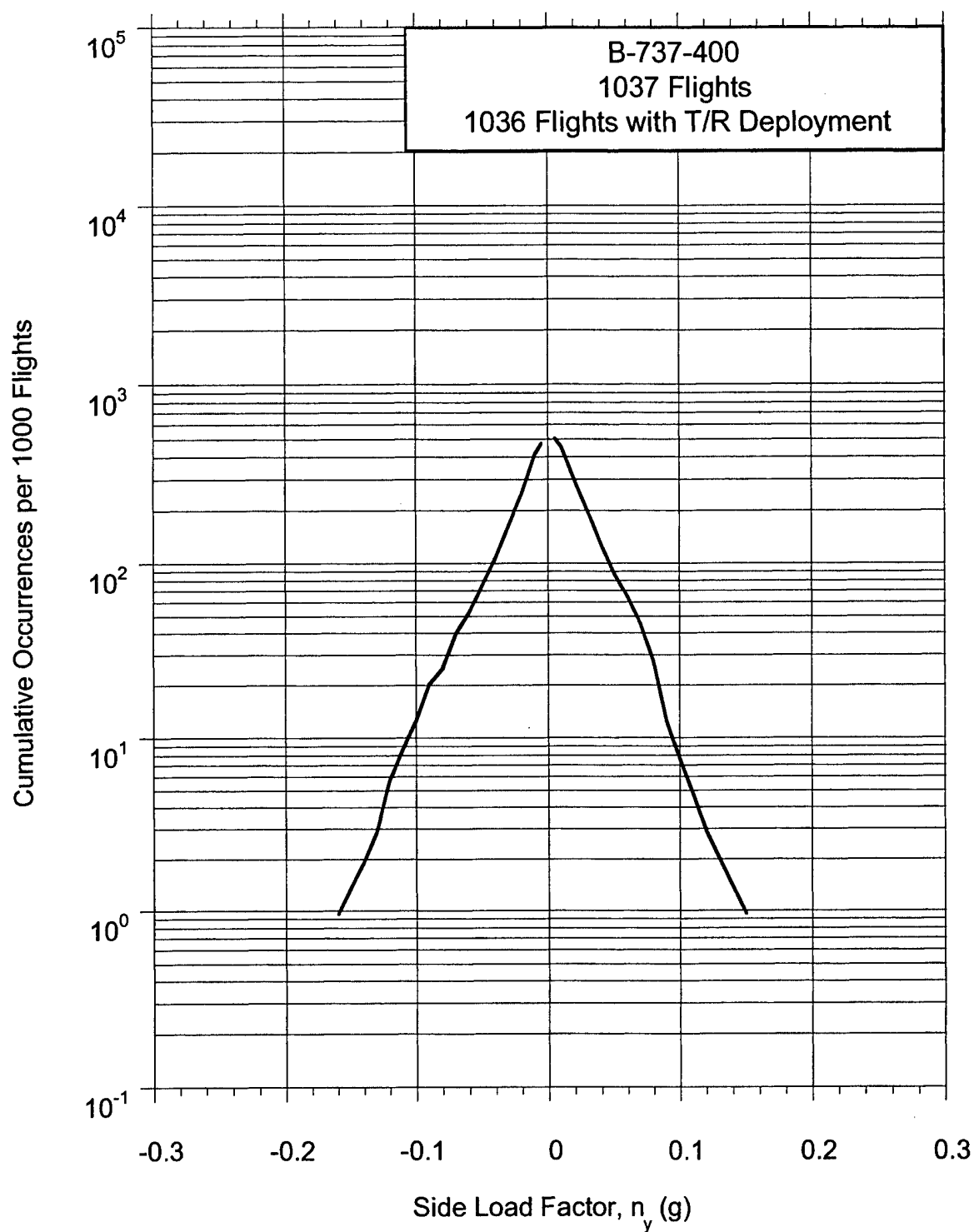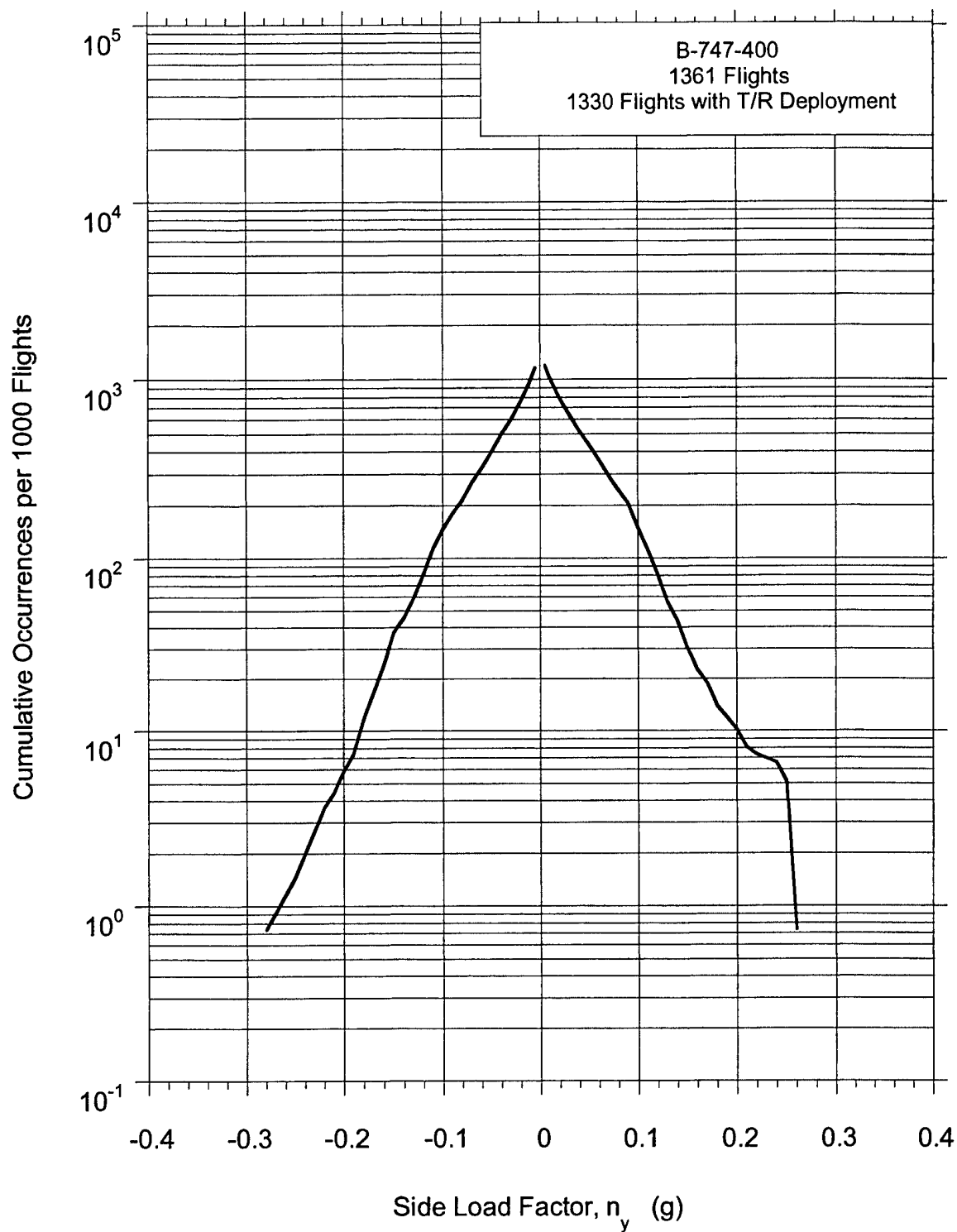
FIGURE A-6. CUMULATIVE FREQUENCY OF SIDE LOAD FACTOR AFTER
TOUCHDOWN AND BEFORE THRUST REVERSER DEPLOYMENT
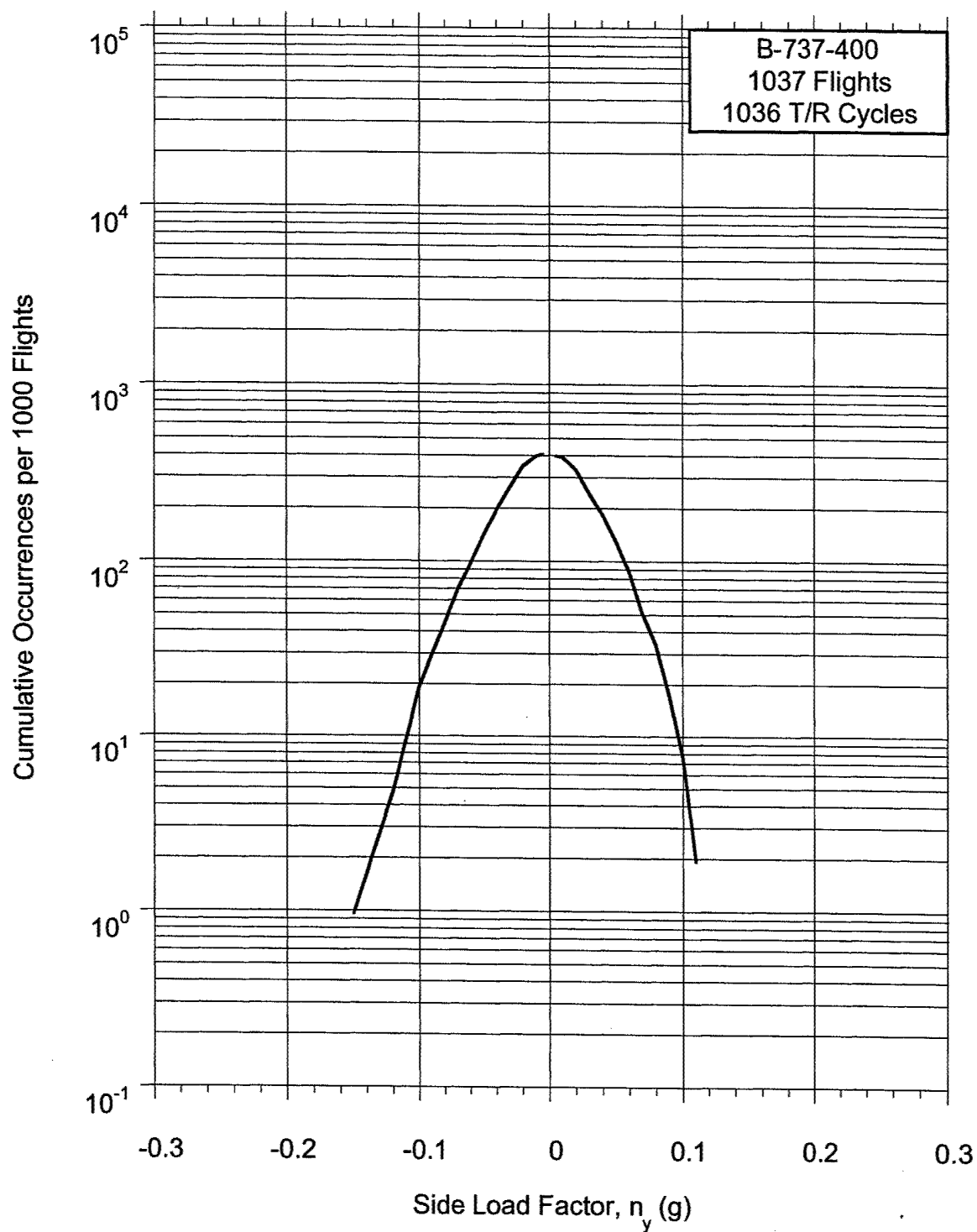
FIGURE A-7. CUMULATIVE FREQUENCY OF MAXIMUM SIDE LOAD FACTOR AT
THRUST REVERSER DEPLOYMENT
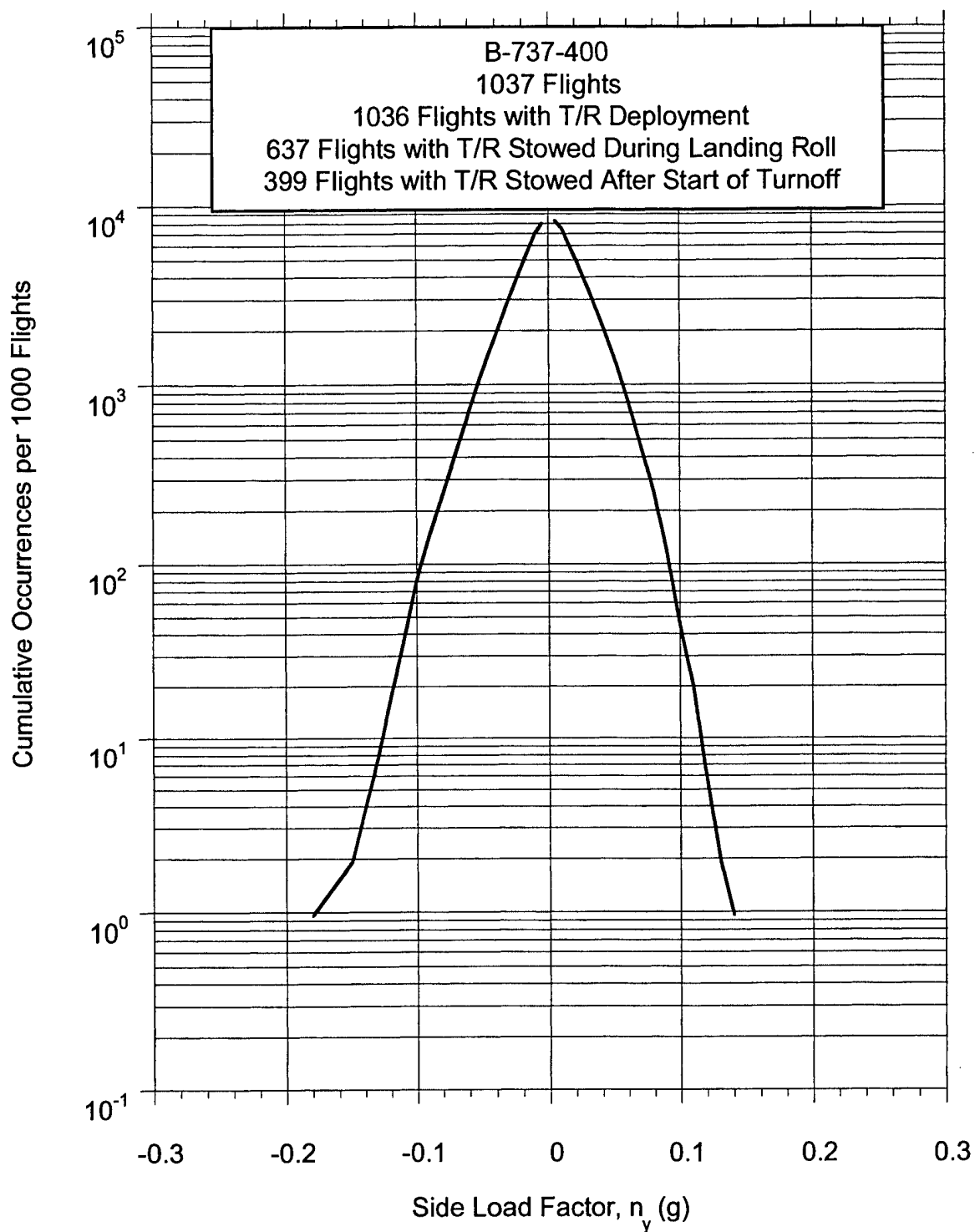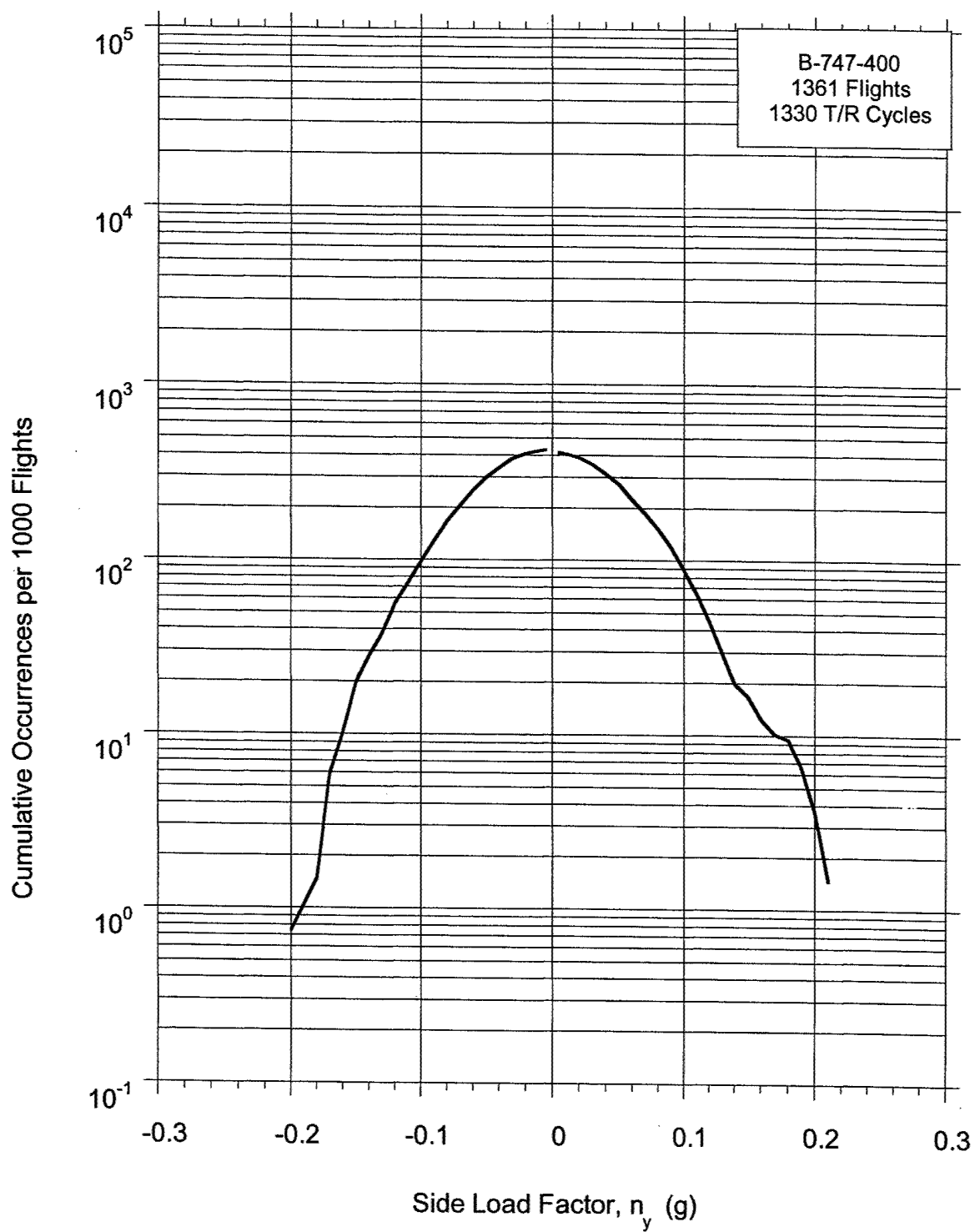
FIGURE A-8. CUMULATIVE FREQUENCY OF SIDE LOAD FACTOR WHILE
THRUST REVERSER IS DEPLOYED
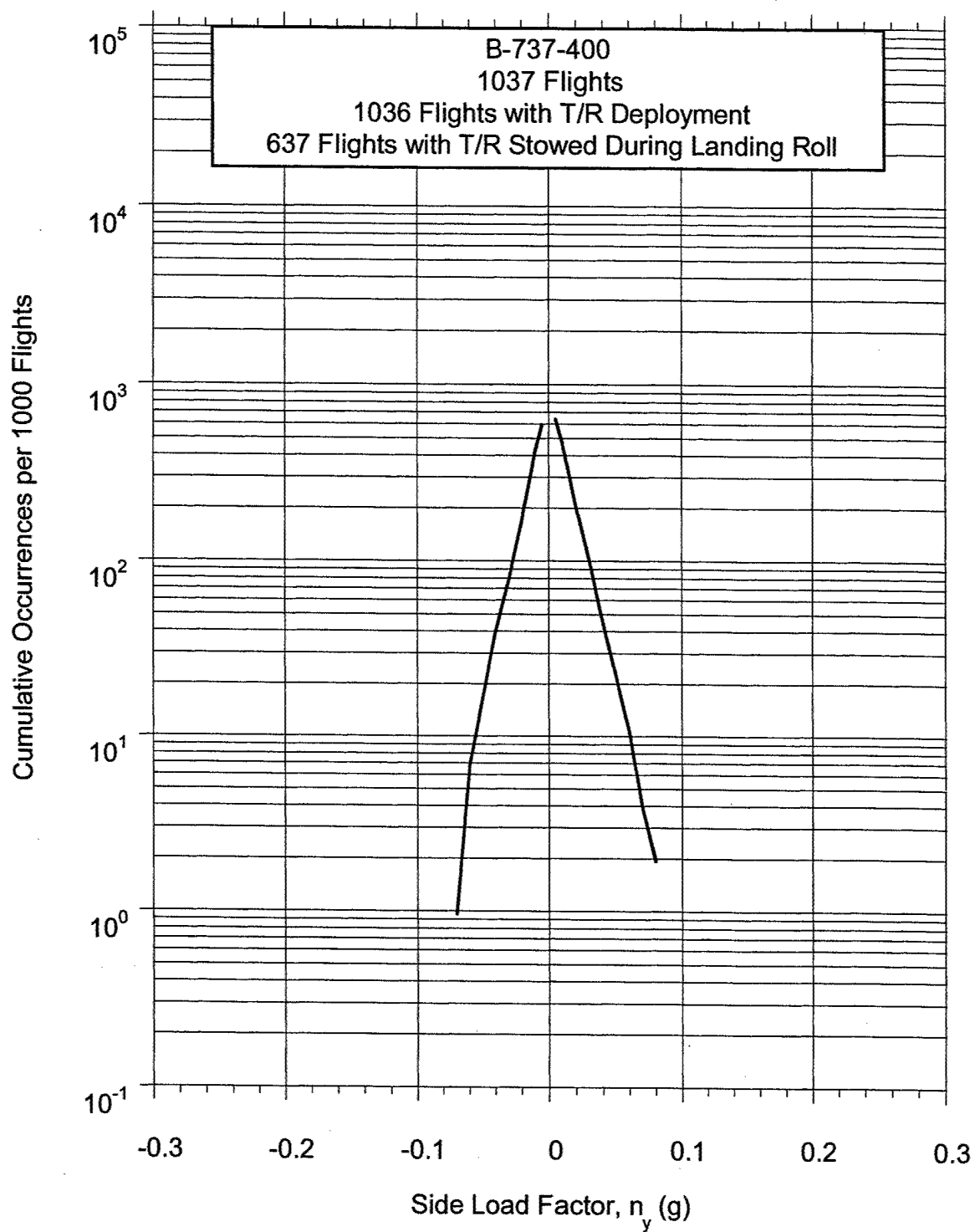
FIGURE A-9. CUMULATIVE FREQUENCY OF SIDE LOAD FACTOR AFTER
THRUST REVERSER STOWED DURING LANDING ROLL
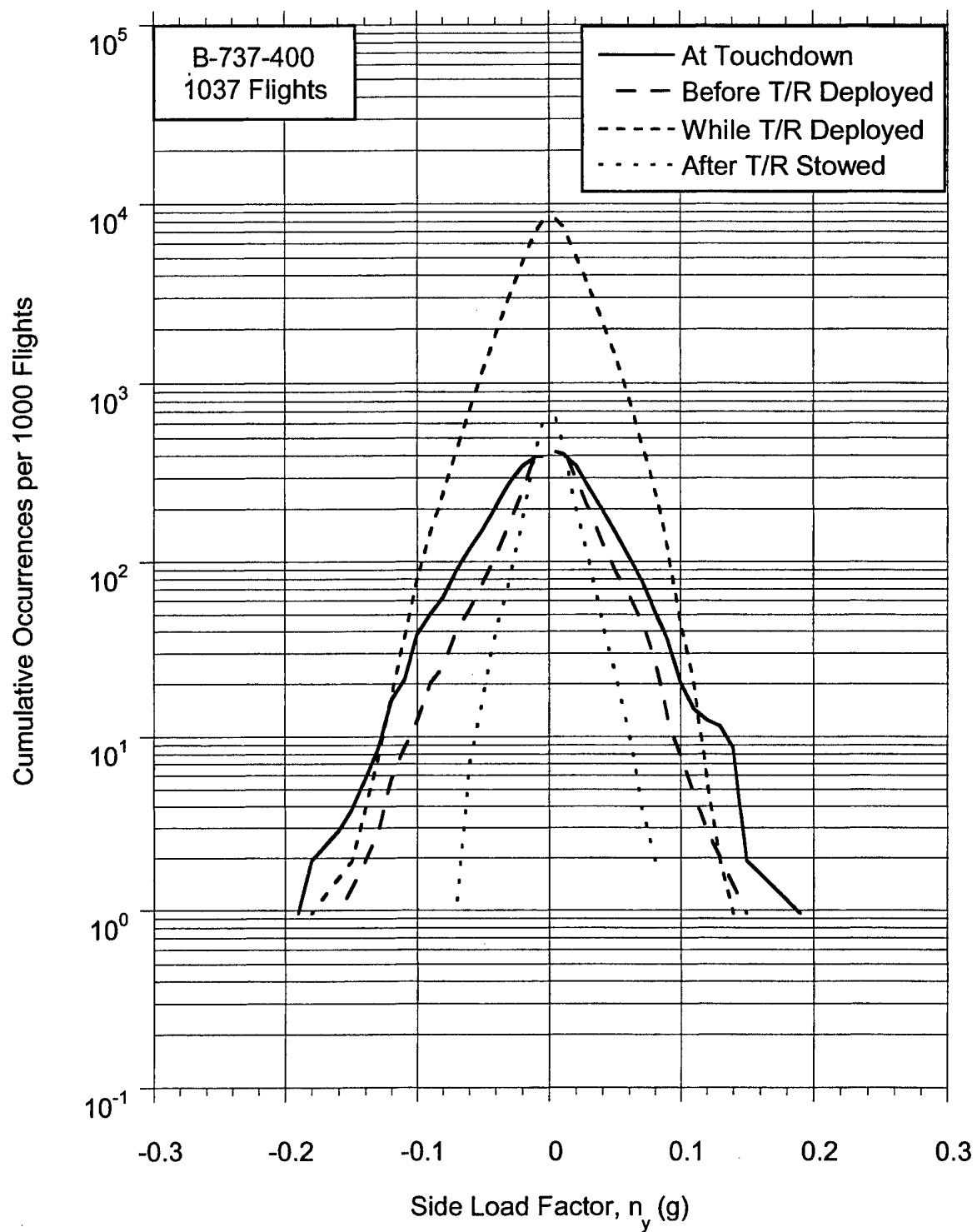
FIGURE A-10. CUMULATIVE FREQUENCY OF SIDE LOAD FACTOR AT
TOUCHDOWN AND DURING LANDING ROLL
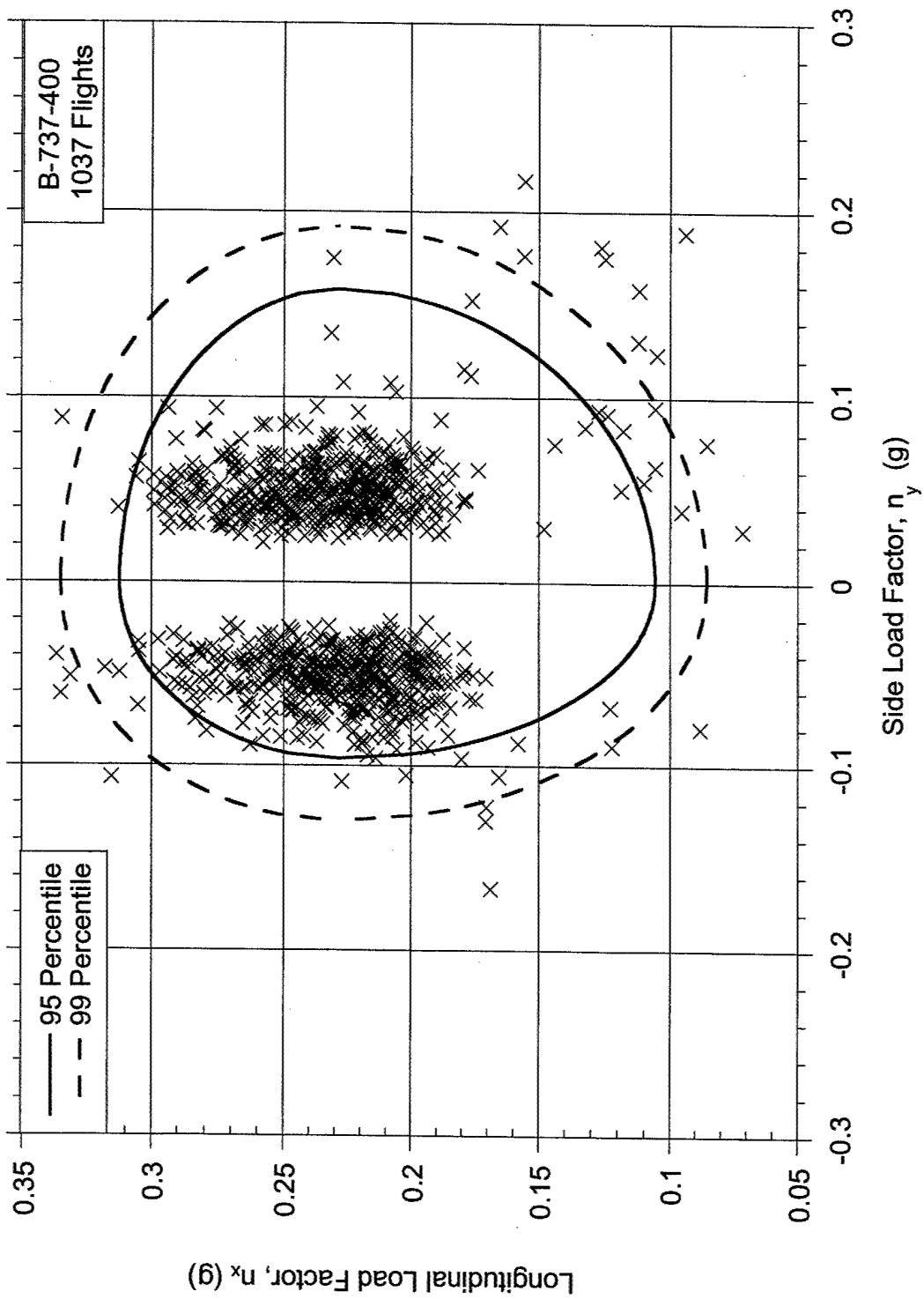
FIGURE A-11. COINCIDENT LONGITUDINAL LOAD FACTOR AT MAXIMUM SIDE LOAD FACTOR DURING TAKEOFF ROLL
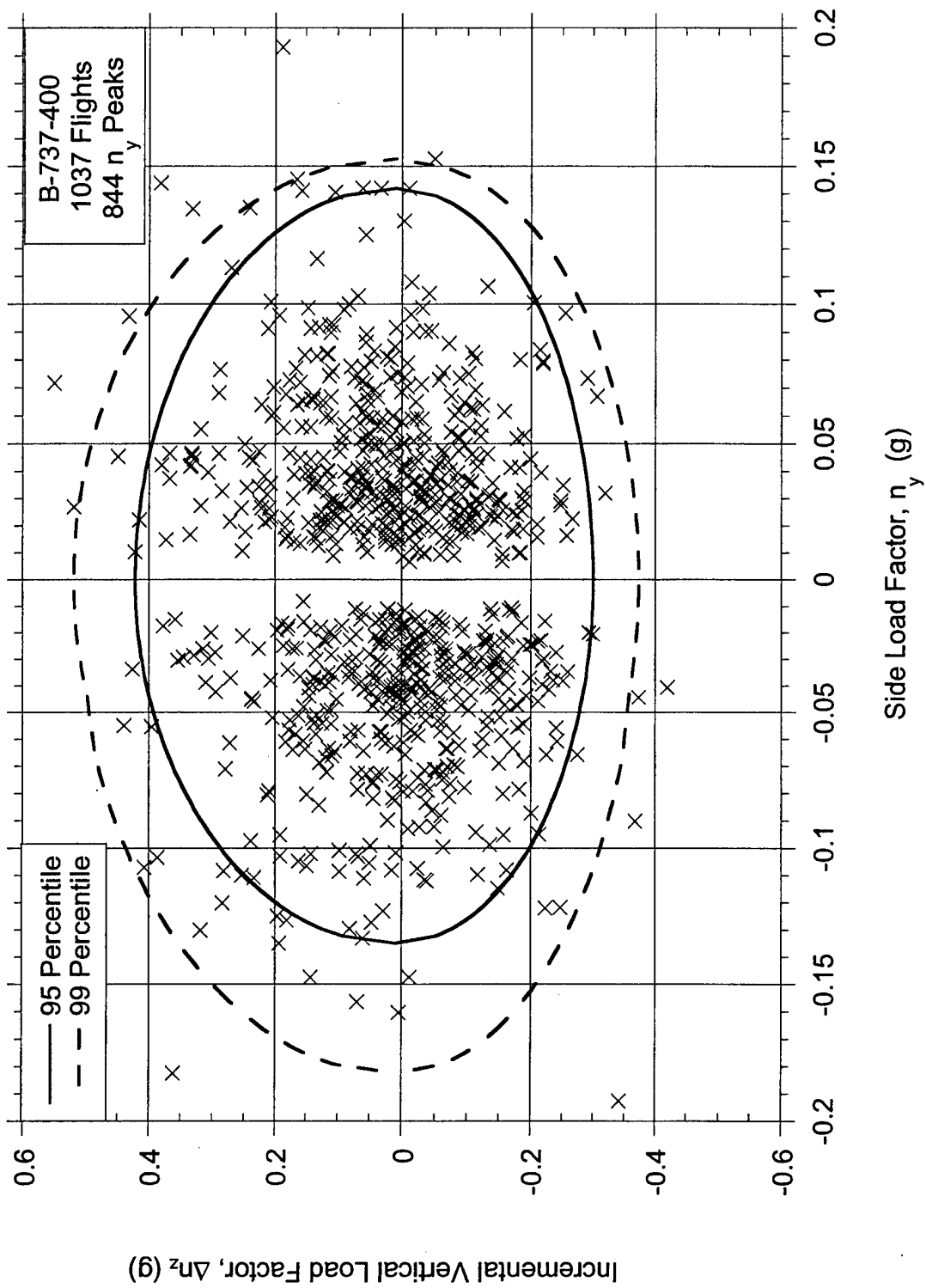
FIGURE A-12. COINCIDENT INCREMENTAL VERTICAL LOAD FACTOR AT MAXIMUM SIDE LOAD FACTOR AT TOUCHDOWN
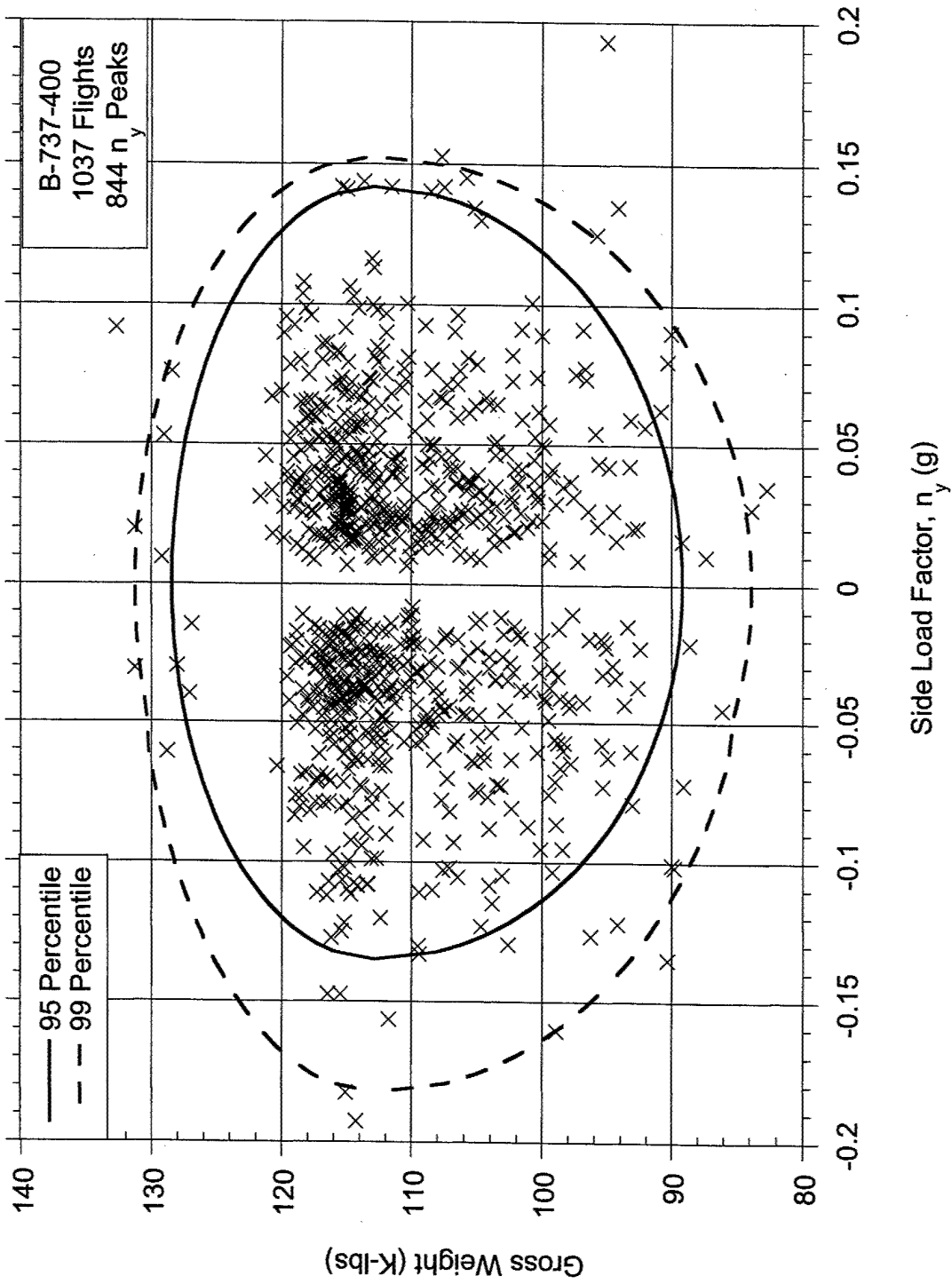
FIGURE A-13. COINCIDENT GROSS WEIGHT AT MAXIMUM SIDE LOAD FACTOR AT TOUCHDOWN
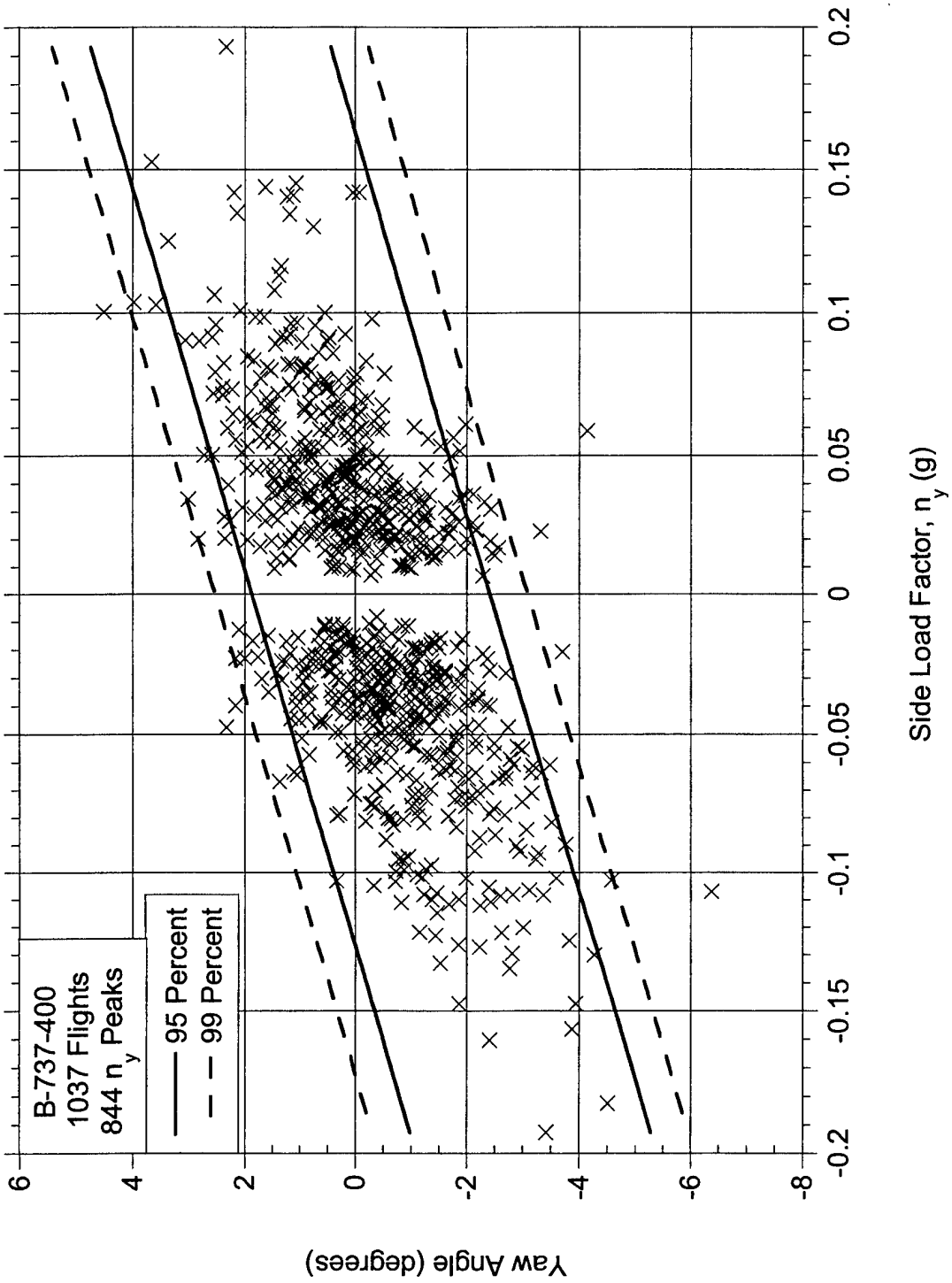
FIGURE A-14. YAW ANGLE AND MAXIMUM SIDE LOAD FACTOR AT TOUCHDOWN
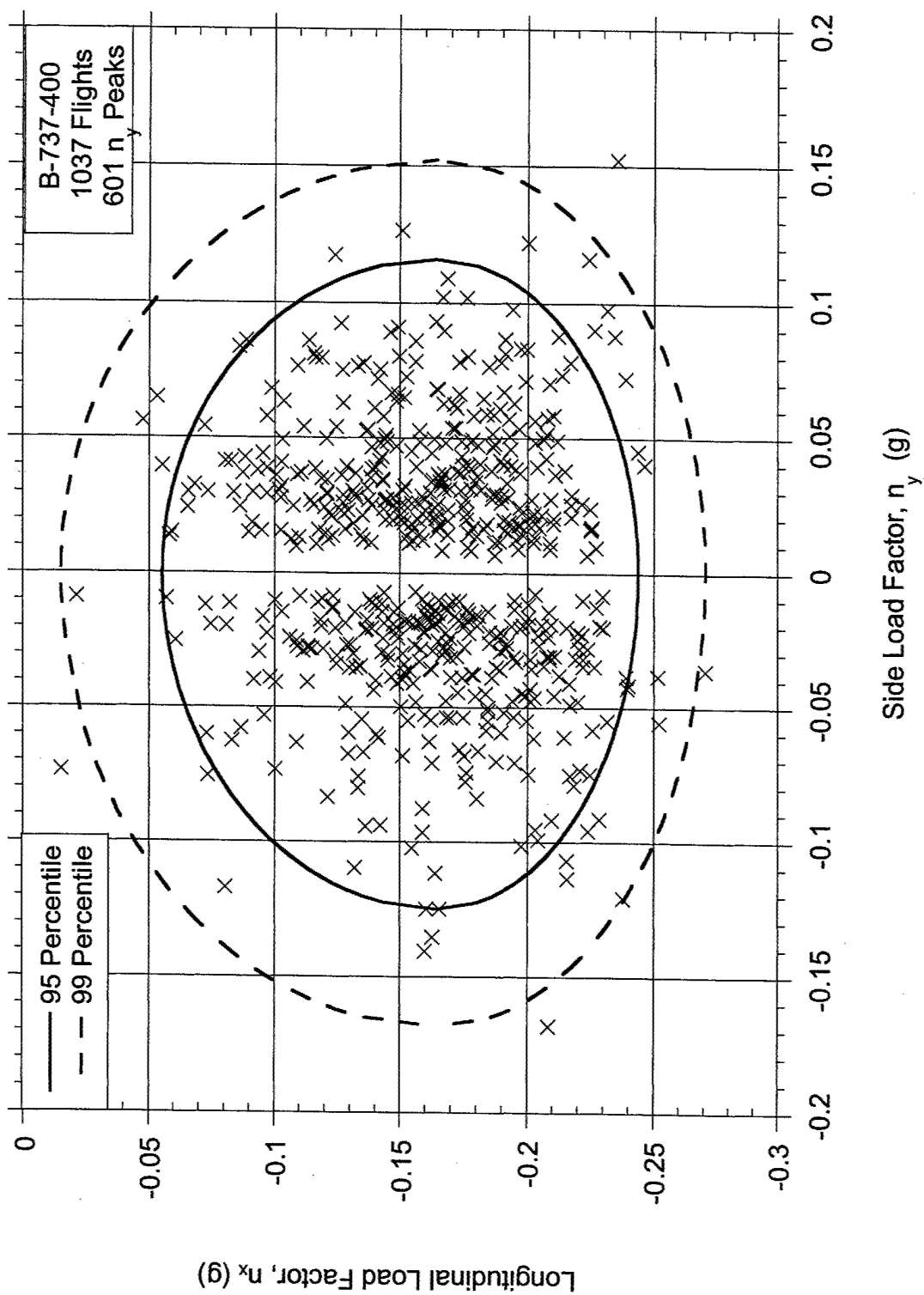
FIGURE A-15. COINCIDENT LONGITUDINAL LOAD FACTOR AT MAXIMUM SIDE LOAD FACTOR BEFORE THRUST REVERSER DEPLOYMENT

A-15
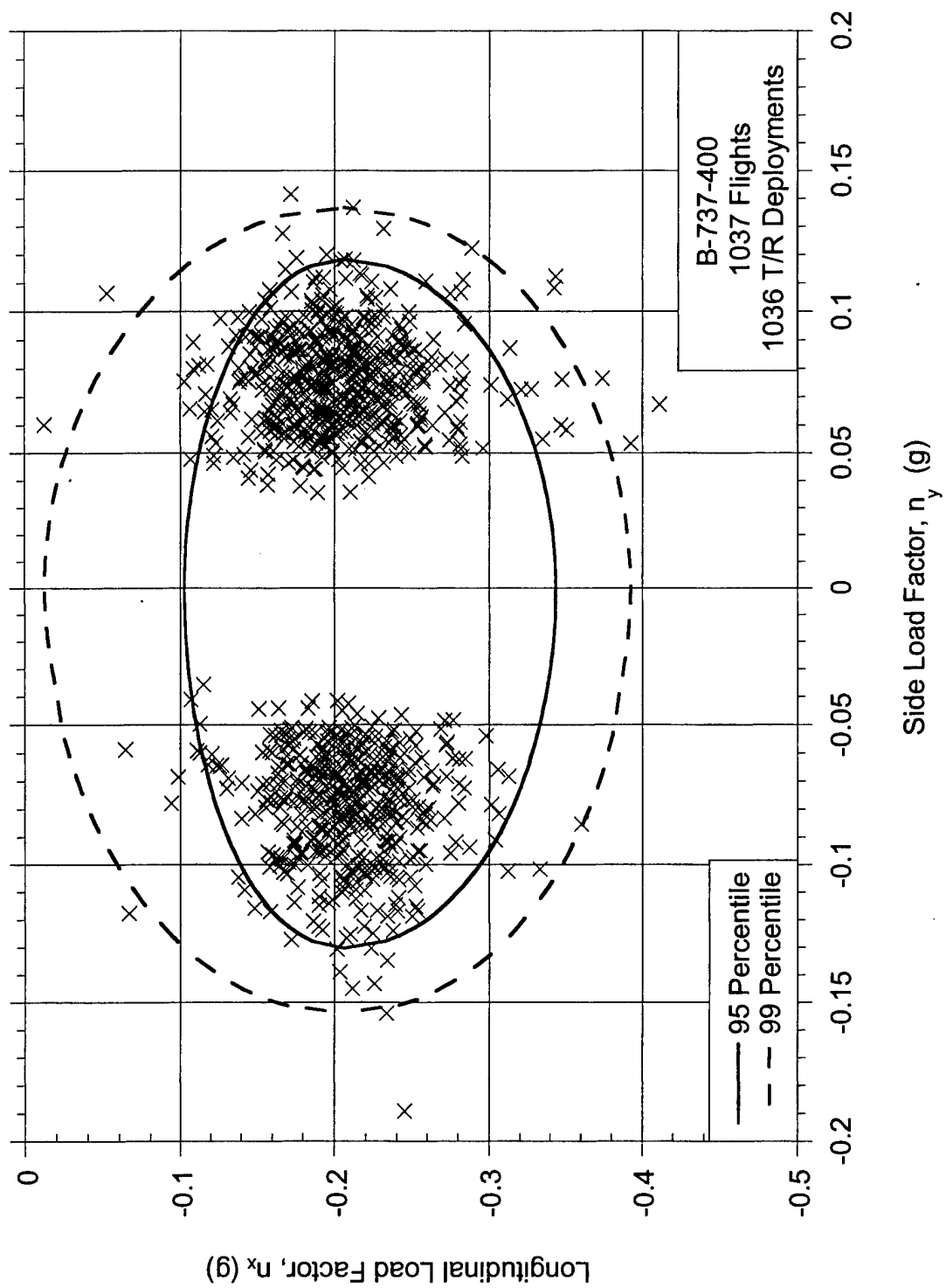
FIGURE A-16. COINCIDENT LONGITUDINAL LOAD FACTOR AT MAXIMUM SIDE LOAD FACTOR WHILE THRUST REVERSER IS DEPLOYED
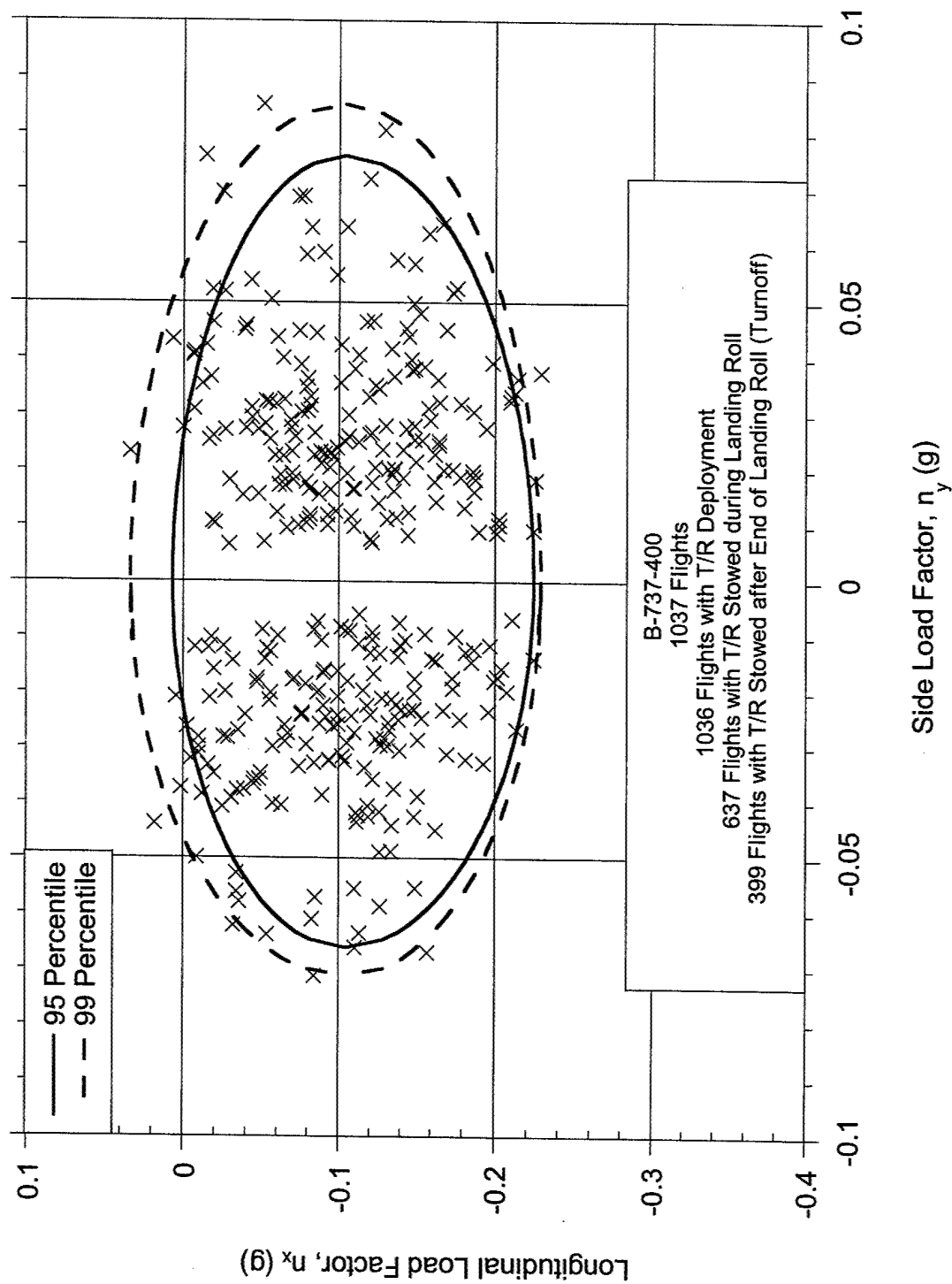
FIGURE A-17. COINCIDENT LONGITUDINAL LOAD FACTOR AT MAXIMUM SIDE LOAD FACTOR AFTER THRUST REVERSER STOWAGE DURING LANDING ROLL
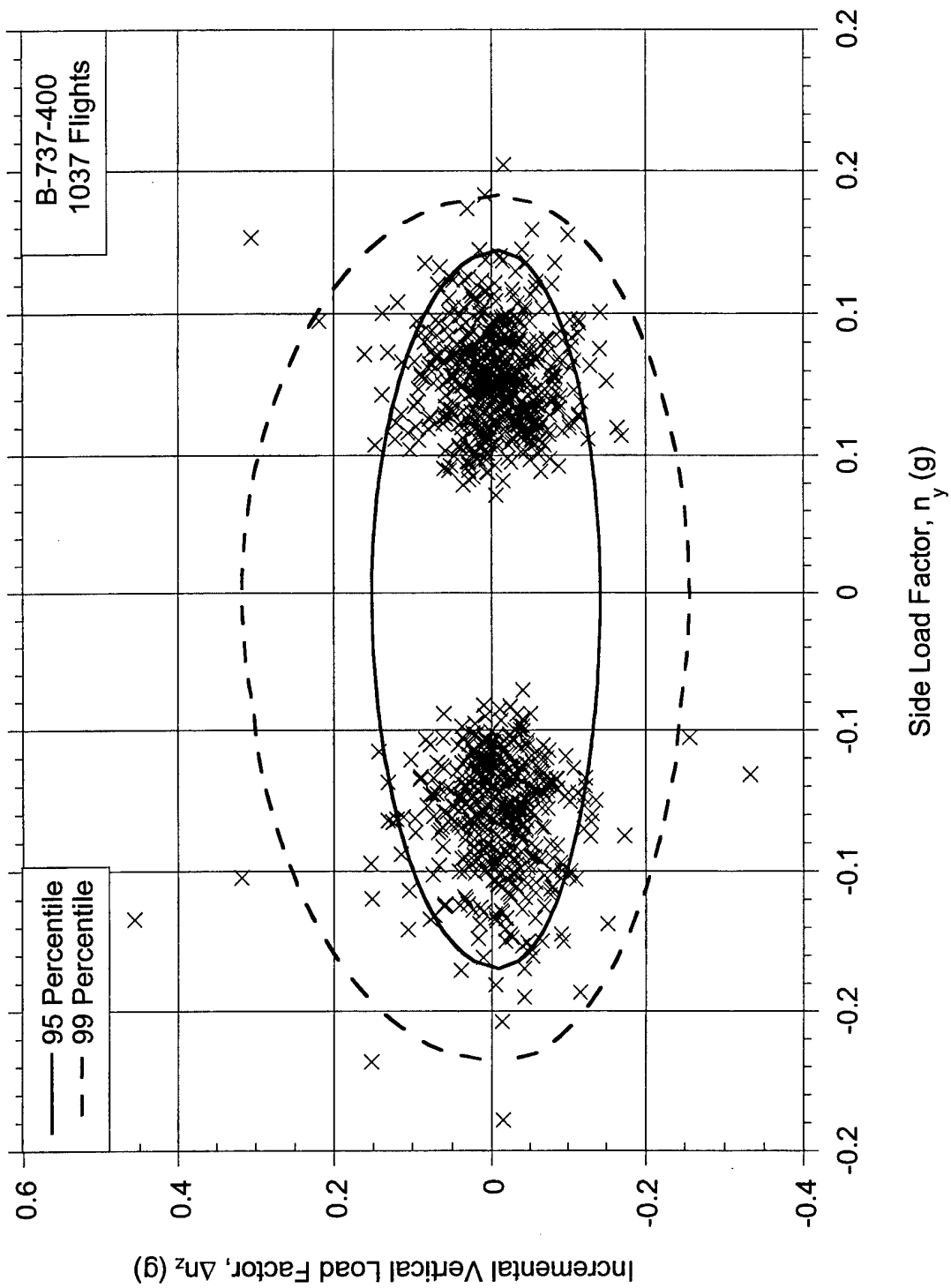
FIGURE A-18. COINCIDENT INCREMENTAL VERTICAL LOAD FACTOR AT MAXIMUM SIDE LOAD FACTOR DURING LANDING ROLL

A-18
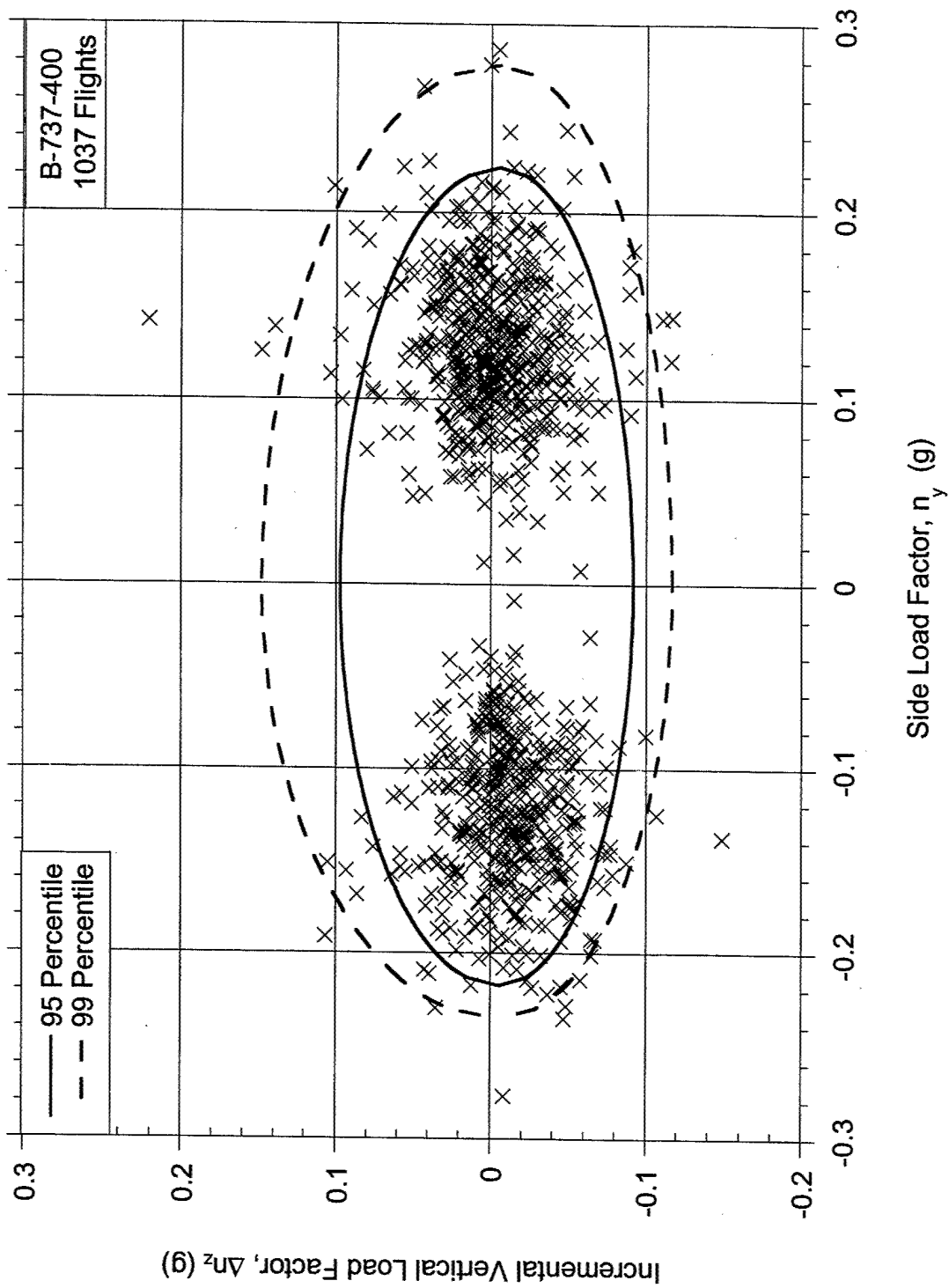
FIGURE A-19. COINCIDENT INCREMENTAL VERTICAL LOAD FACTOR AT MAXIMUM SIDE LOAD FACTOR DURING RUNWAY TURNOFF AFTER LANDING
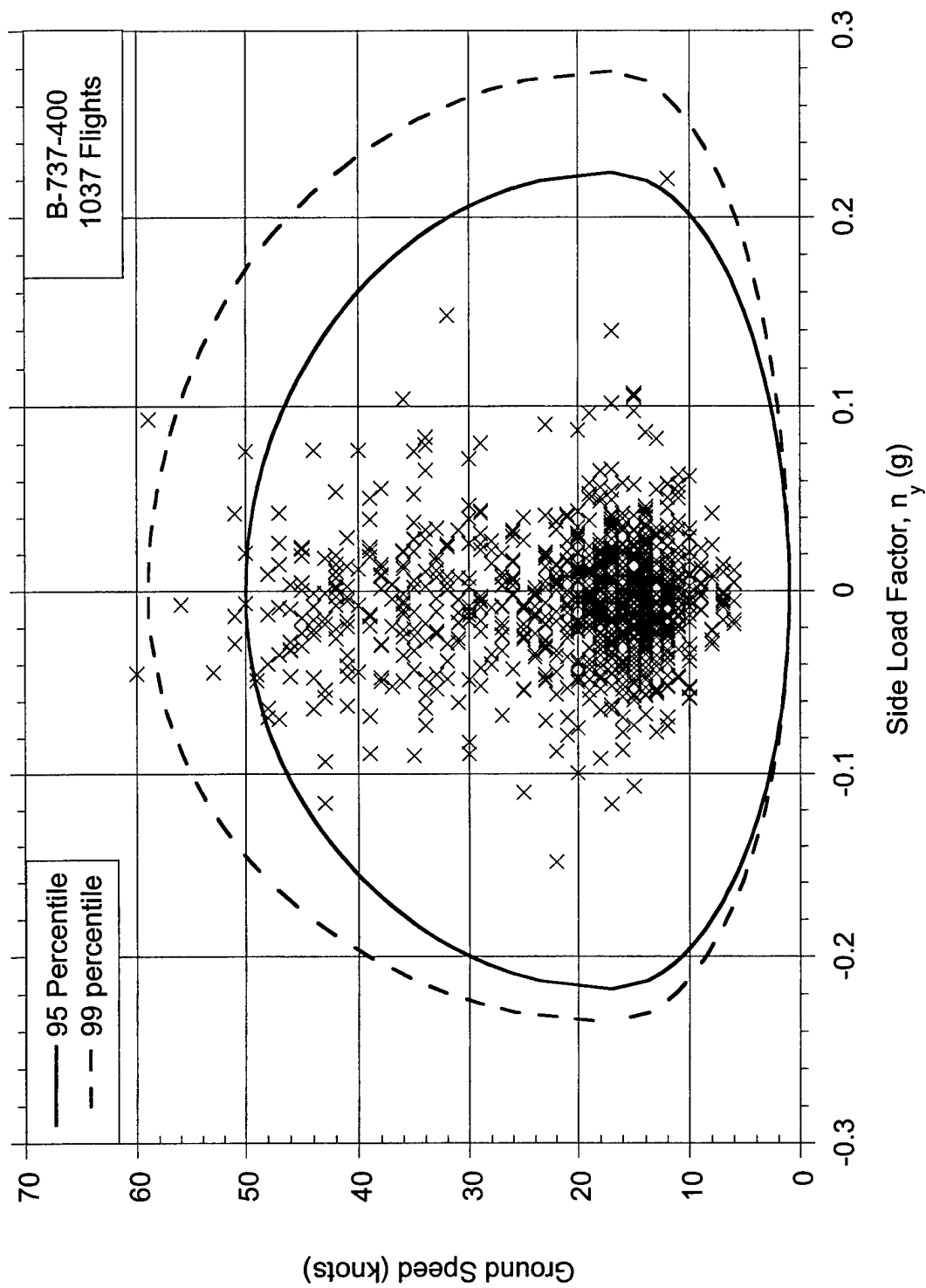
FIGURE A-20. COINCIDENT GROUND SPEED AT MAXIMUM SIDE LOAD FACTOR DURING RUNWAY TURNOFF AFTER LANDING
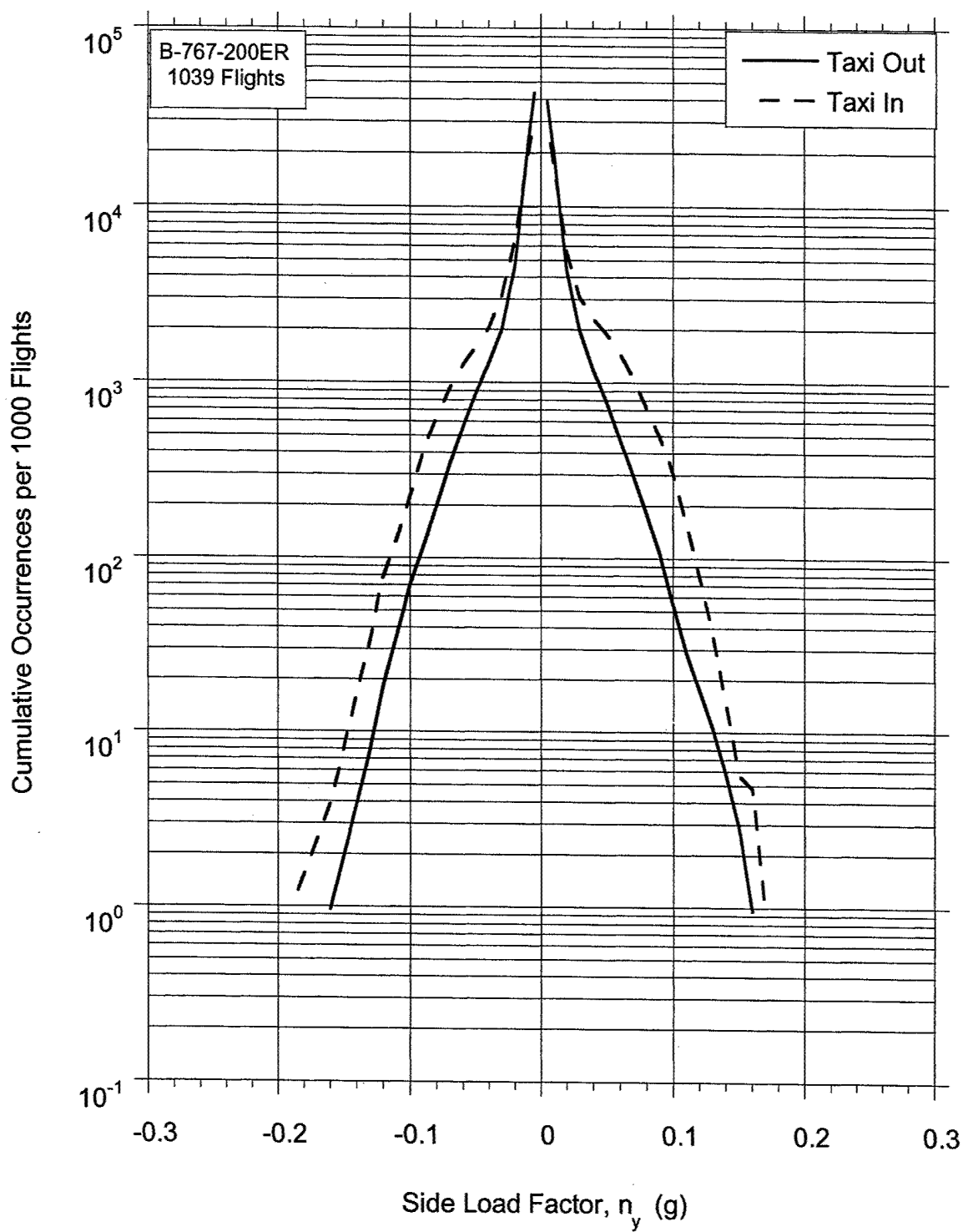
FIGURE B-1. CUMULATIVE FREQUENCY OF SIDE LOAD FACTOR DURING TAXI
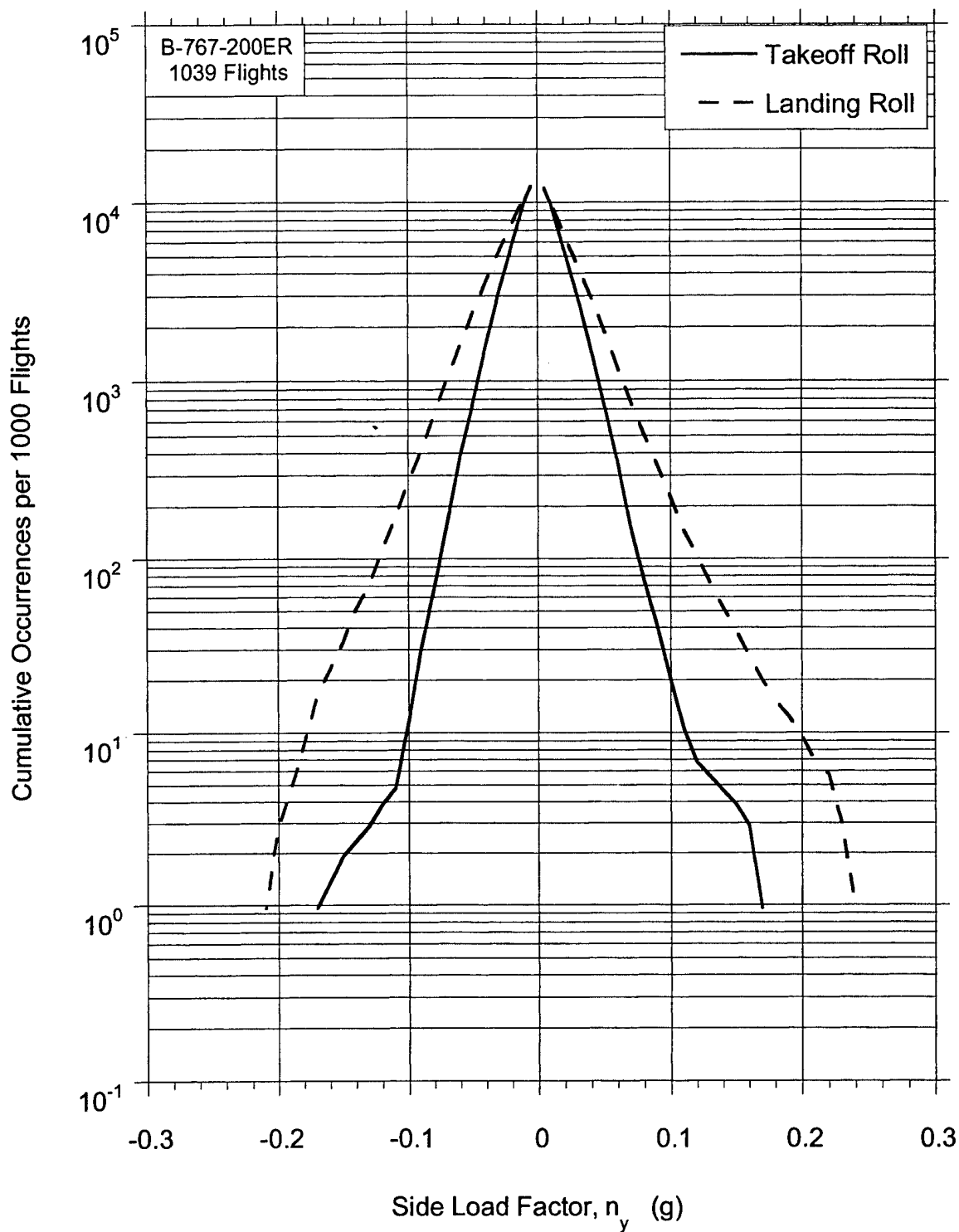
FIGURE B-2. CUMULATIVE FREQUENCY OF SIDE LOAD FACTOR DURING
TAKEOFF AND LANDING ROLL
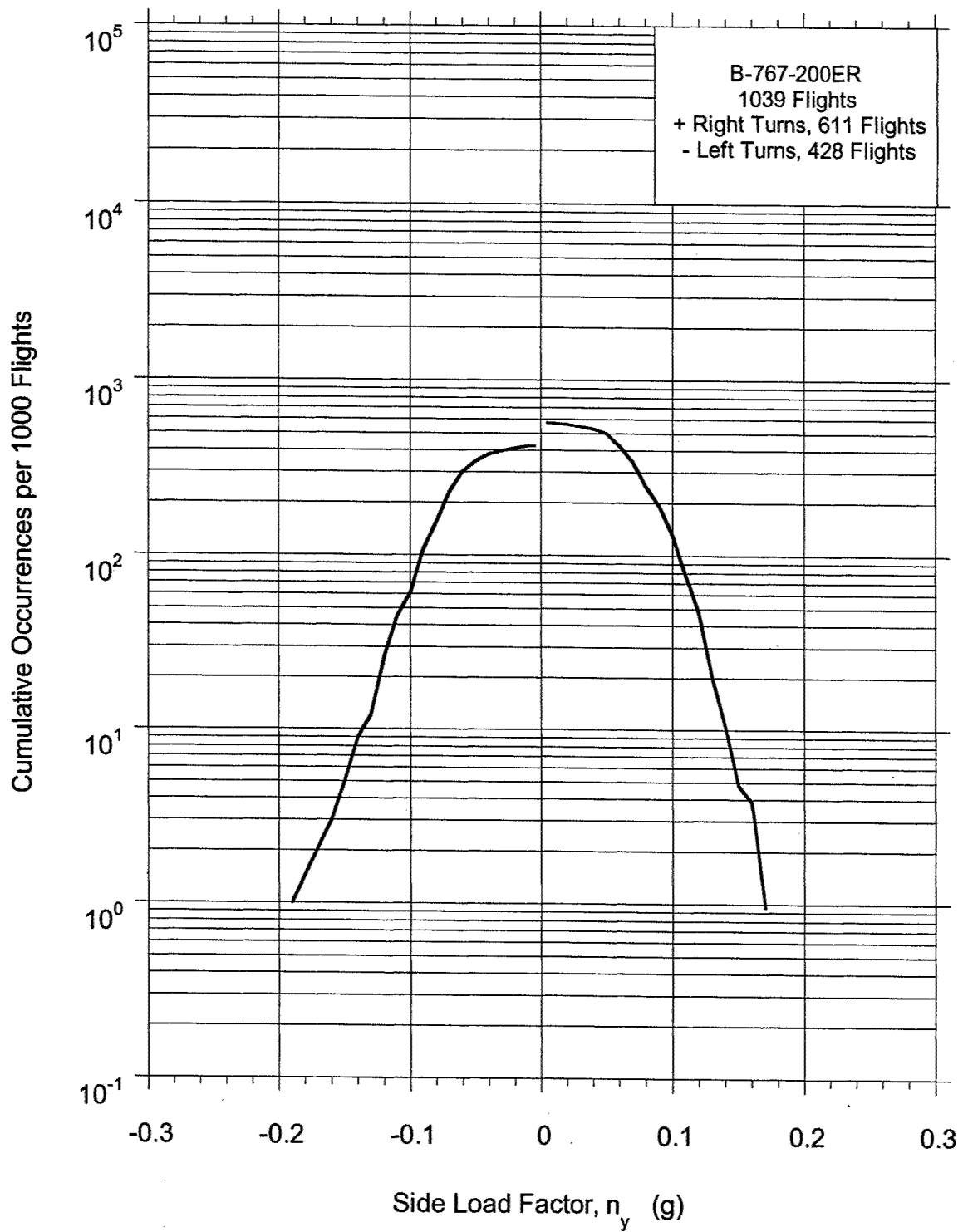
FIGURE B-3. CUMULATIVE FREQUENCY OF MAXIMUM SIDE LOAD FACTOR
DURING RUNWAY TURNOFF
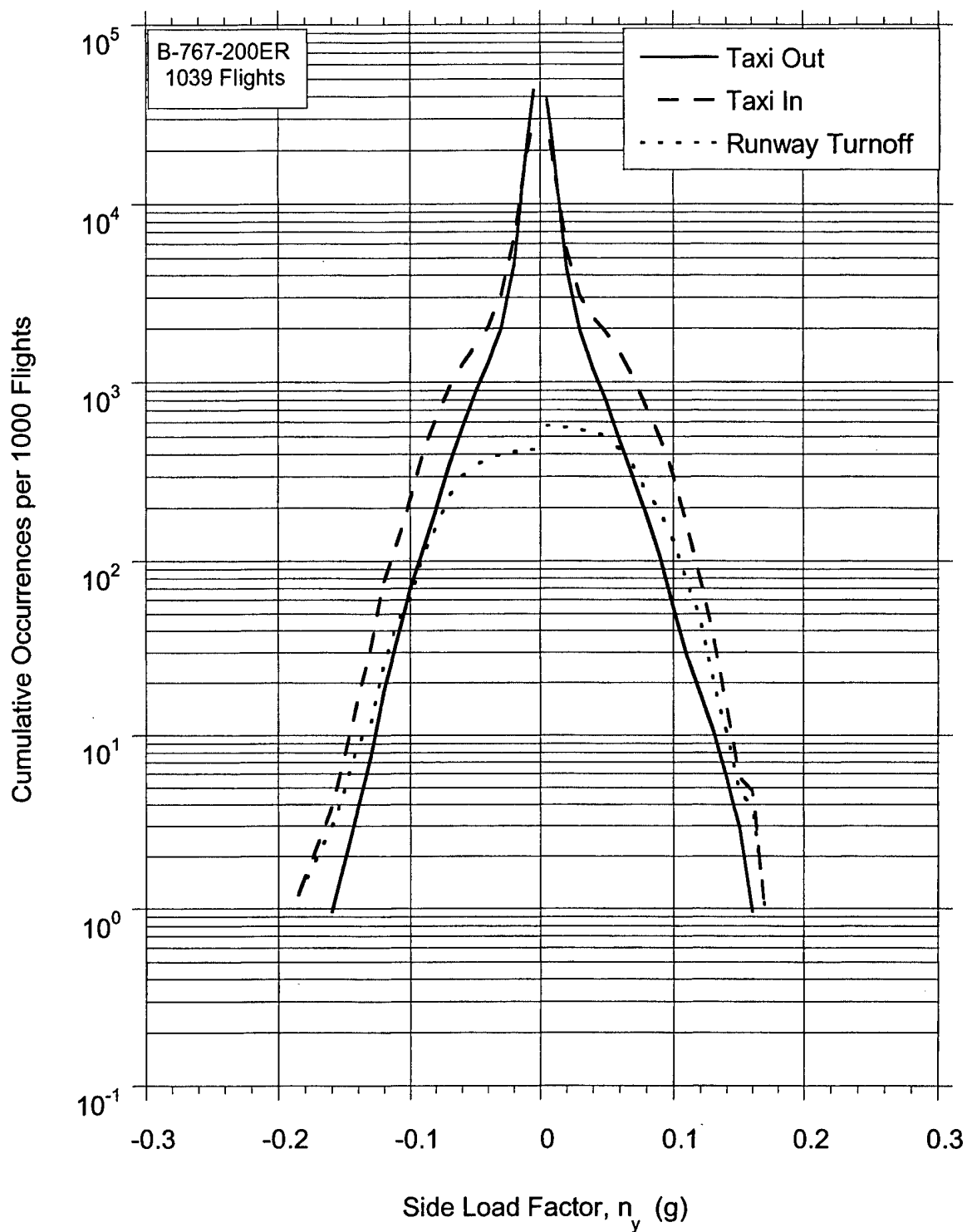
FIGURE B-4. CUMULATIVE FREQUENCY OF SIDE LOAD FACTOR DURING TAXI-IN, TAXI-OUT, AND RUNWAY TURNOFF
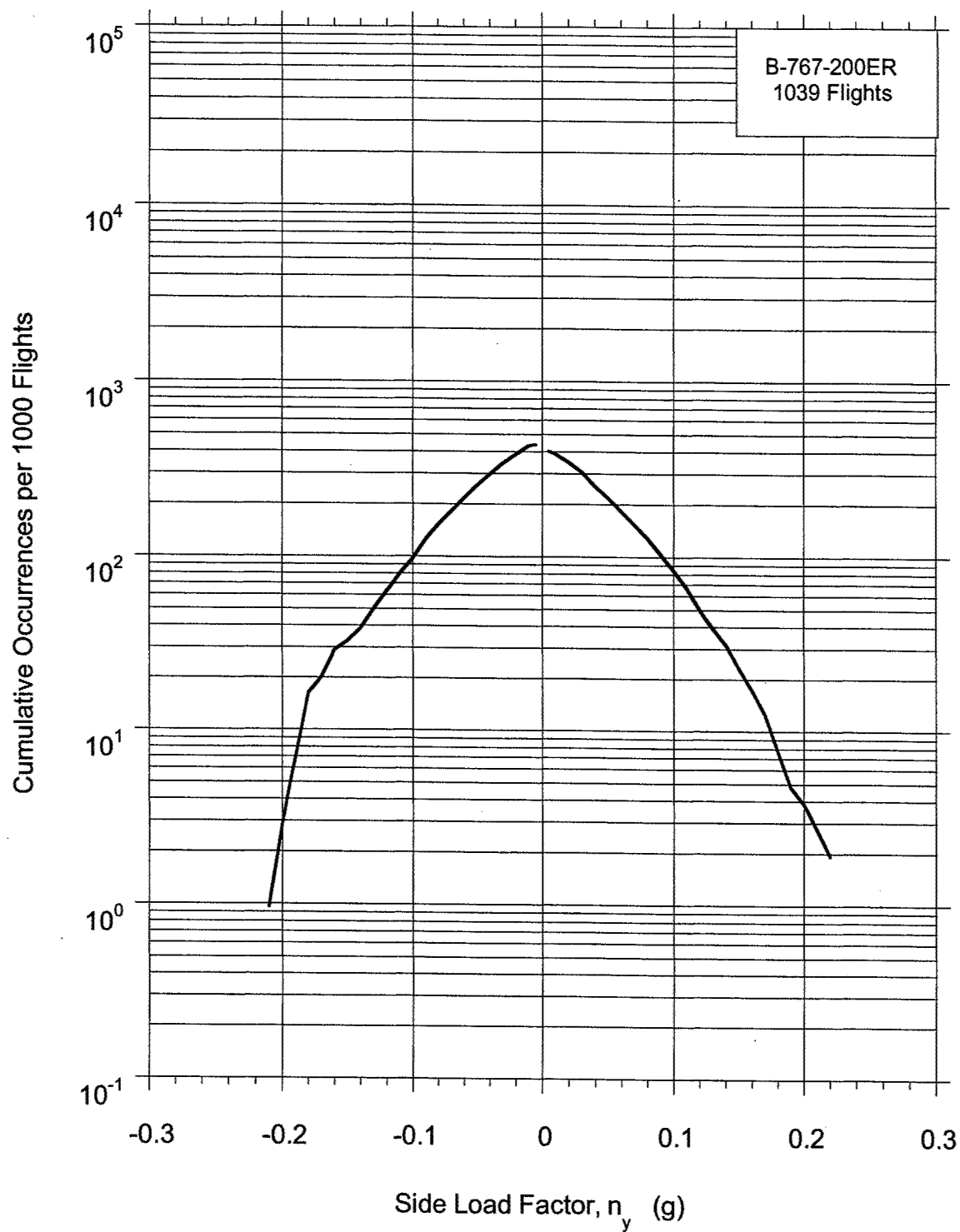
FIGURE B-5. CUMULATIVE FREQUENCY OF MAXIMUM SIDE LOAD FACTOR AT TOUCHDOWN
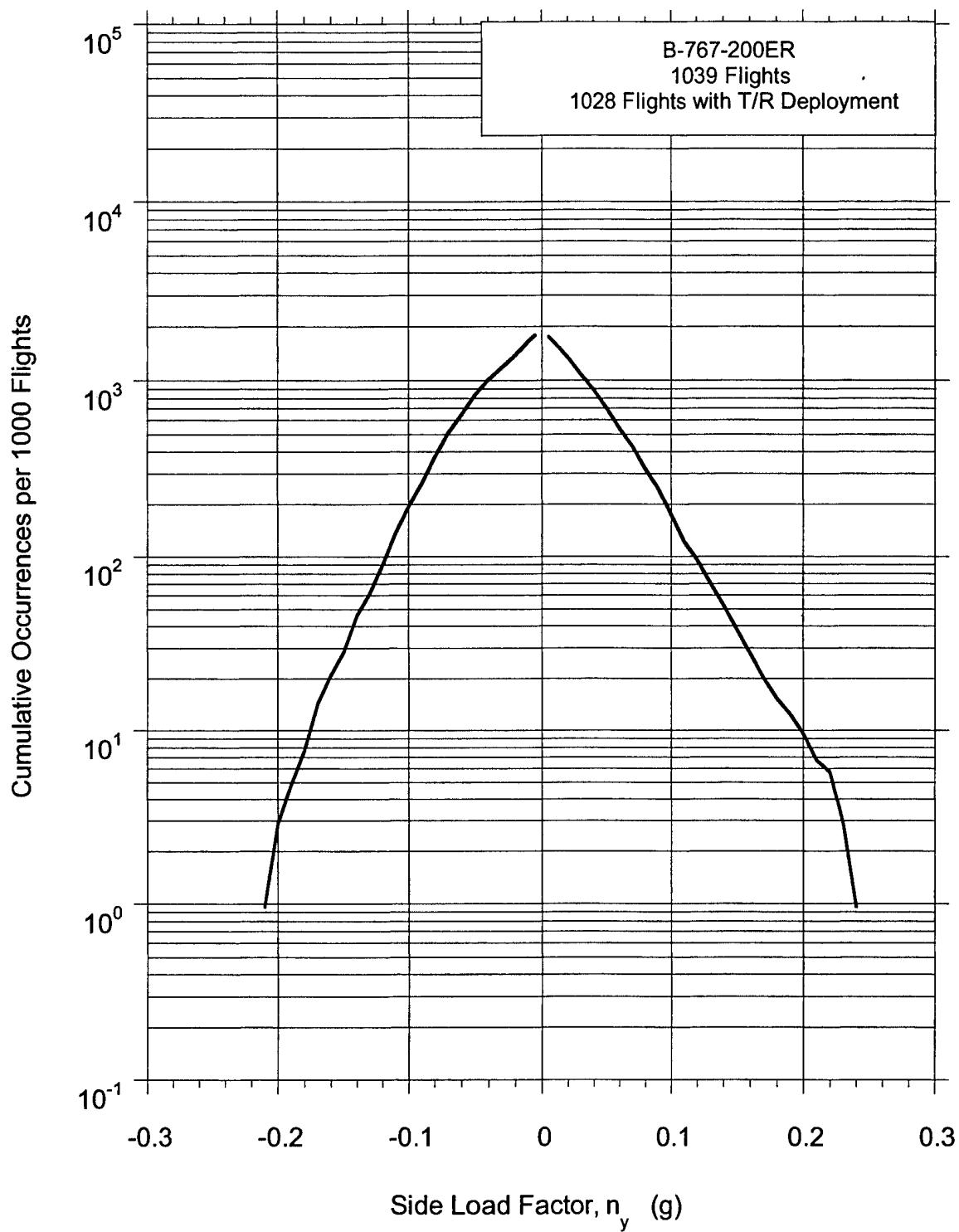
FIGURE B-6. CUMULATIVE FREQUENCY OF SIDE LOAD FACTOR AFTER
TOUCHDOWN AND BEFORE THRUST REVERSER DEPLOYMENT
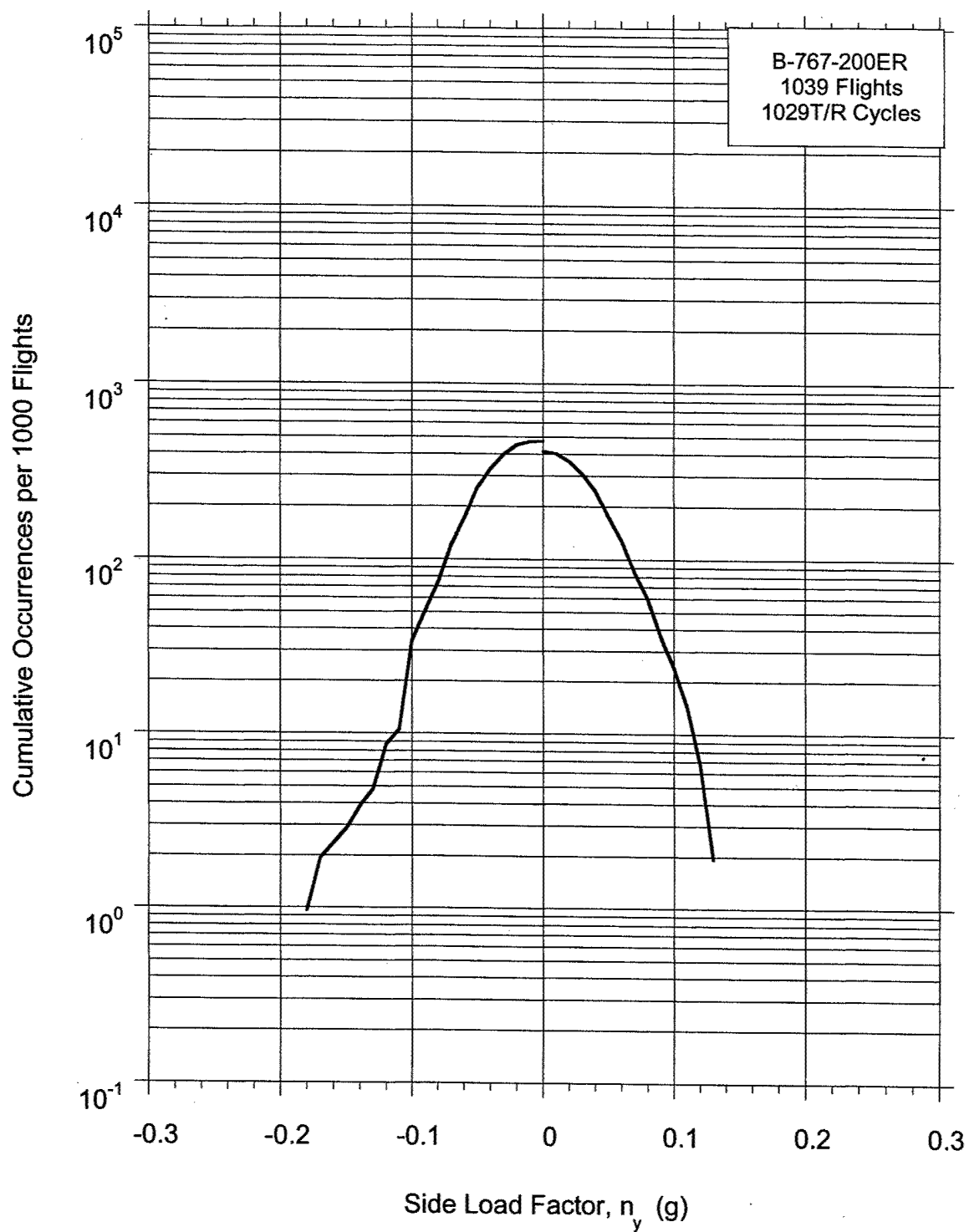
FIGURE B-7. CUMULATIVE FREQUENCY OF MAXIMUM SIDE LOAD FACTOR AT THRUST REVERSER DEPLOYMENT
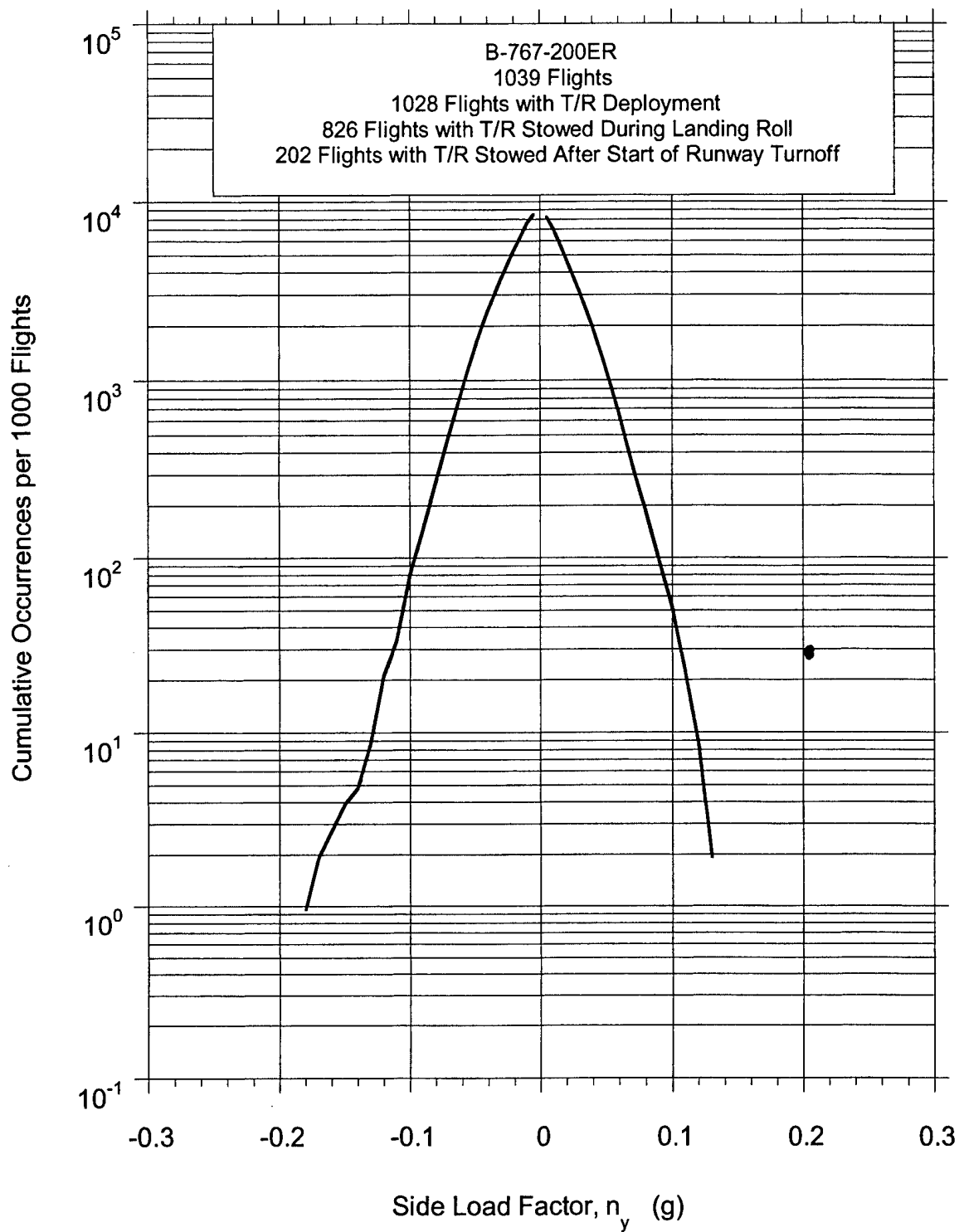
FIGURE B-8. CUMULATIVE FREQUENCY OF SIDE LOAD FACTOR WHILE
THRUST REVERSER IS DEPLOYED
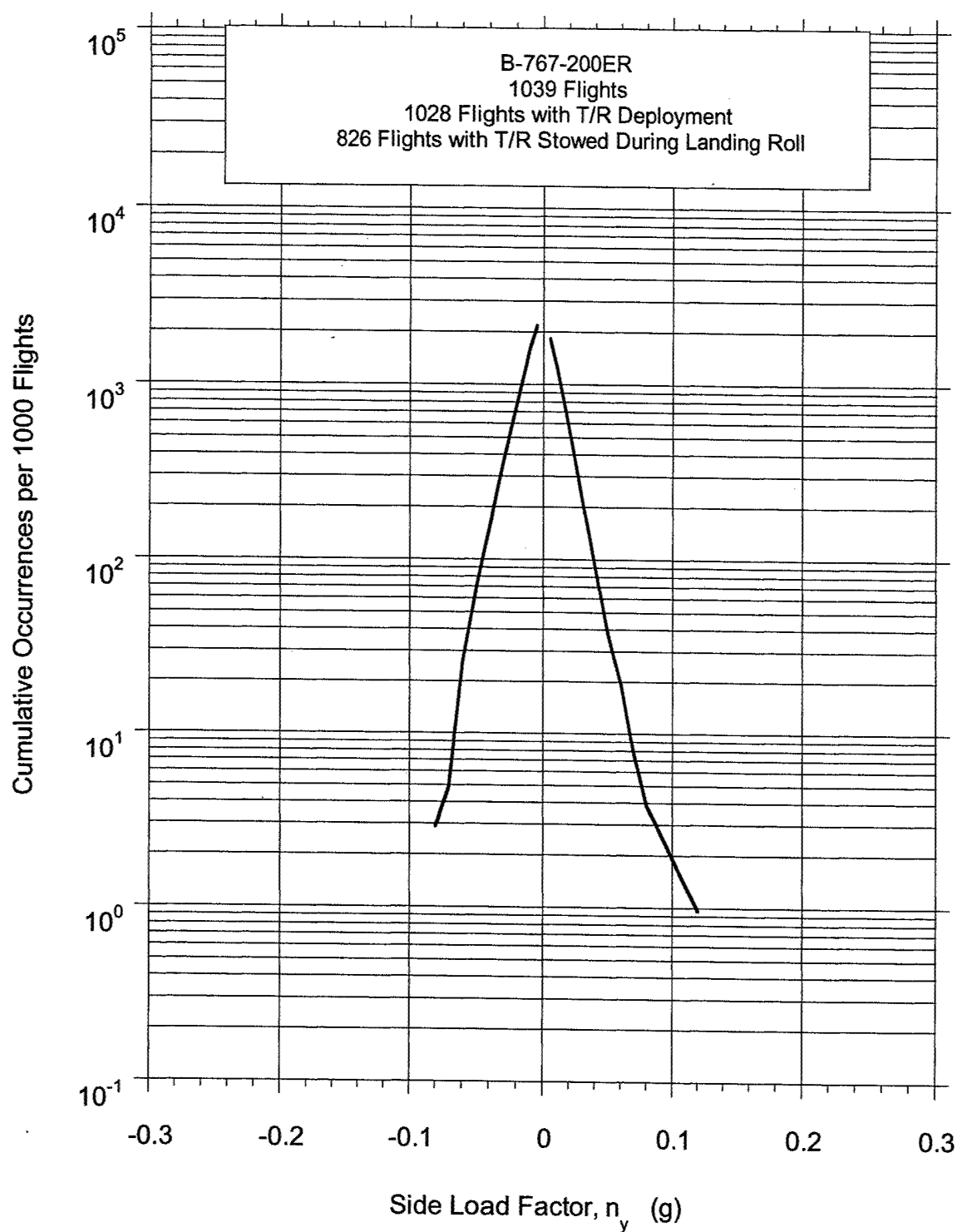
FIGURE B-9. CUMULATIVE FREQUENCY OF SIDE LOAD FACTOR AFTER
THRUST REVERSER STOWED DURING LANDING ROLL
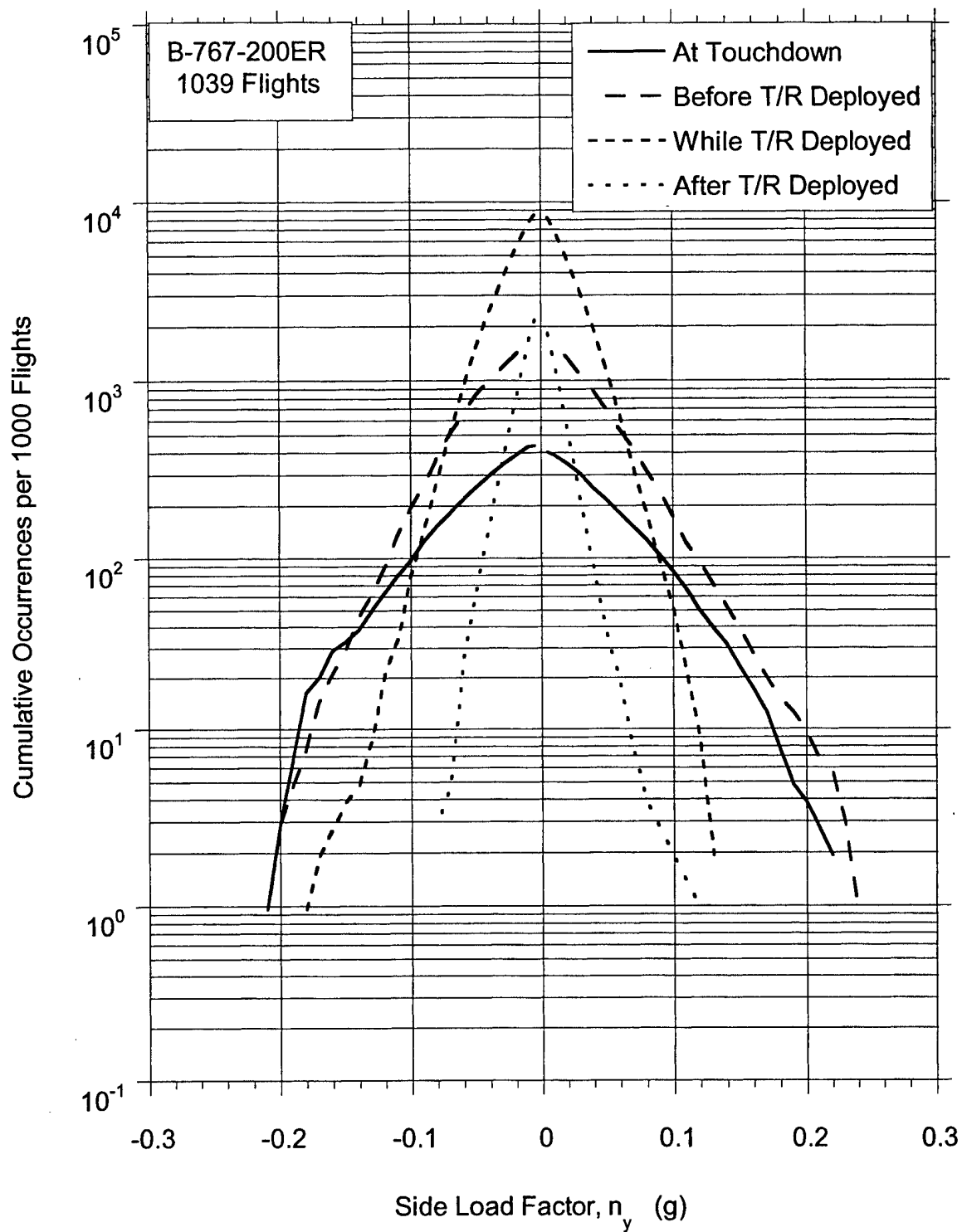
FIGURE B-10. CUMULATIVE FREQUENCY OF SIDE LOAD FACTOR AT
TOUCHDOWN AND DURING LANDING ROLL
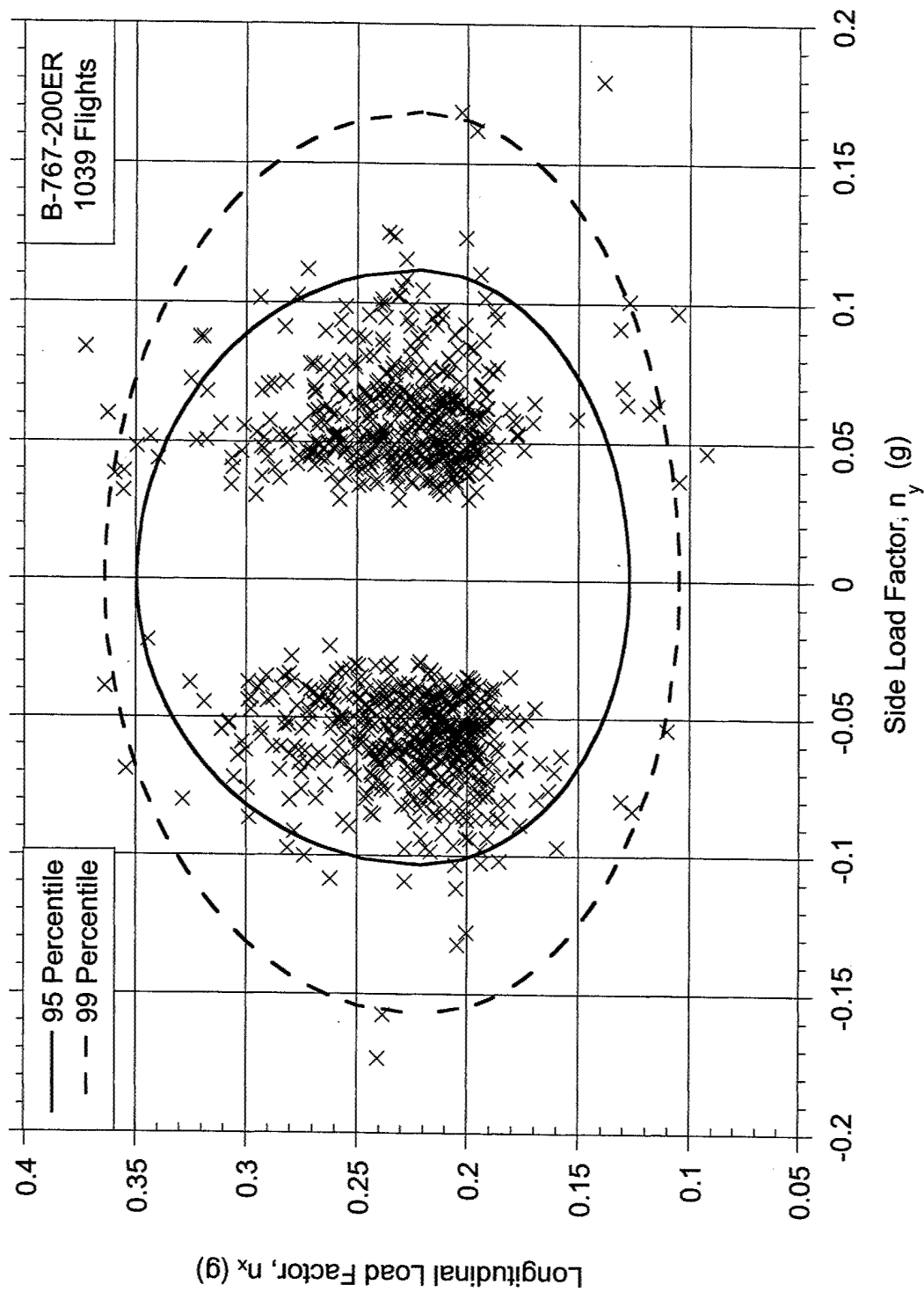
FIGURE B-11. COINCIDENT LONGITUDINAL LOAD FACTOR AT MAXIMUM SIDE LOAD FACTOR DURING TAKEOFF ROLL
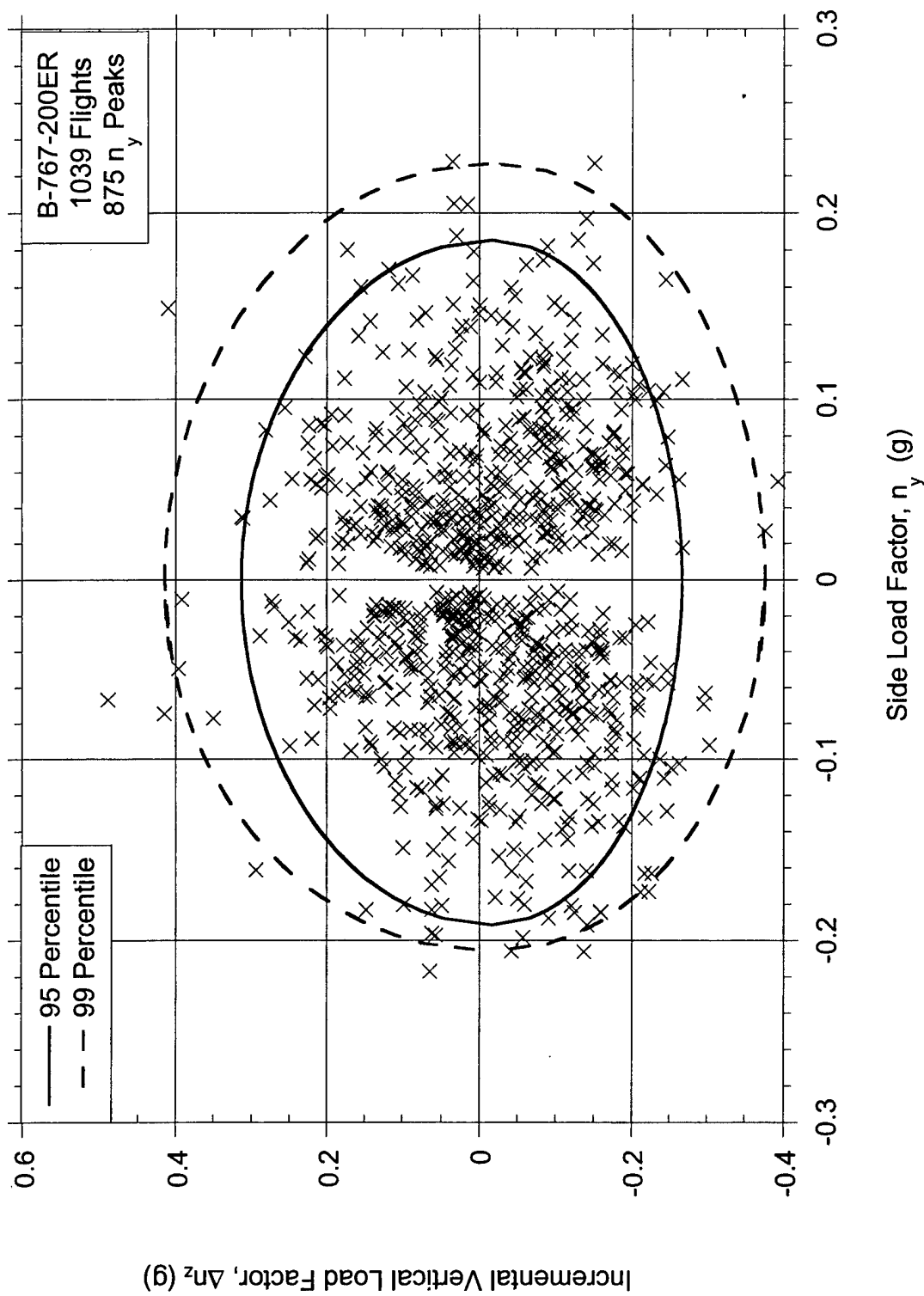
FIGURE B-12. COINCIDENT INCREMENTAL VERTICAL LOAD FACTOR AT MAXIMUM SIDE LOAD FACTOR AT TOUCHDOWN
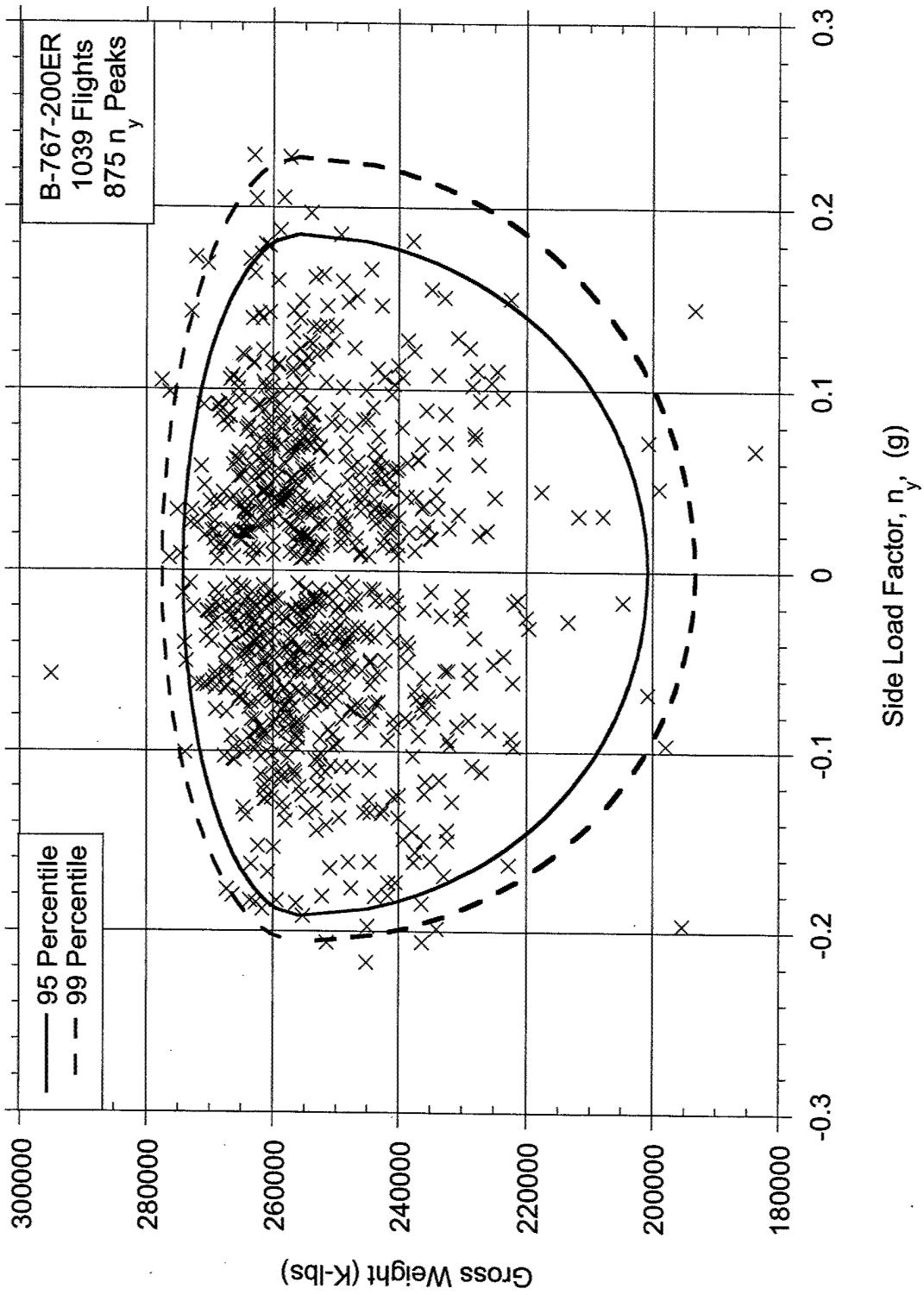
FIGURE B-13. COINCIDENT GROSS WEIGHT AT MAXIMUM SIDE LOAD FACTOR AT TOUCHDOWN
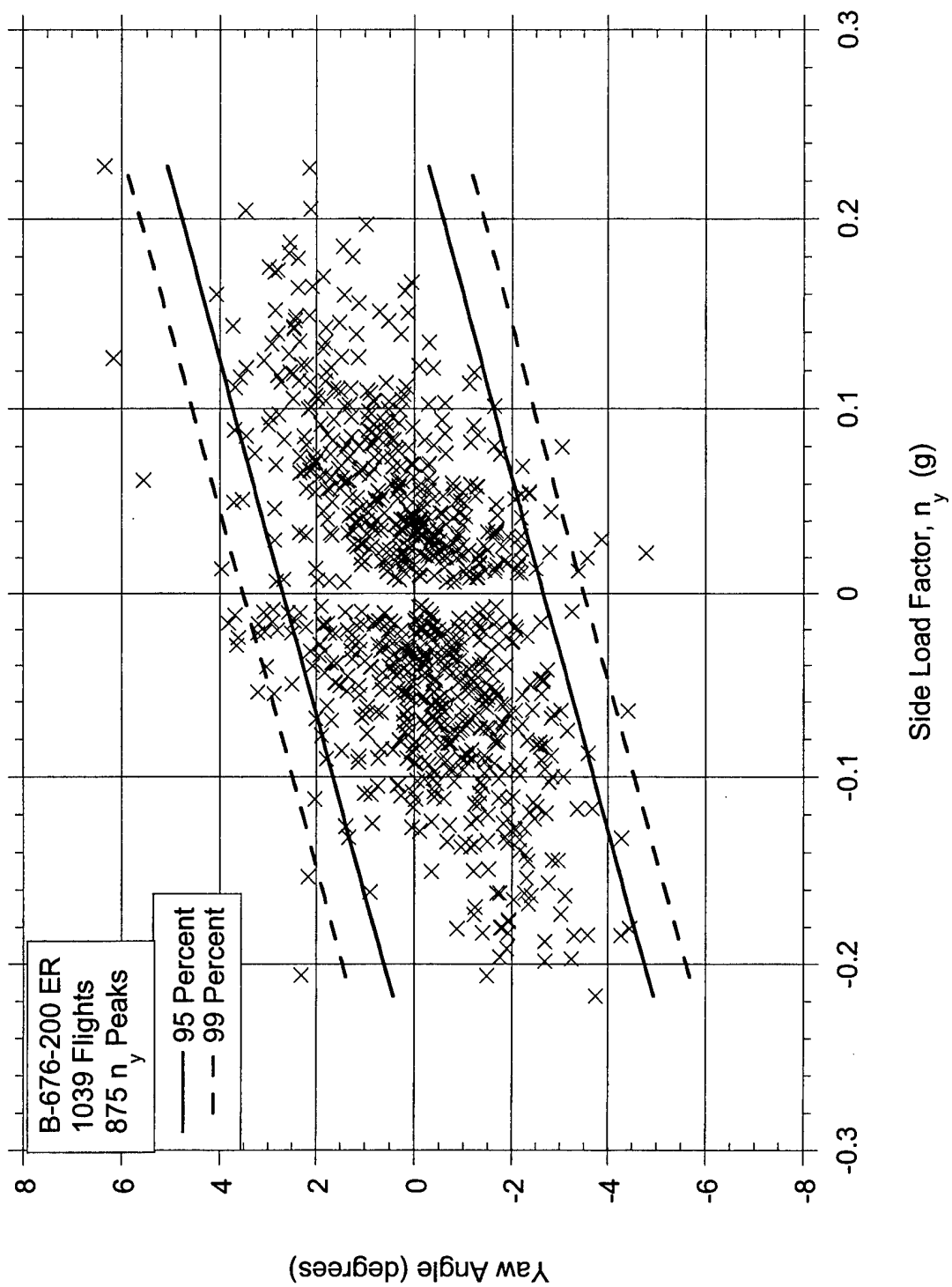
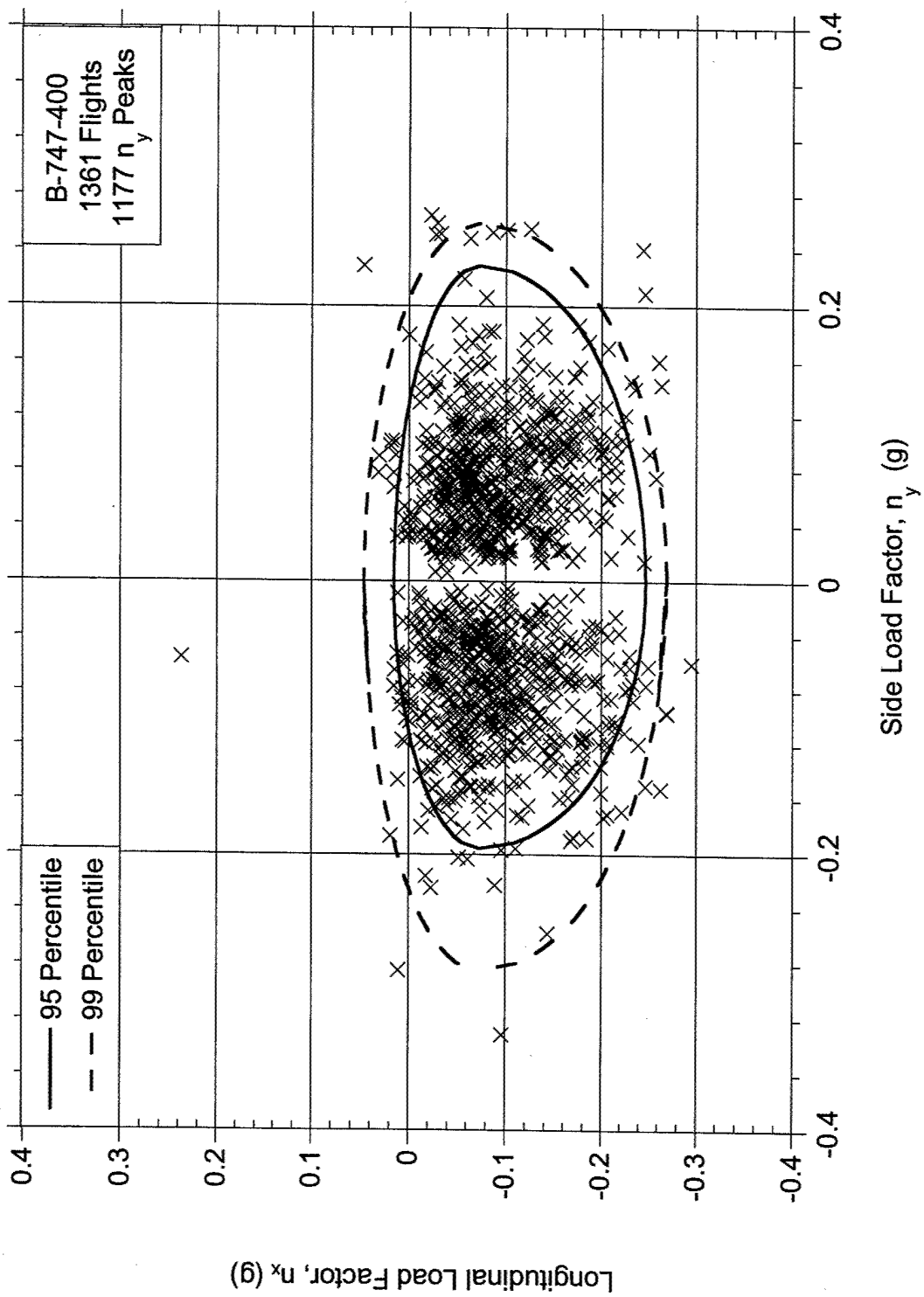FIGURE B-14. YAW ANGLE AND MAXIMUM SIDE LOAD FACTOR AT TOUCHDOWN
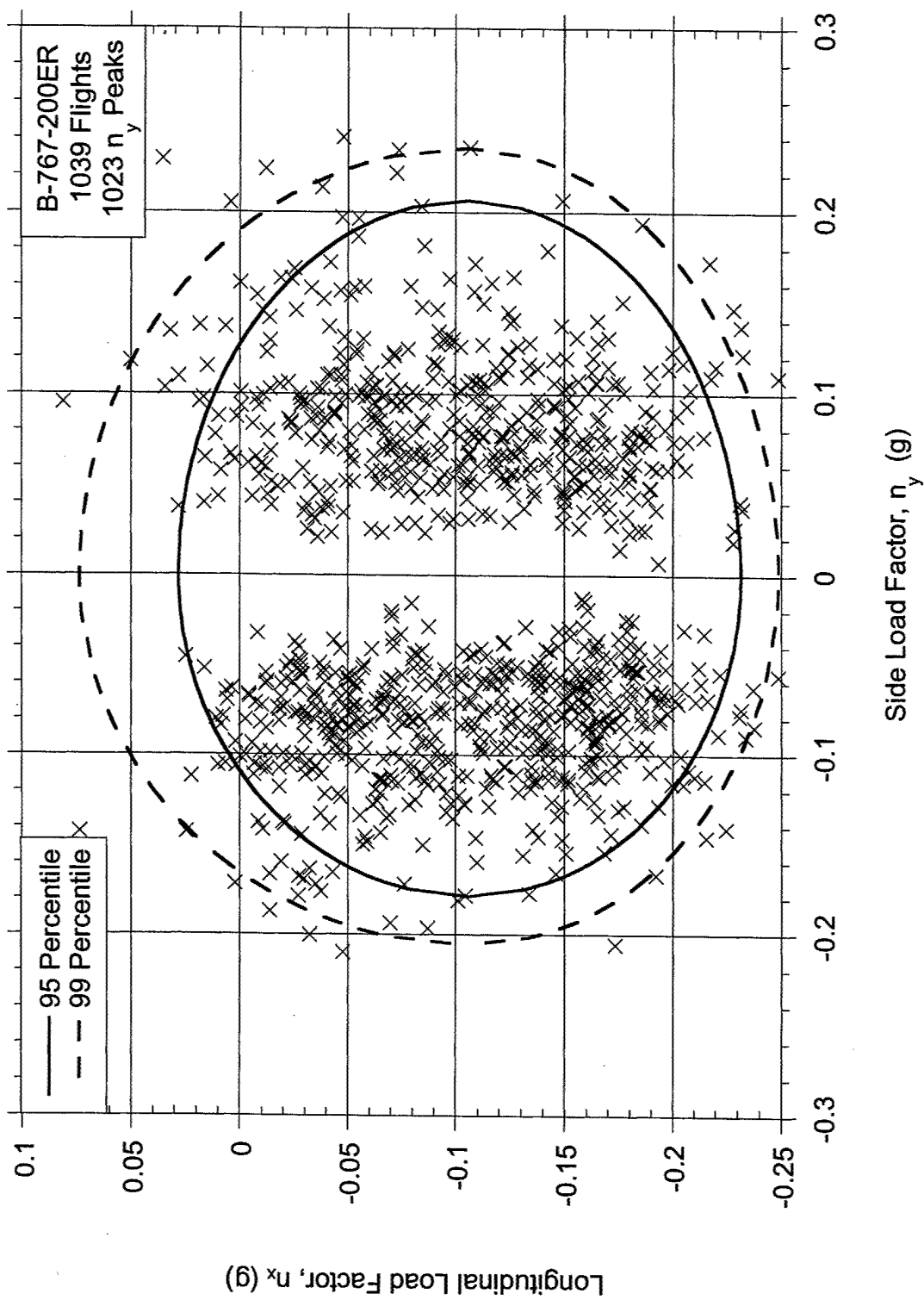
FIGURE B-15. COINCIDENT LONGITUDINAL LOAD FACTOR AT MAXIMUM SIDE LOAD FACTOR BEFORE THRUST REVERSER DEPLOYMENT
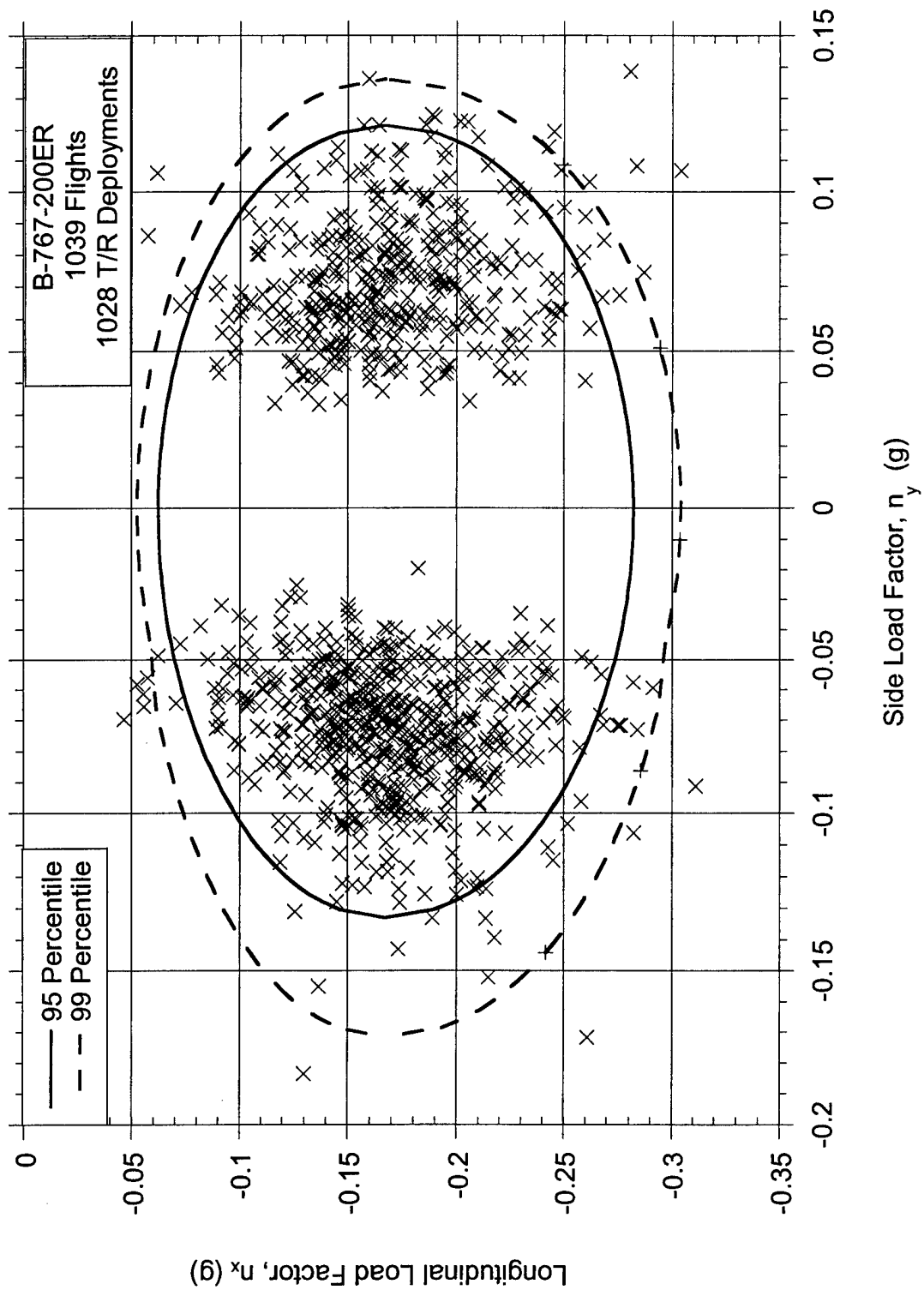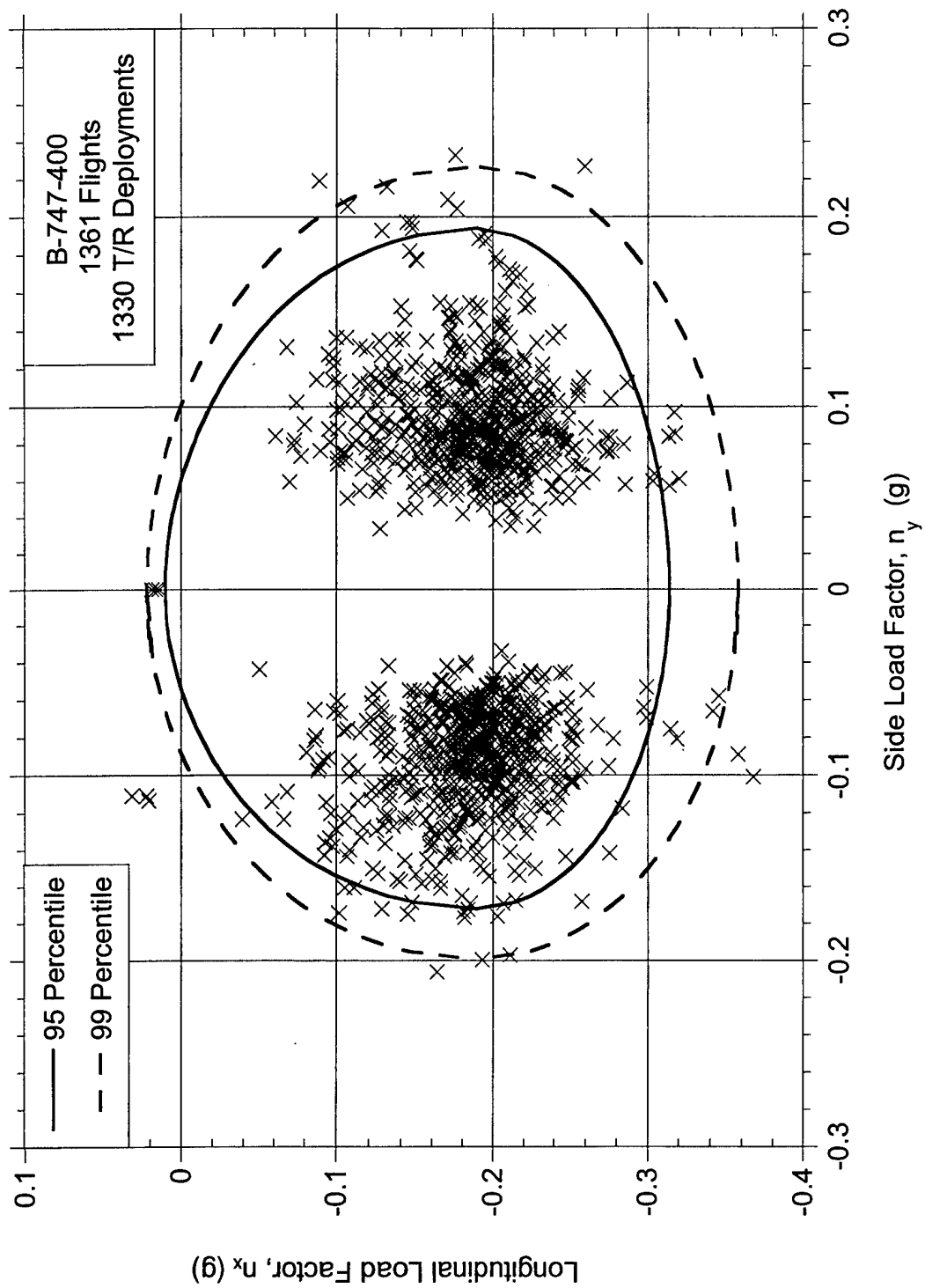
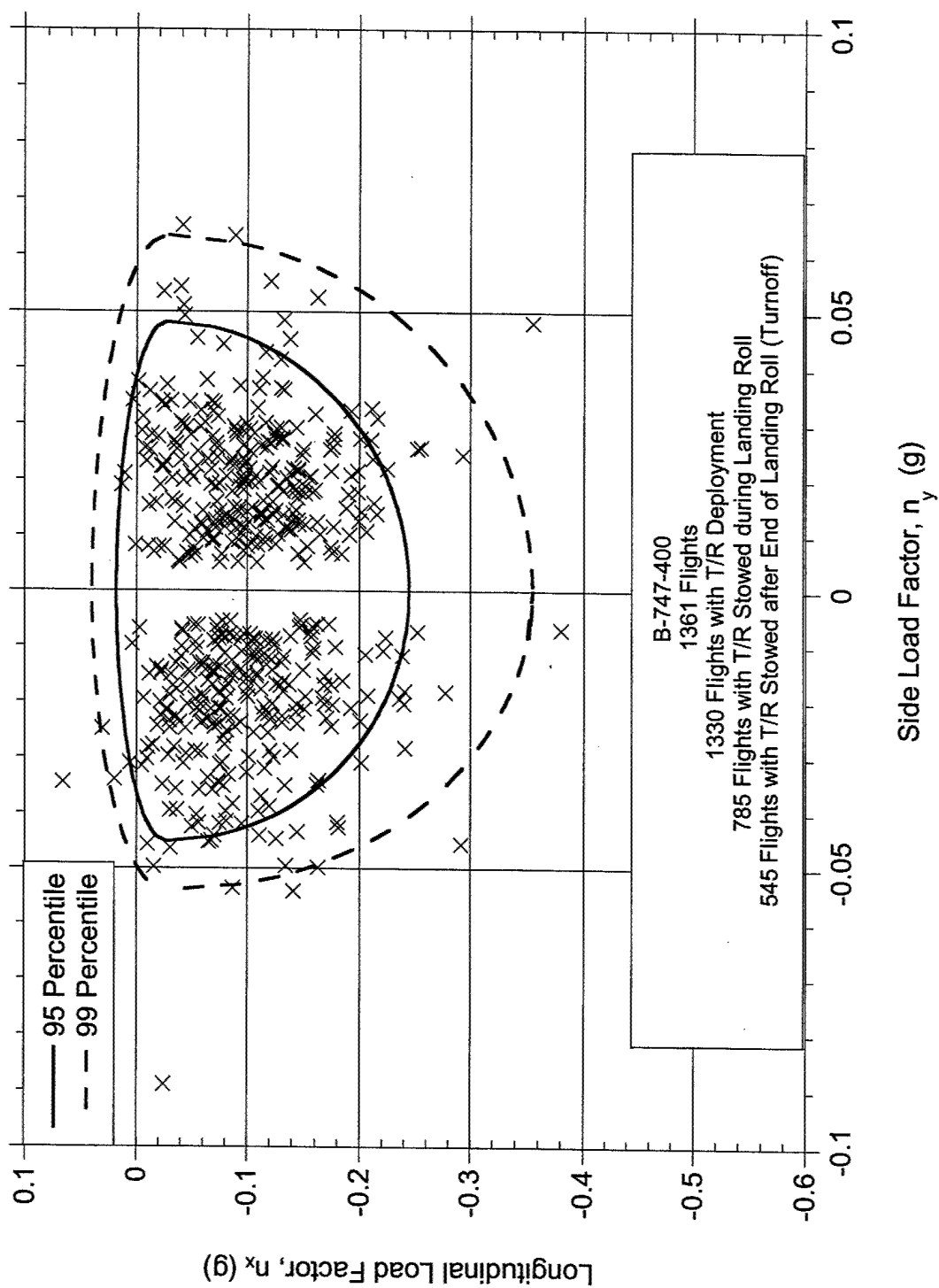FIGURE B-16. COINCIDENT LONGITUDINAL LOAD FACTOR AT MAXIMUM SIDE LOAD FACTOR WHILE THRUST REVERSER IS DEPLOYED
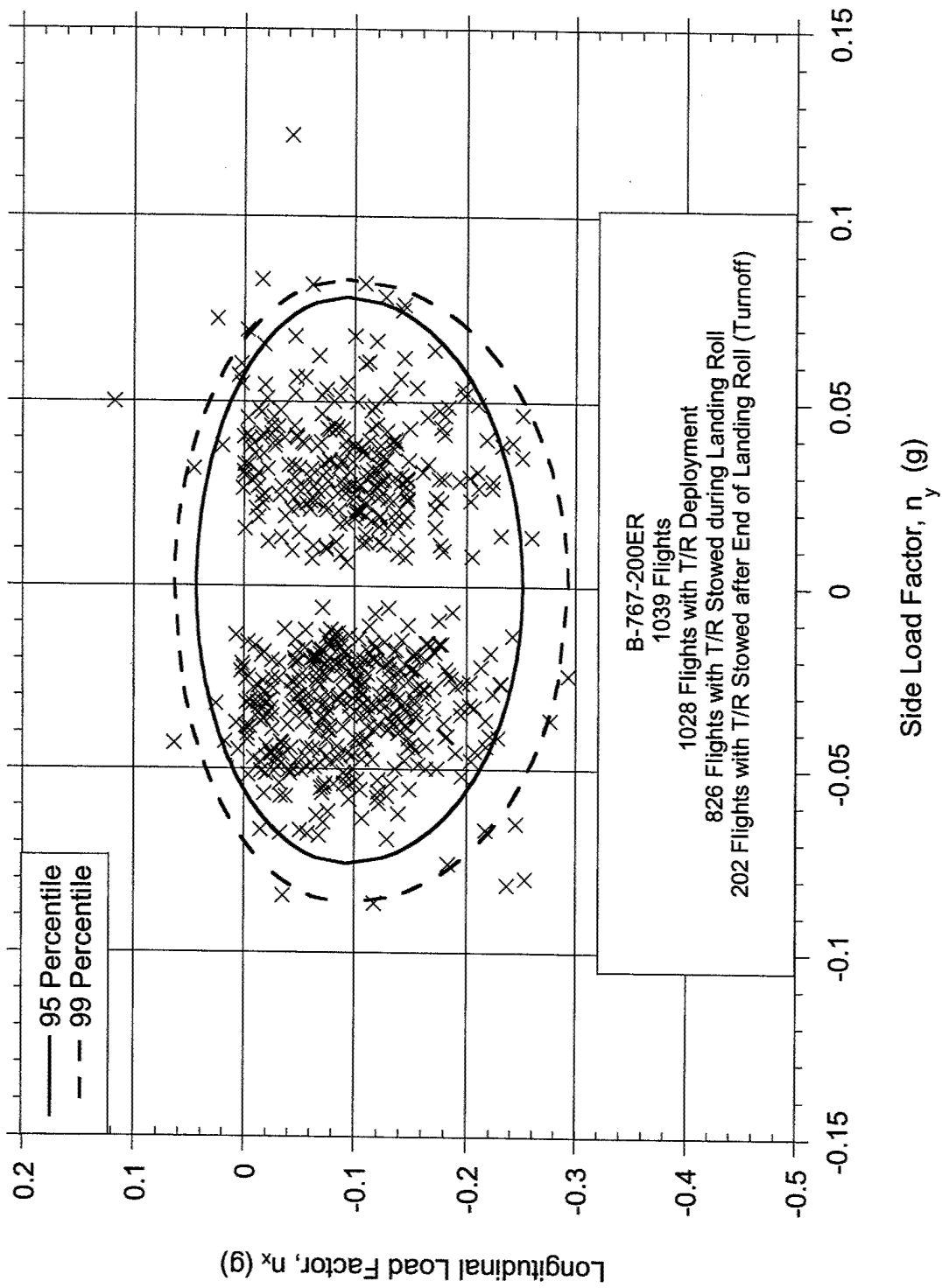
FIGURE B-17. COINCIDENT LONGITUDINAL LOAD FACTOR AT MAXIMUM SIDE LOAD FACTOR AFTER THRUST REVERSER STOWAGE DURING LANDING ROLL
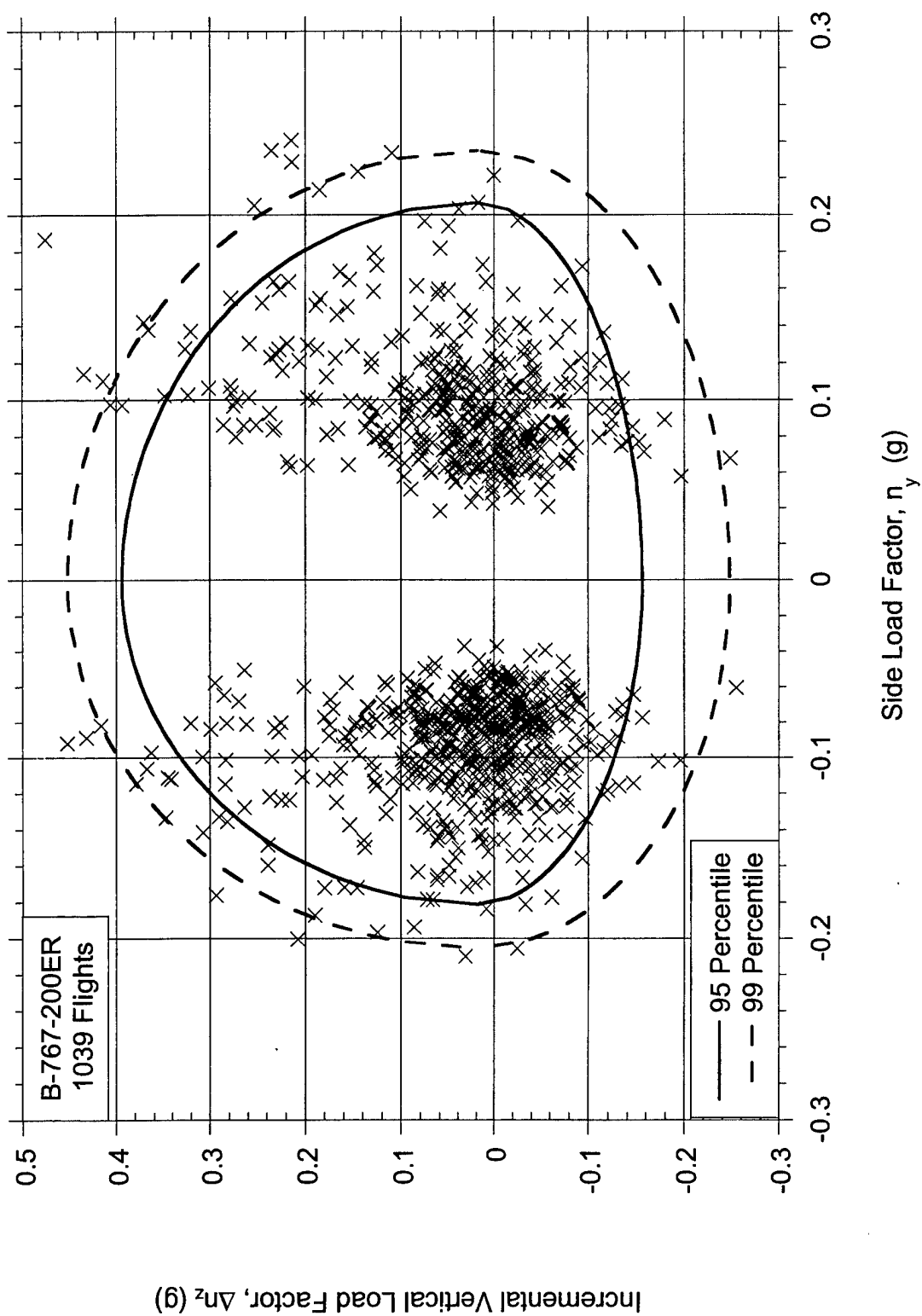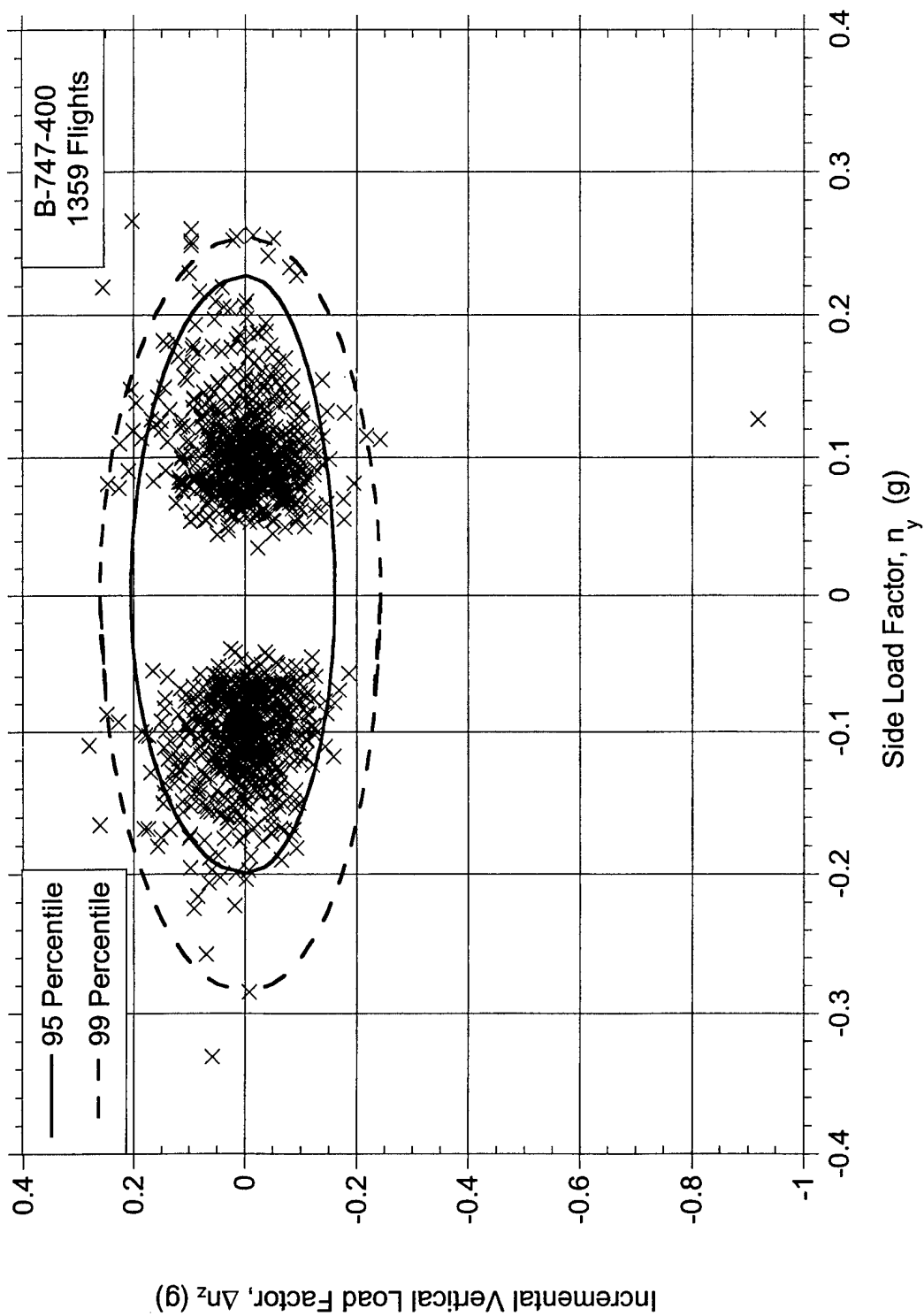
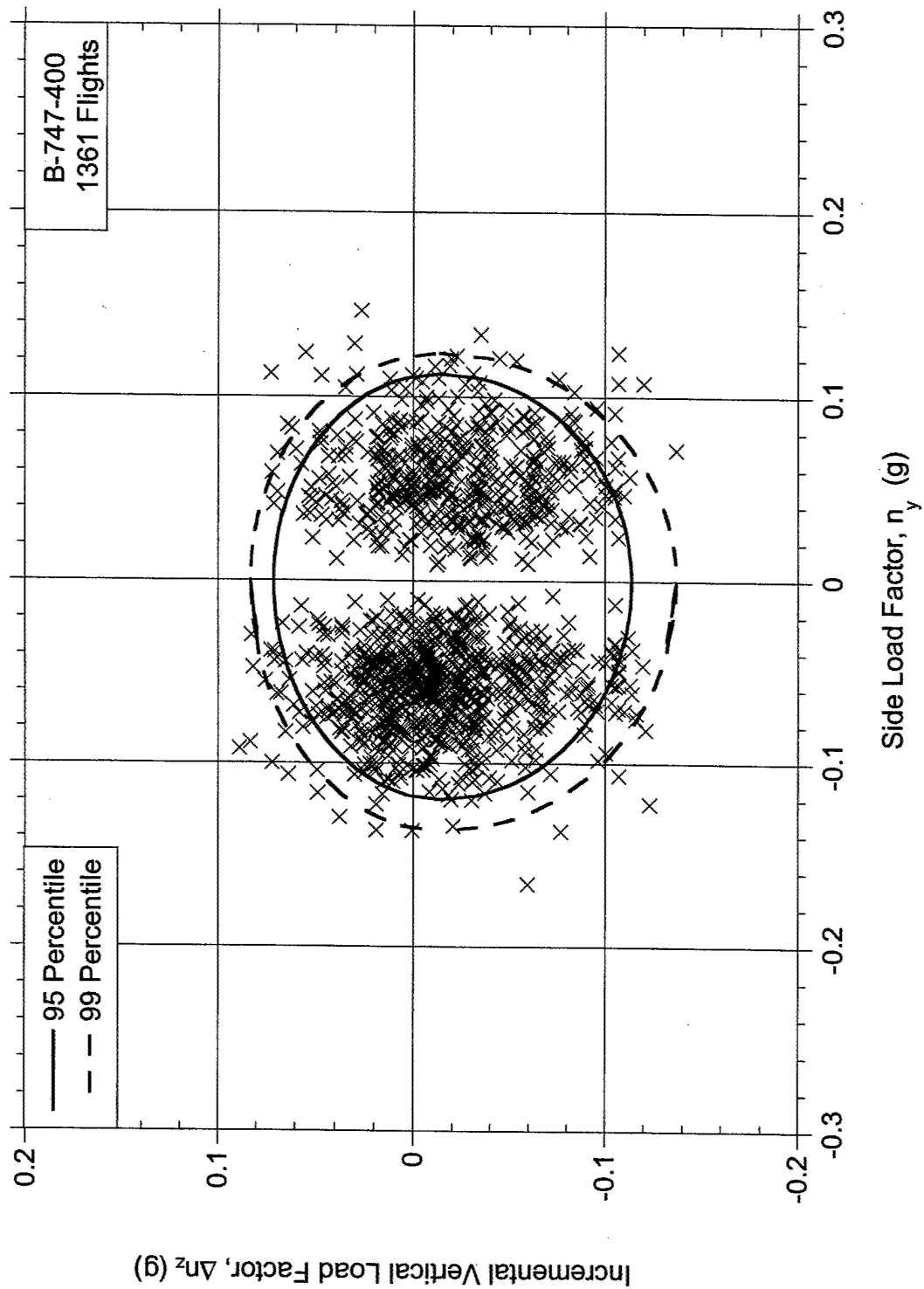FIGURE B-18. COINCIDENT INCREMENTAL VERTICAL LOAD FACTOR AT MAXIMUM SIDE LOAD FACTOR DURING LANDING ROLL
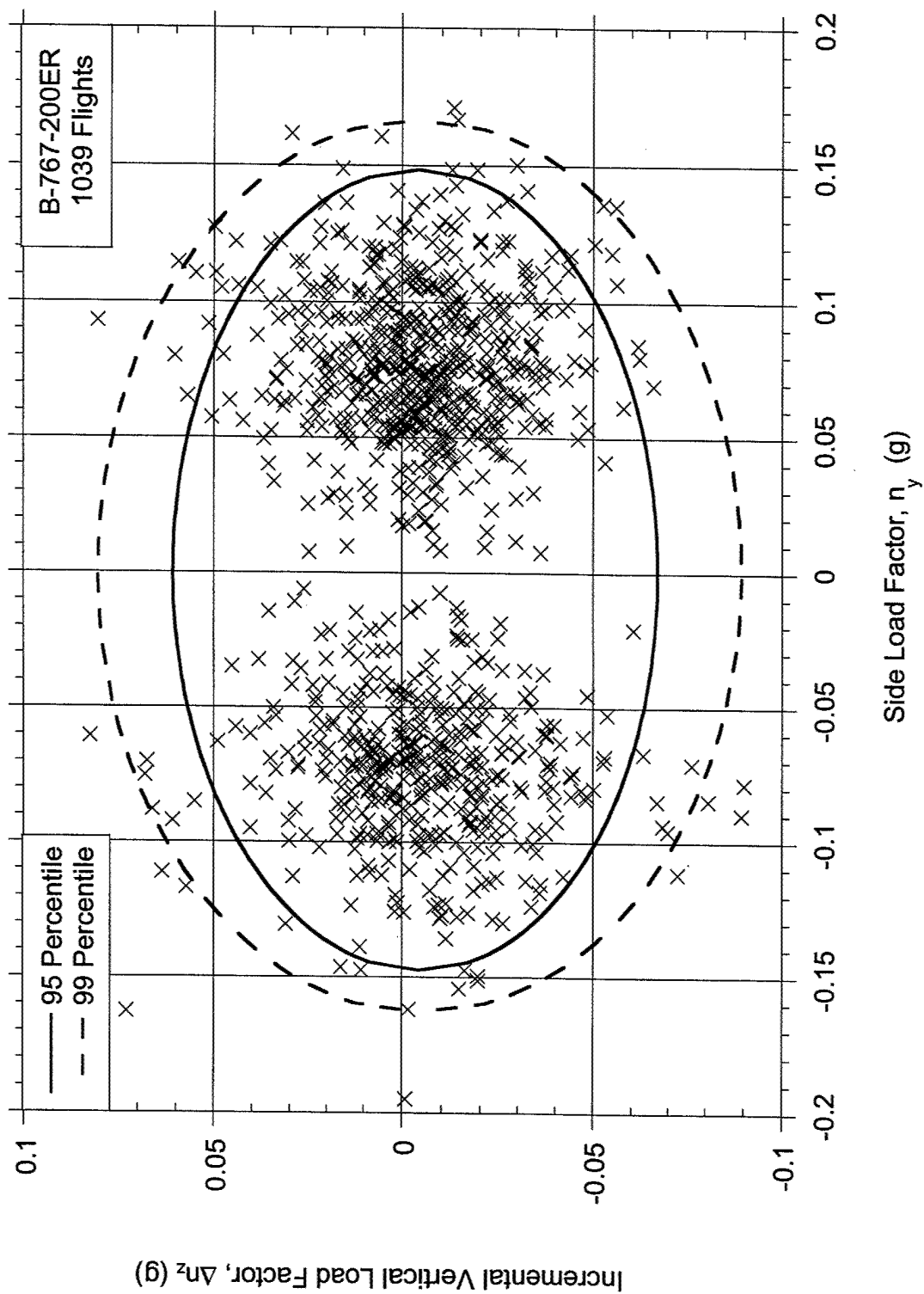
FIGURE B-19. COINCIDENT INCREMENTAL VERTICAL LOAD FACTOR AT MAXIMUM SIDE LOAD FACTOR DURING RUNWAY TURNOFF AFTER LANDING
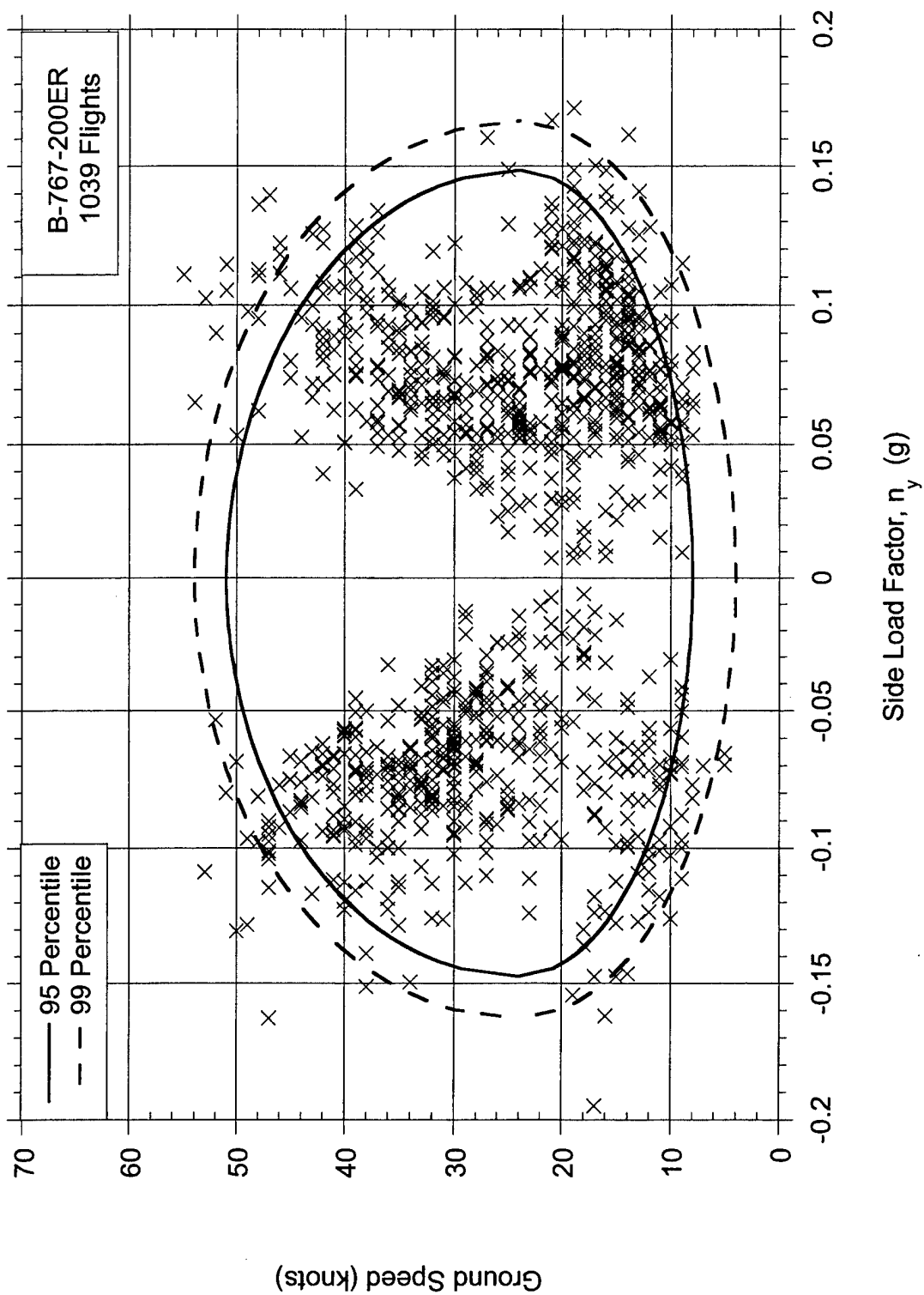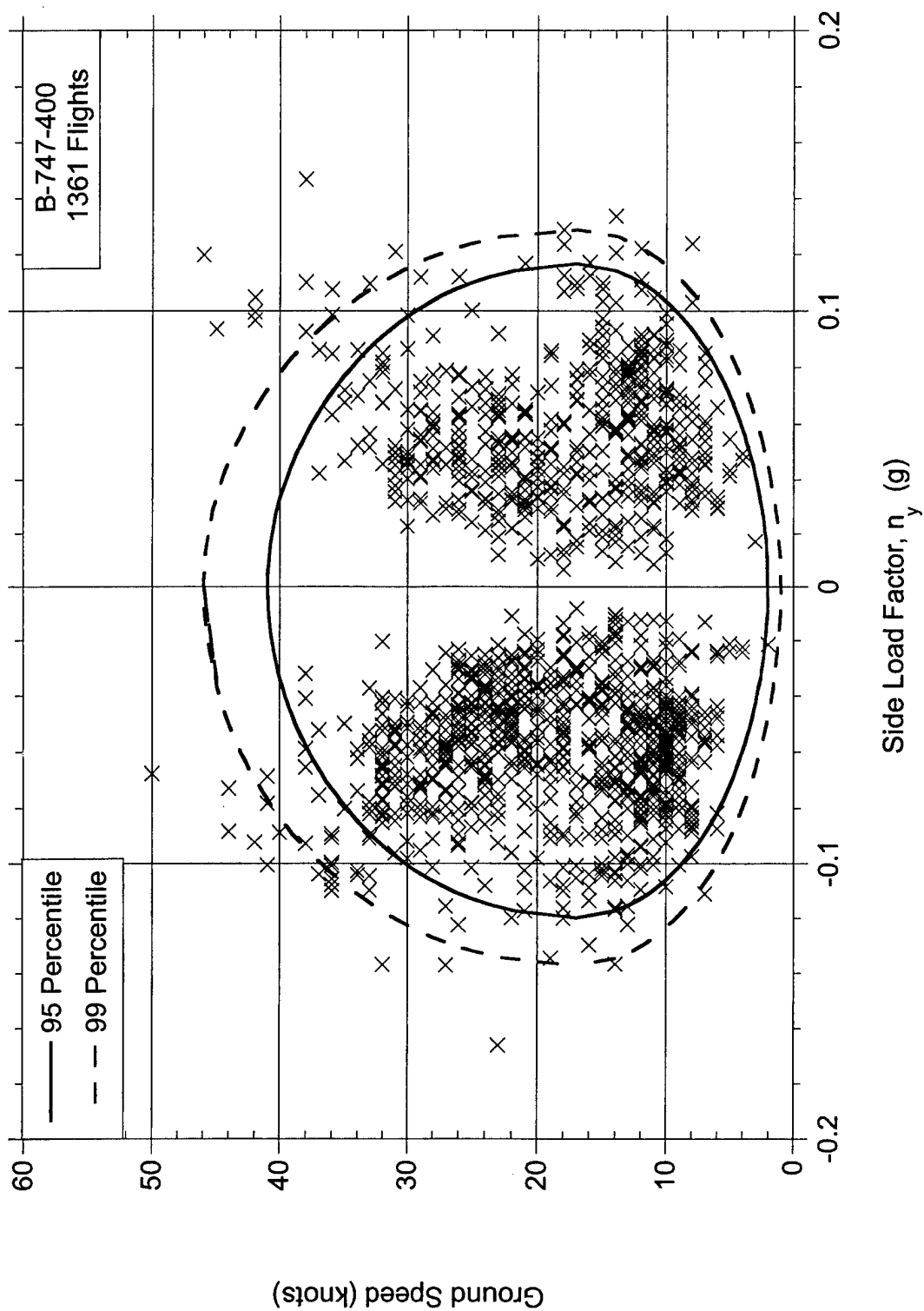
FIGURE B-20. COINCIDENT GROUND SPEED AT MAXIMUM SIDE LOAD FACTOR DURING RUNWAY TURNOFF AFTER LANDING

FIGURE C-1. CUMULATIVE FREQUENCY OF SIDE LOAD FACTOR DURING TAXI

FIGURE C-2. CUMULATIVE FREQUENCY OF SIDE LOAD FACTOR DURING
TAKEOFF AND LANDING ROLL

FIGURE C-3. CUMULATIVE FREQUENCY OF MAXIMUM SIDE LOAD FACTOR
DURING RUNWAY TURNOFF

FIGURE C-4. CUMULATIVE FREQUENCY OF SIDE LOAD FACTOR DURING
TAXI-IN, TAXI-OUT, AND RUNWAY TURNOFF

FIGURE C-5. CUMULATIVE FREQUENCY OF MAXIMUM SIDE LOAD FACTOR AT TOUCHDOWN

FIGURE C-6. CUMULATIVE FREQUENCY OF SIDE LOAD FACTOR AFTER
TOUCHDOWN AND BEFORE THRUST REVERSER DEPLOYMENT

FIGURE C-7. CUMULATIVE FREQUENCY OF MAXIMUM SIDE LOAD FACTOR
AT THRUST REVERSER DEPLOYMENT
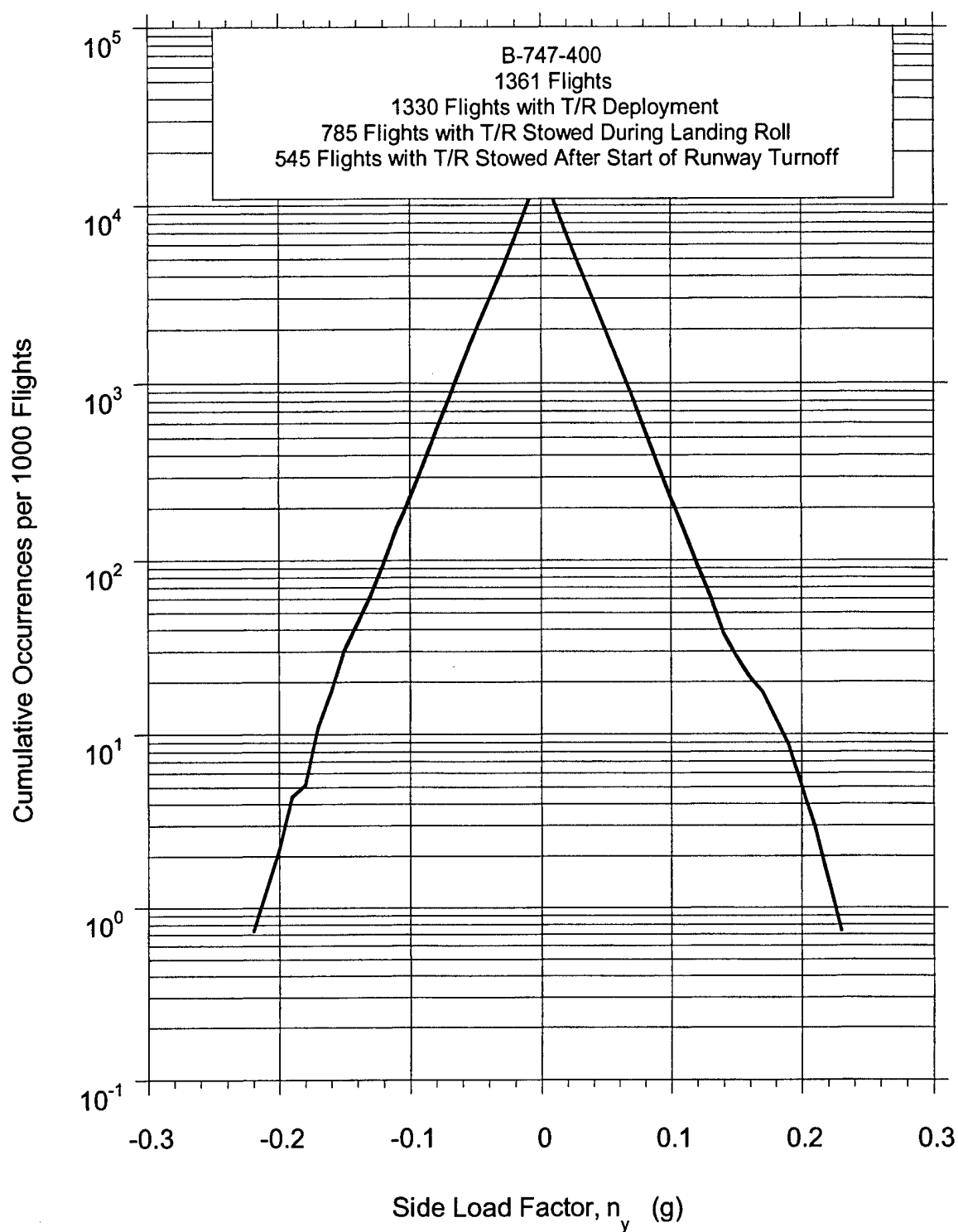
FIGURE C-8. CUMULATIVE FREQUENCY OF SIDE LOAD FACTOR WHILE
THRUST REVERSER IS DEPLOYED
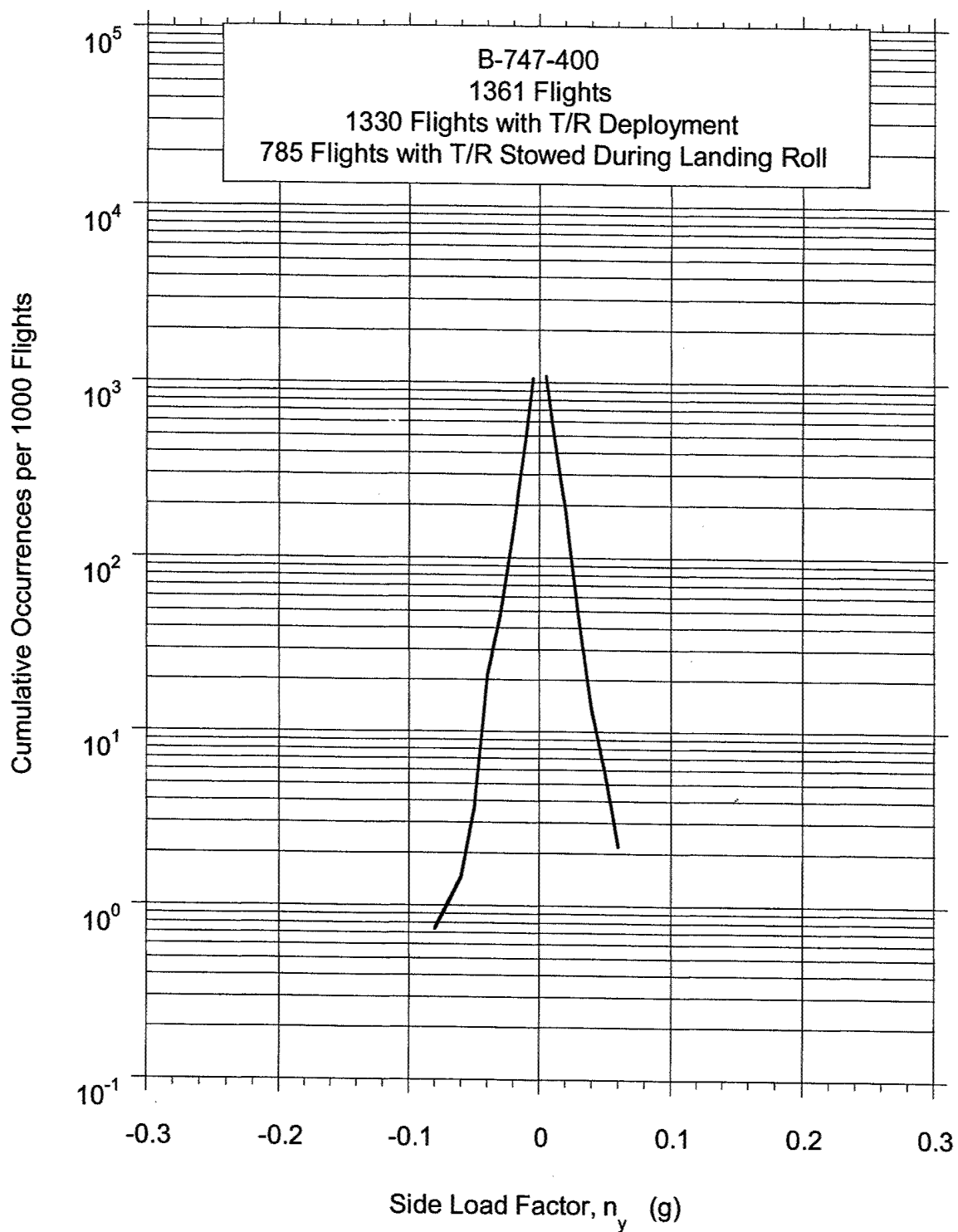
FIGURE C-9. CUMULATIVE FREQUENCY OF SIDE LOAD FACTOR AFTER
THRUST REVERSER STOWED DURING LANDING ROLL
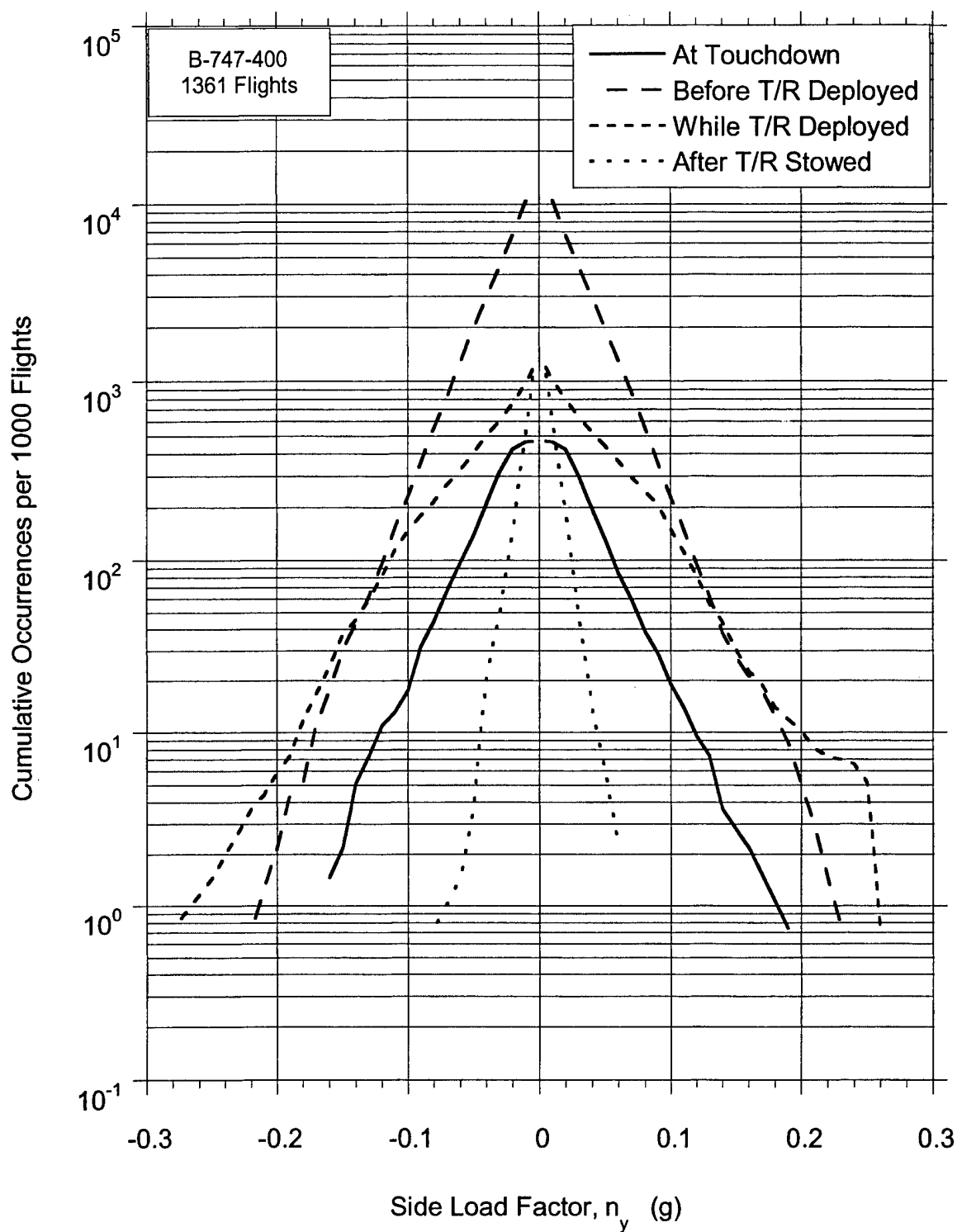
FIGURE C-10. CUMULATIVE FREQUENCY OF SIDE LOAD FACTOR AT
TOUCHDOWN AND DURING LANDING ROLL

C-10
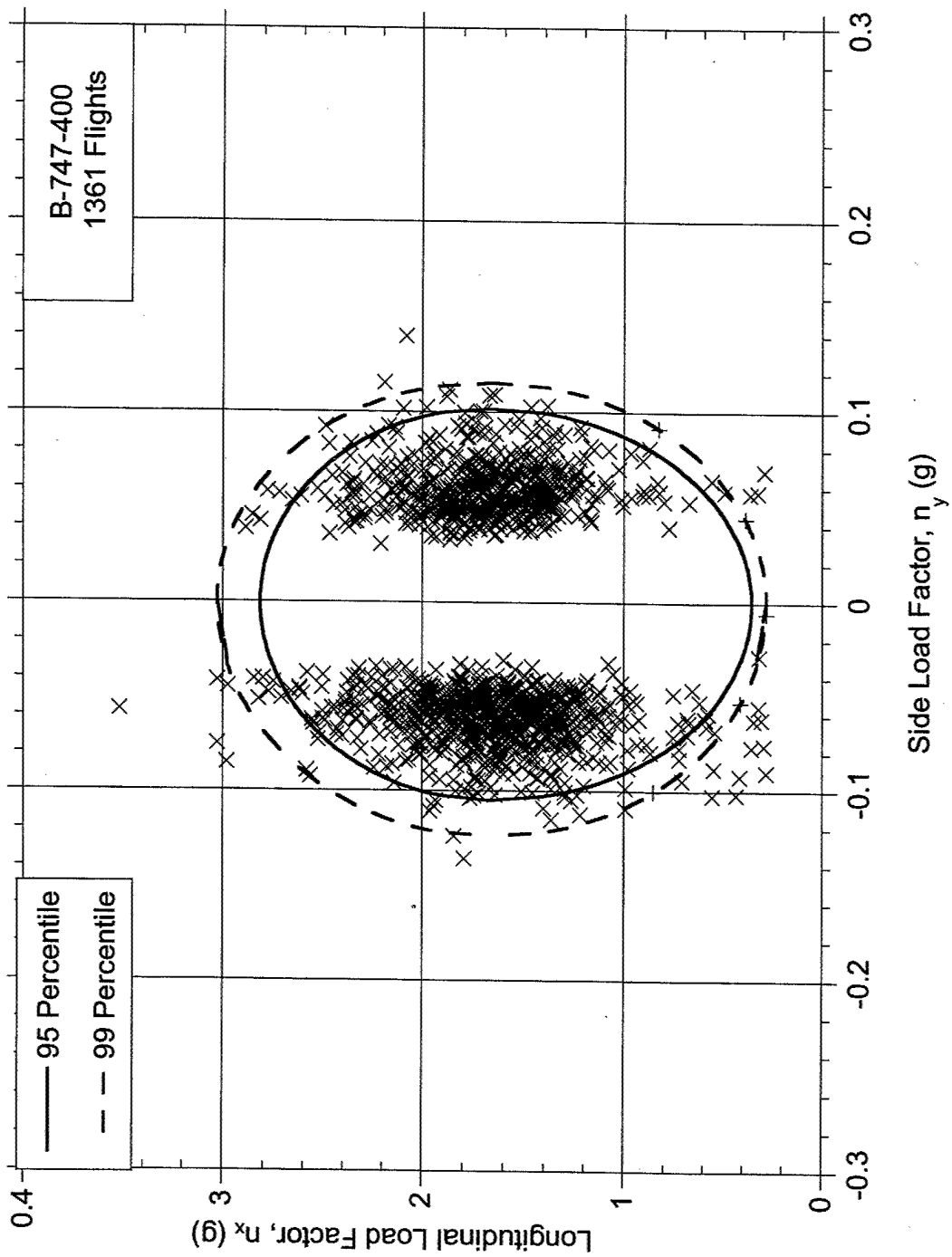
FIGURE C-11. COINCIDENT LONGITUDINAL LOAD FACTOR AT MAXIMUM SIDE LOAD FACTOR DURING TAKEOFF ROLL
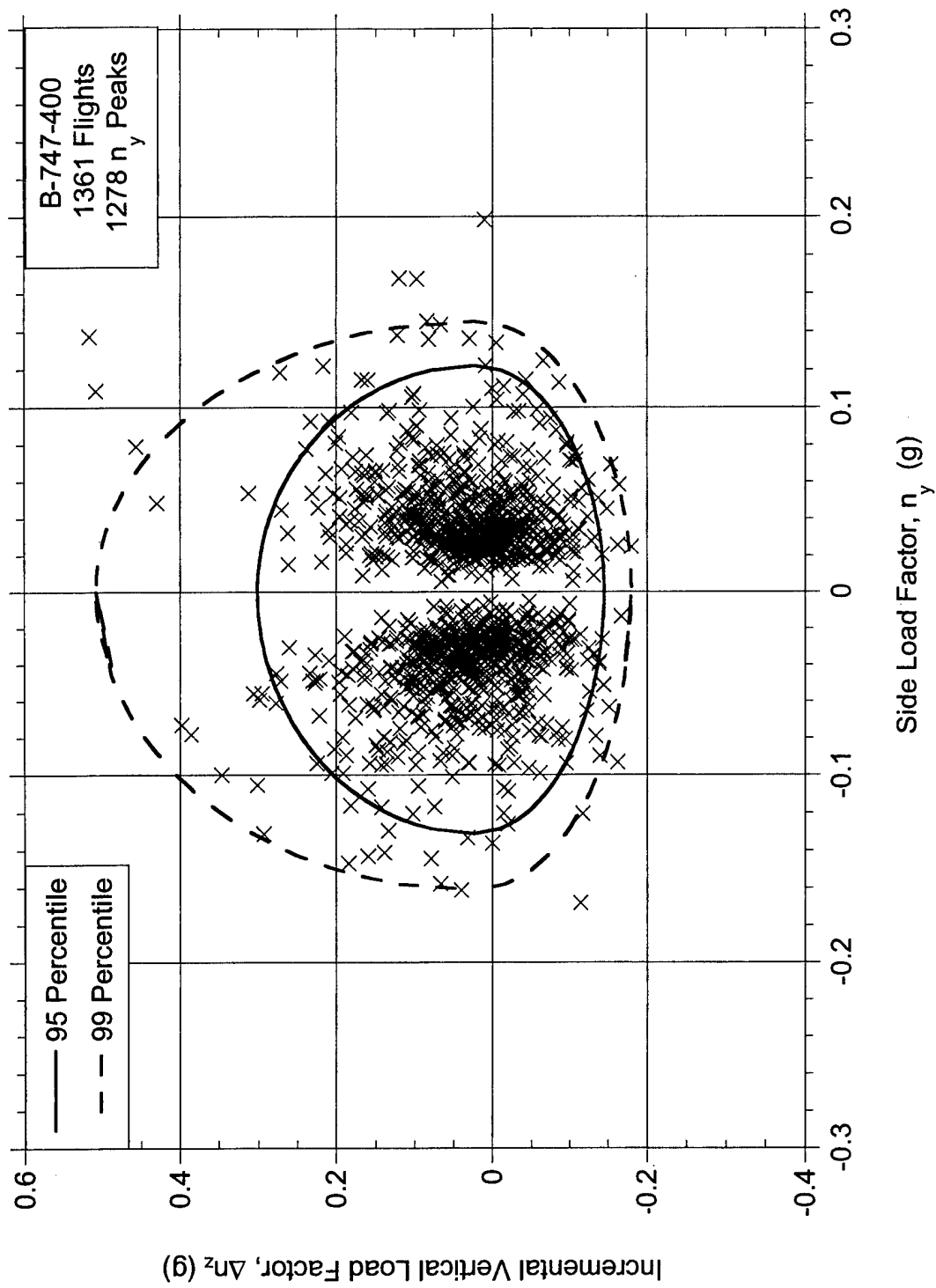
FIGURE C-12. COINCIDENT INCREMENTAL VERTICAL LOAD FACTOR AT MAXIMUM SIDE LOAD FACTOR AT TOUCHDOWN
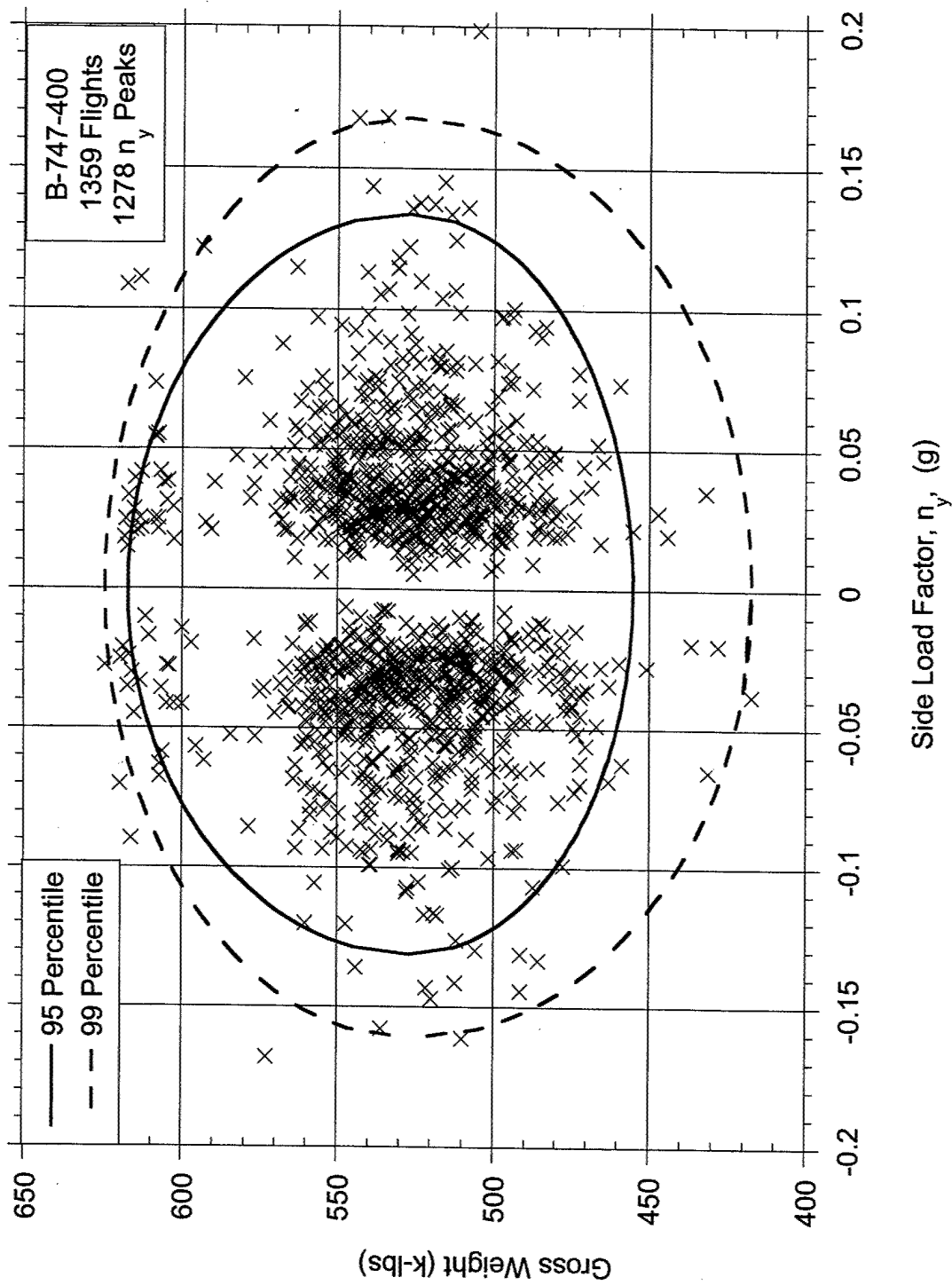
FIGURE C-13. COINCIDENT GROSS WEIGHT AT MAXIMUM SIDE LOAD FACTOR AT TOUCHDOWN
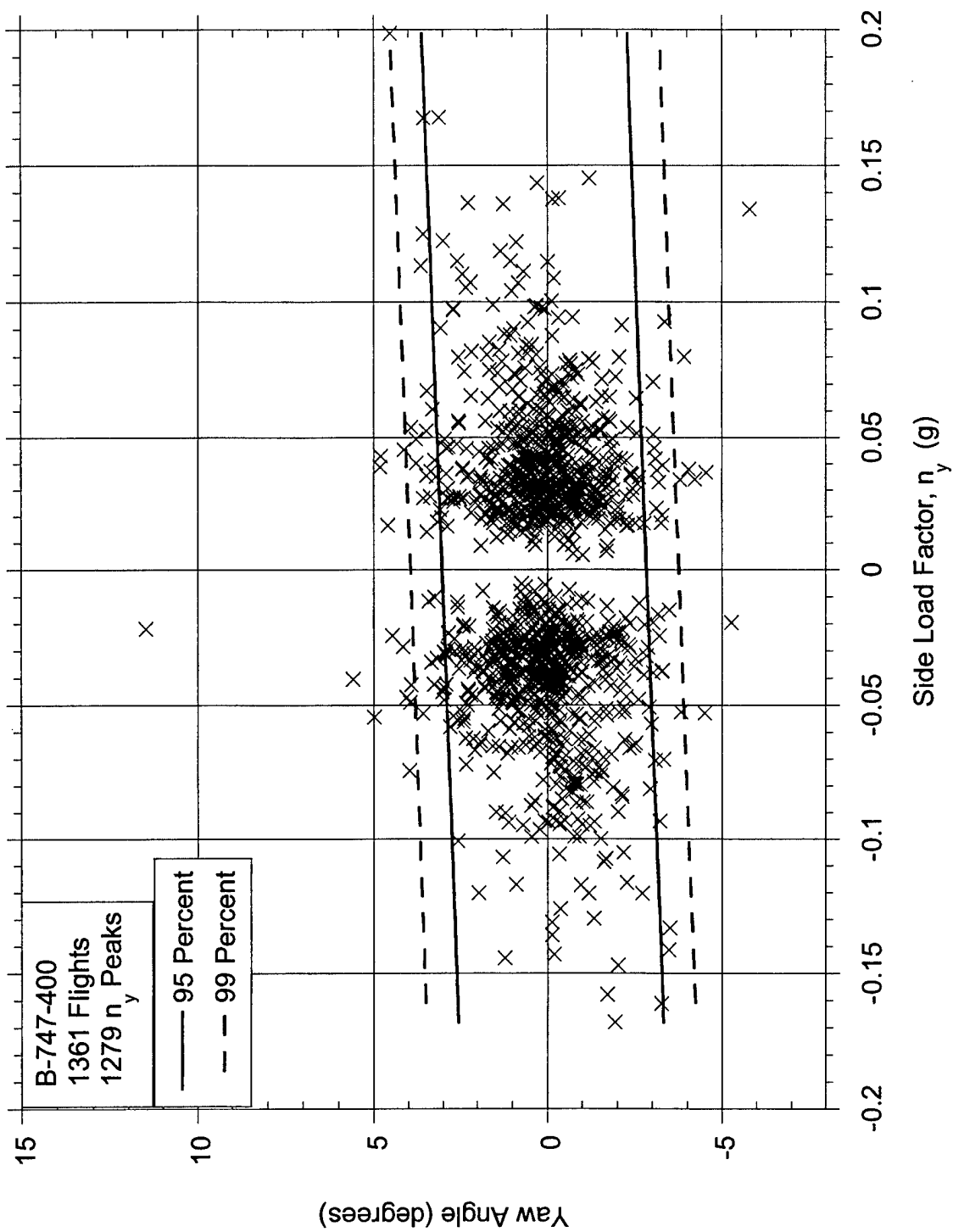
FIGURE C-14. YAW ANGLE AND MAXIMUM SIDE LOAD FACTOR AT TOUCHDOWN

FIGURE C-15. COINCIDENT LONGITUDINAL LOAD FACTOR AT MAXIMUM SIDE LOAD FACTOR BEFORE THRUST REVERSER DEPLOYMENT

C-15

FIGURE C-16. COINCIDENT LONGITUDINAL LOAD FACTOR AT MAXIMUM SIDE LOAD FACTOR WHILE THRUST REVERSER IS DEPLOYED

FIGURE C-17. COINCIDENT LONGITUDINAL LOAD FACTOR AT MAXIMUM SIDE LOAD FACTOR AFTER THRUST REVERSER STOWAGE DURING LANDING ROLL

FIGURE C-18. COINCIDENT INCREMENTAL VERTICAL LOAD FACTOR AT MAXIMUM SIDE LOAD FACTOR DURING LANDING ROLL

FIGURE C-19. COINCIDENT INCREMENTAL VERTICAL LOAD FACTOR AT MAXIMUM SIDE LOAD FACTOR DURING RUNWAY TURNOFF AFTER LANDING

FIGURE C-20. COINCIDENT GROUND SPEED AT MAXIMUM SIDE LOAD FACTOR DURING RUNWAY TURNOFF AFTER LANDING

C-20
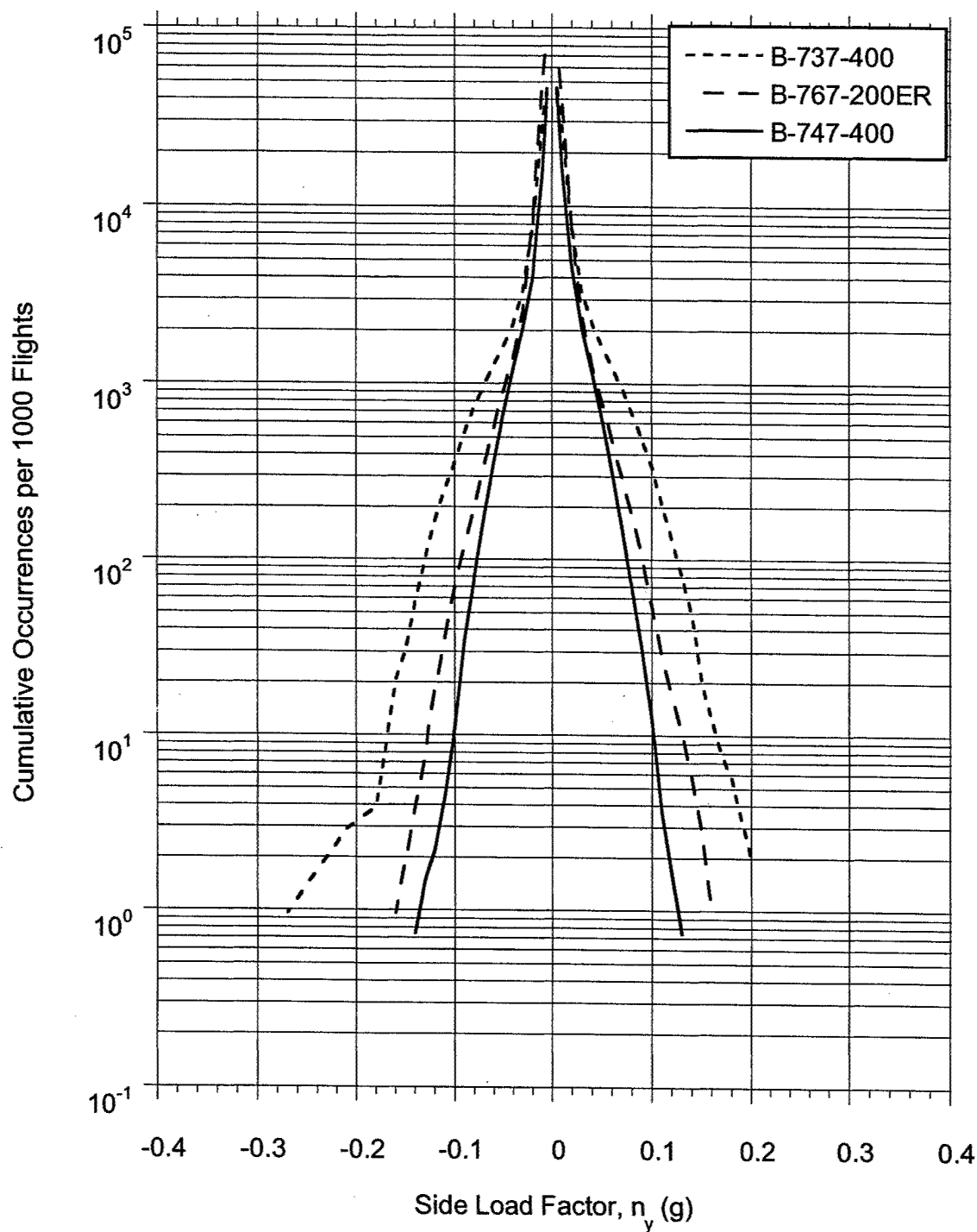
FIGURE D-1a. COMPARISON OF CUMULATIVE FREQUENCY OF SIDE LOAD
FACTOR DURING TAXI-OUT
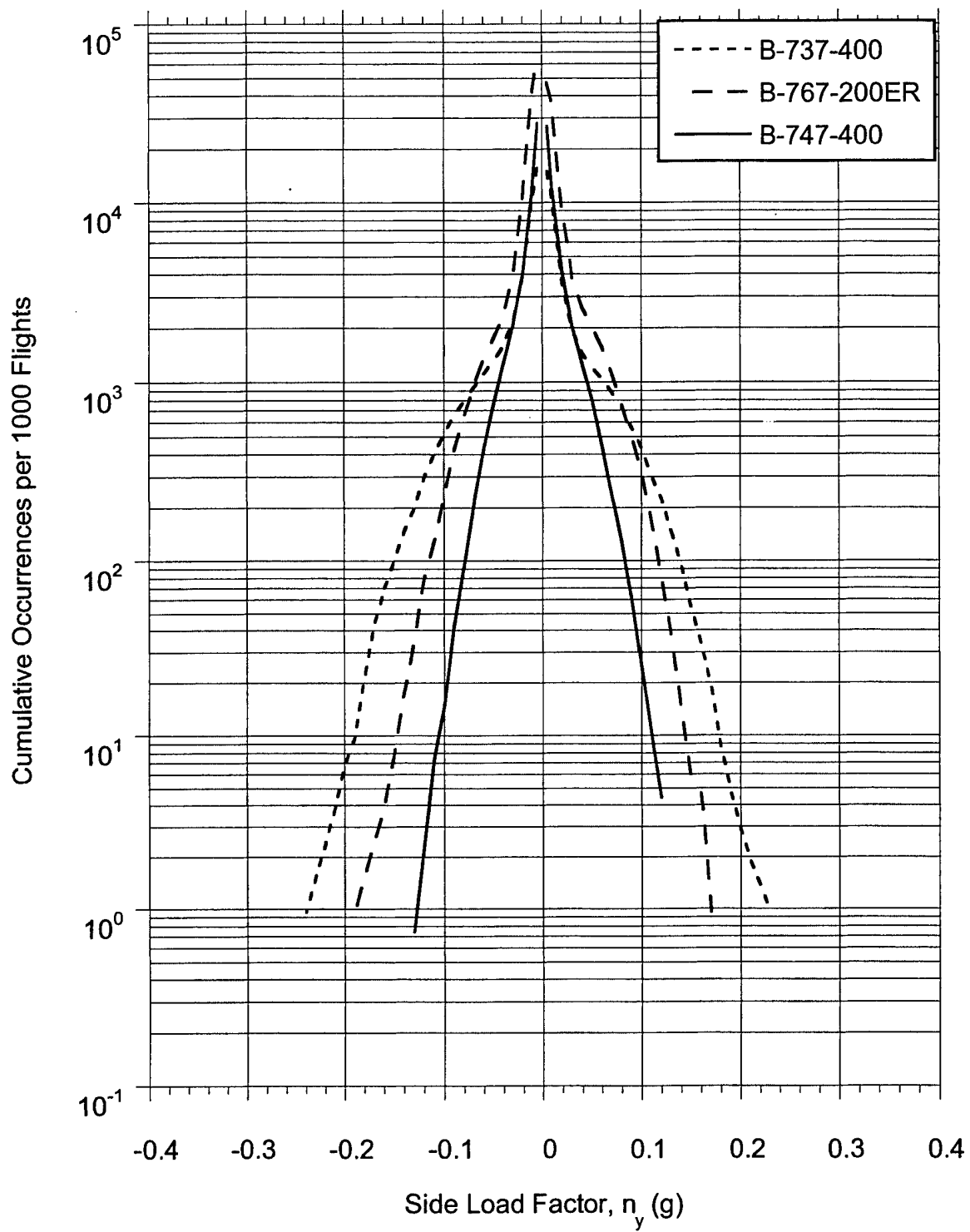
FIGURE D-1b. COMPARISON OF CUMULATIVE FREQUENCY OF SIDE LOAD
FACTOR DURING TAXI-IN
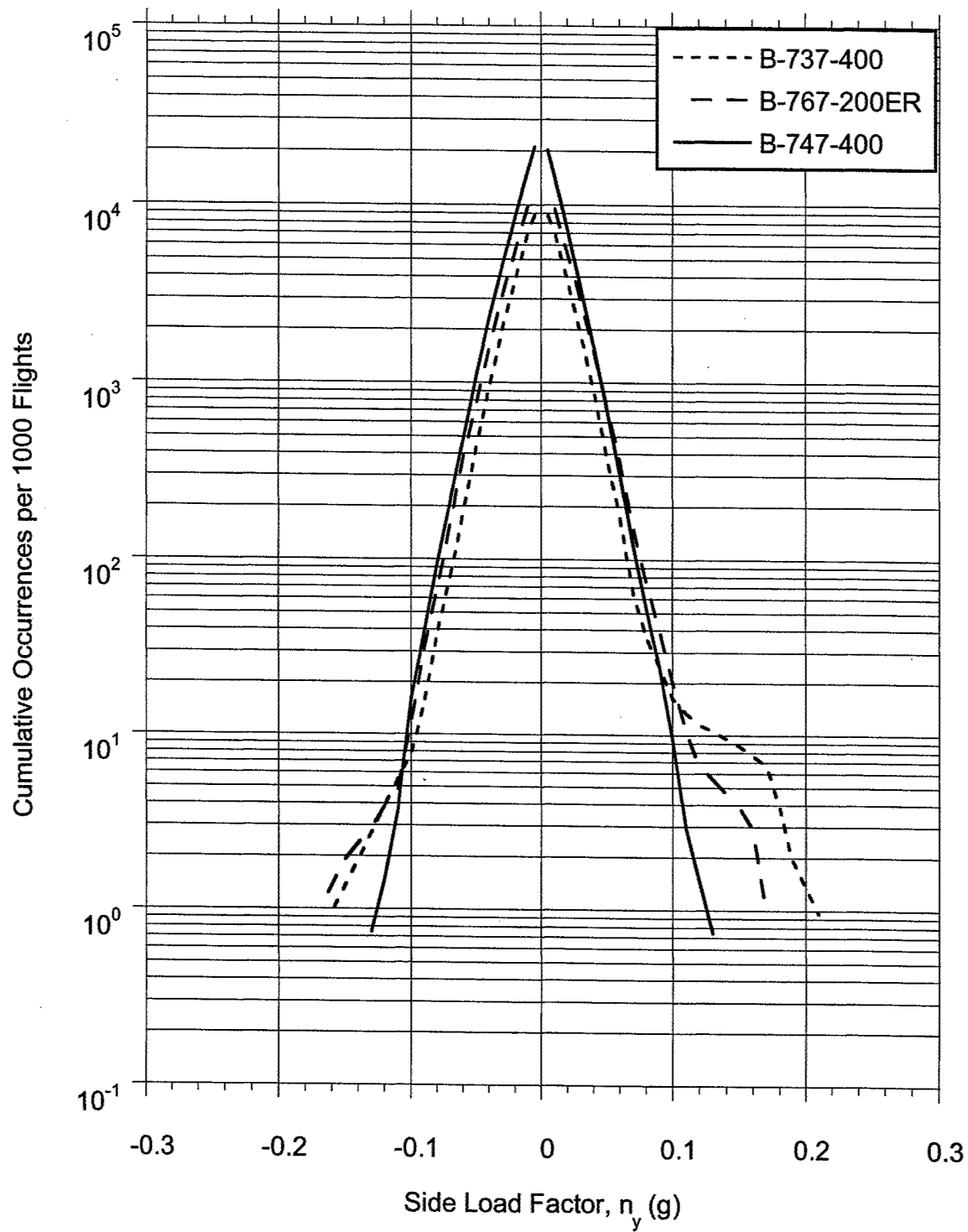
FIGURE D-2a. COMPARISON OF CUMULATIVE FREQUENCY OF SIDE LOAD
FACTOR DURING TAKEOFF ROLL
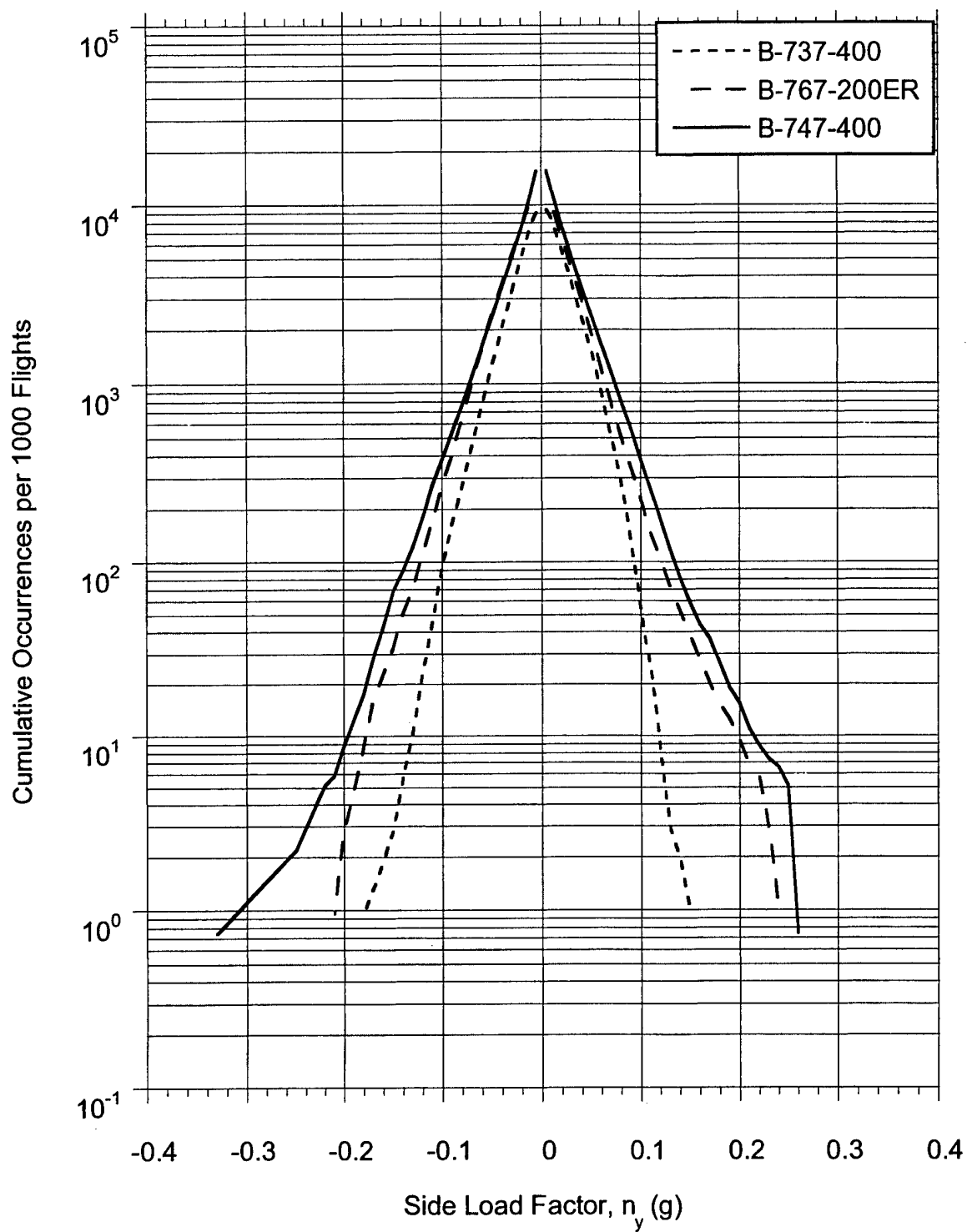
FIGURE D-2b. COMPARISON OF CUMULATIVE FREQUENCY OF SIDE LOAD
FACTOR DURING LANDING ROLL
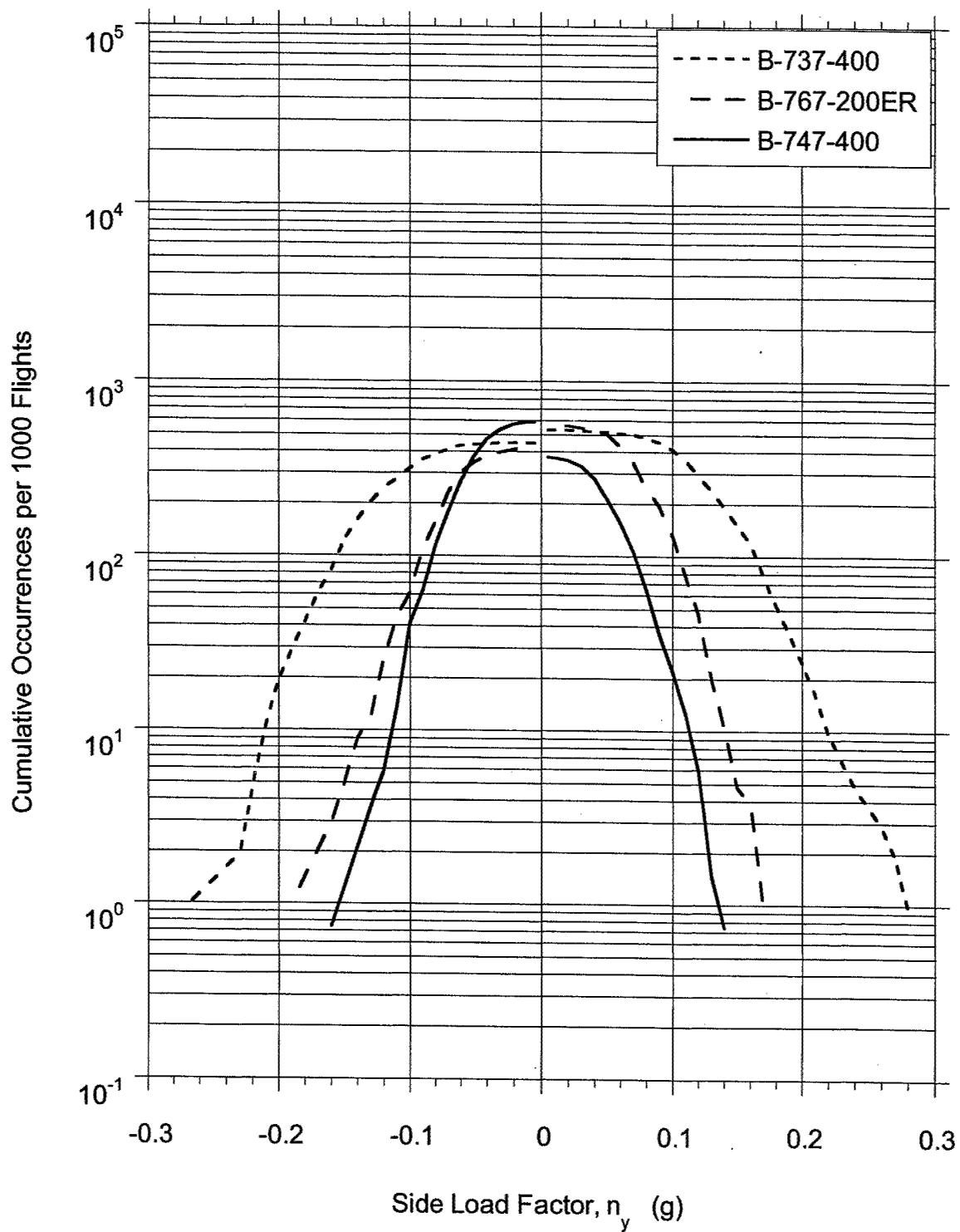
FIGURE D-3. COMPARISON OF CUMULATIVE FREQUENCY OF MAXIMUM SIDE
LOAD FACTOR DURING RUNWAY TURNOFF
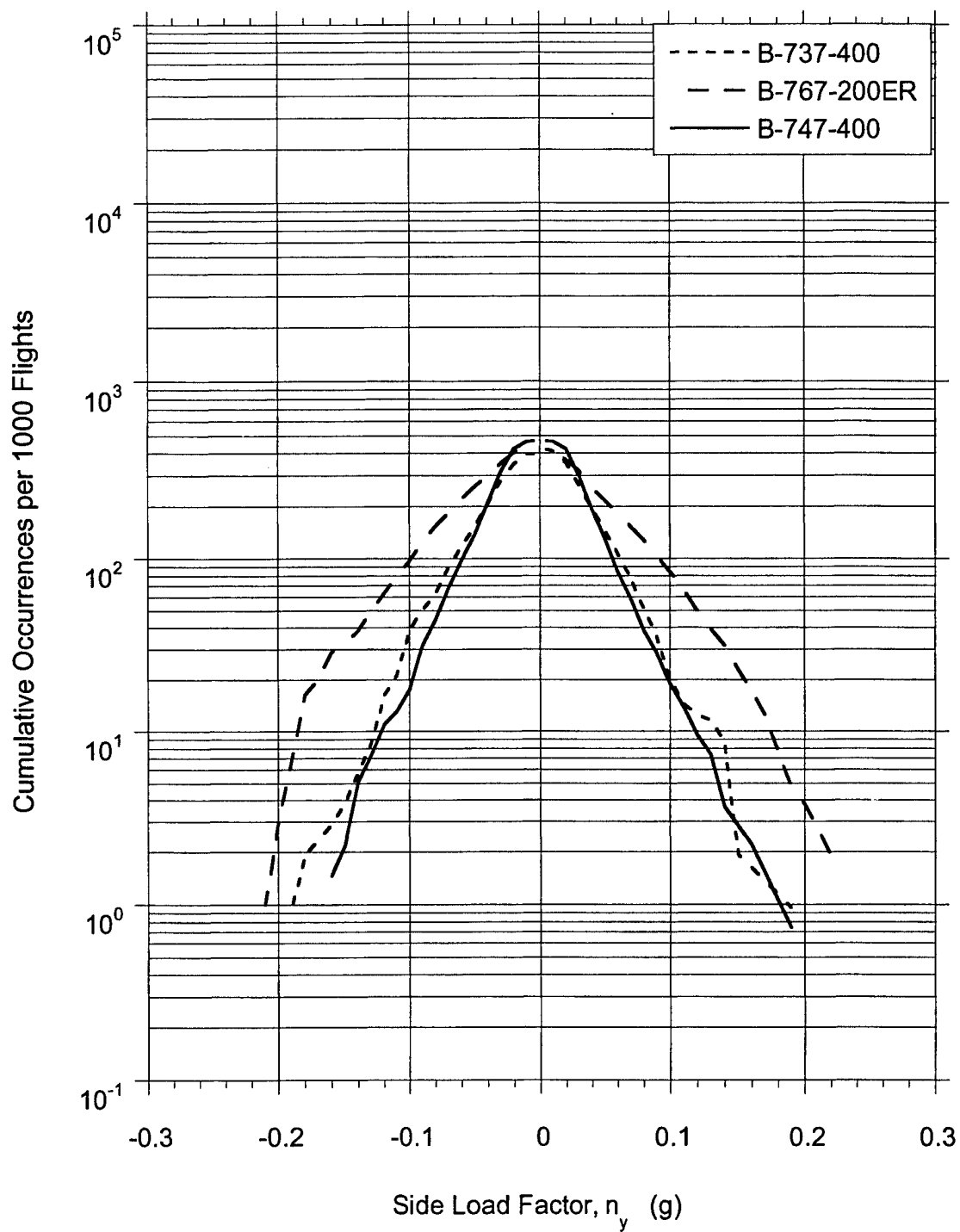
FIGURE D-4. COMPARISON OF CUMULATIVE FREQUENCY OF MAXIMUM SIDE
LOAD FACTOR AT TOUCHDOWN
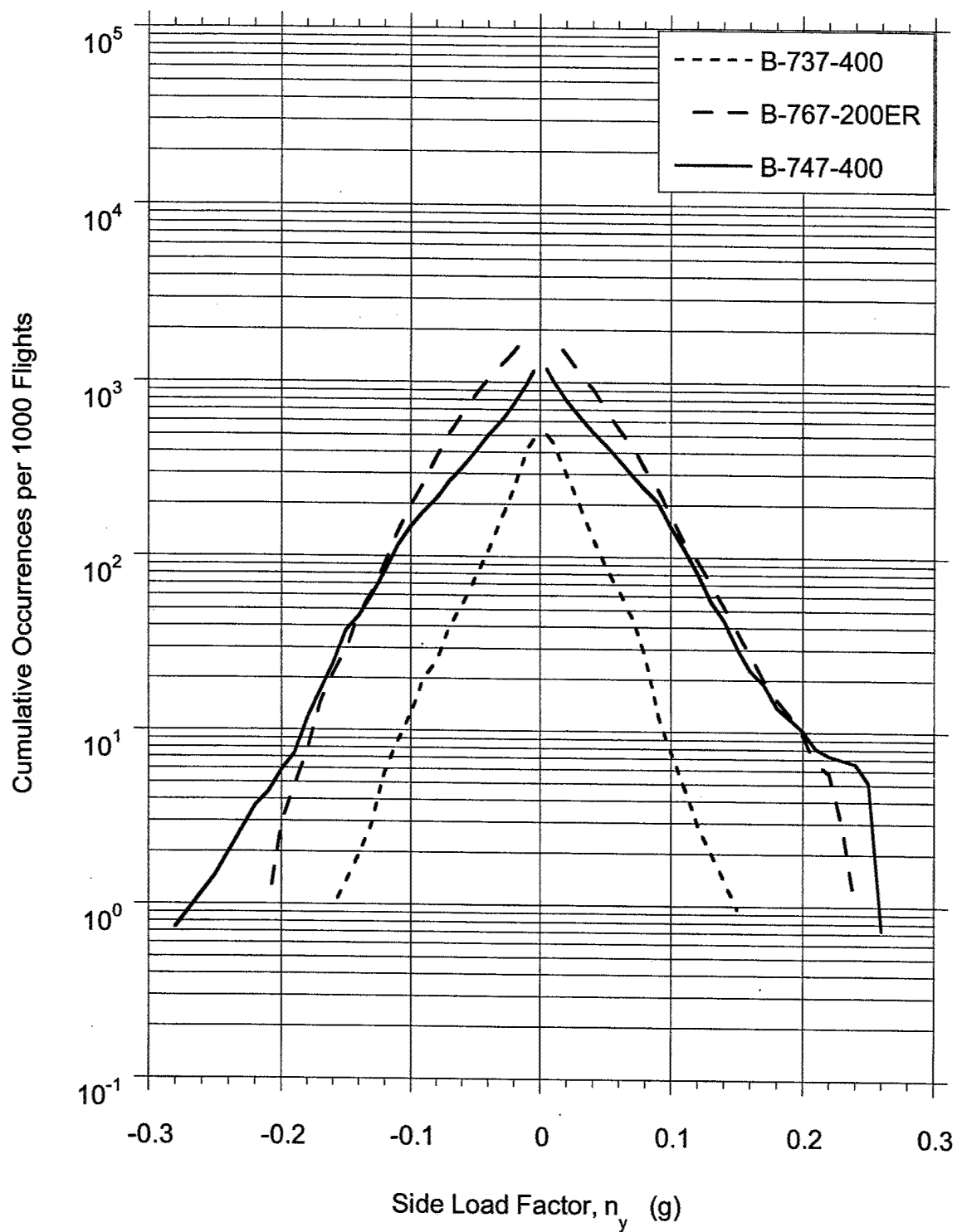
FIGURE D-5. COMPARISON OF CUMULATIVE FREQUENCY OF SIDE LOAD
FACTOR AFTER TOUCHDOWN AND BEFORE THRUST REVERSER DEPLOYMENT
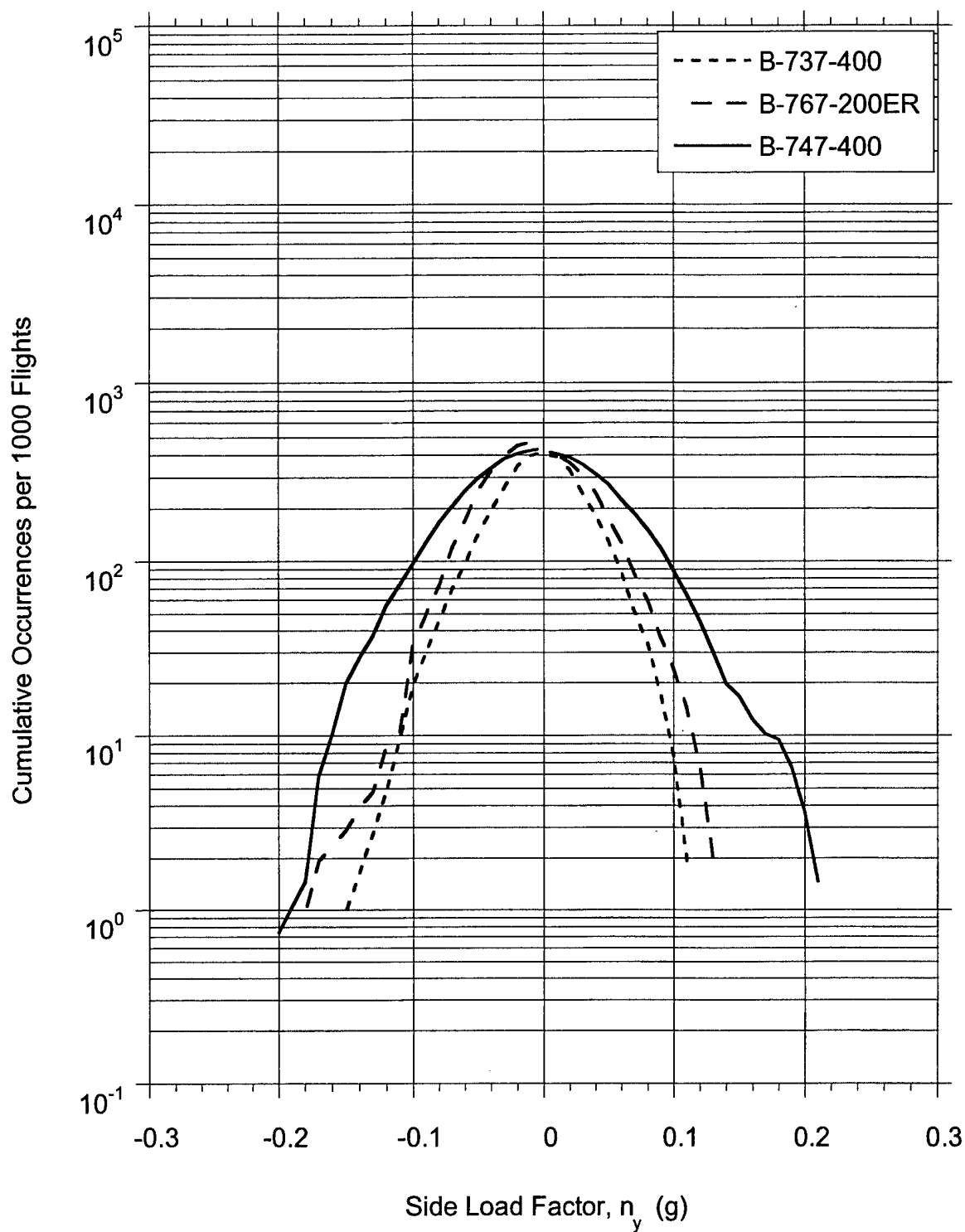
FIGURE D-6. COMPARISON OF CUMULATIVE FREQUENCY OF MAXIMUM SIDE
LOAD FACTOR AT THRUST REVERSER DEPLOYMENT
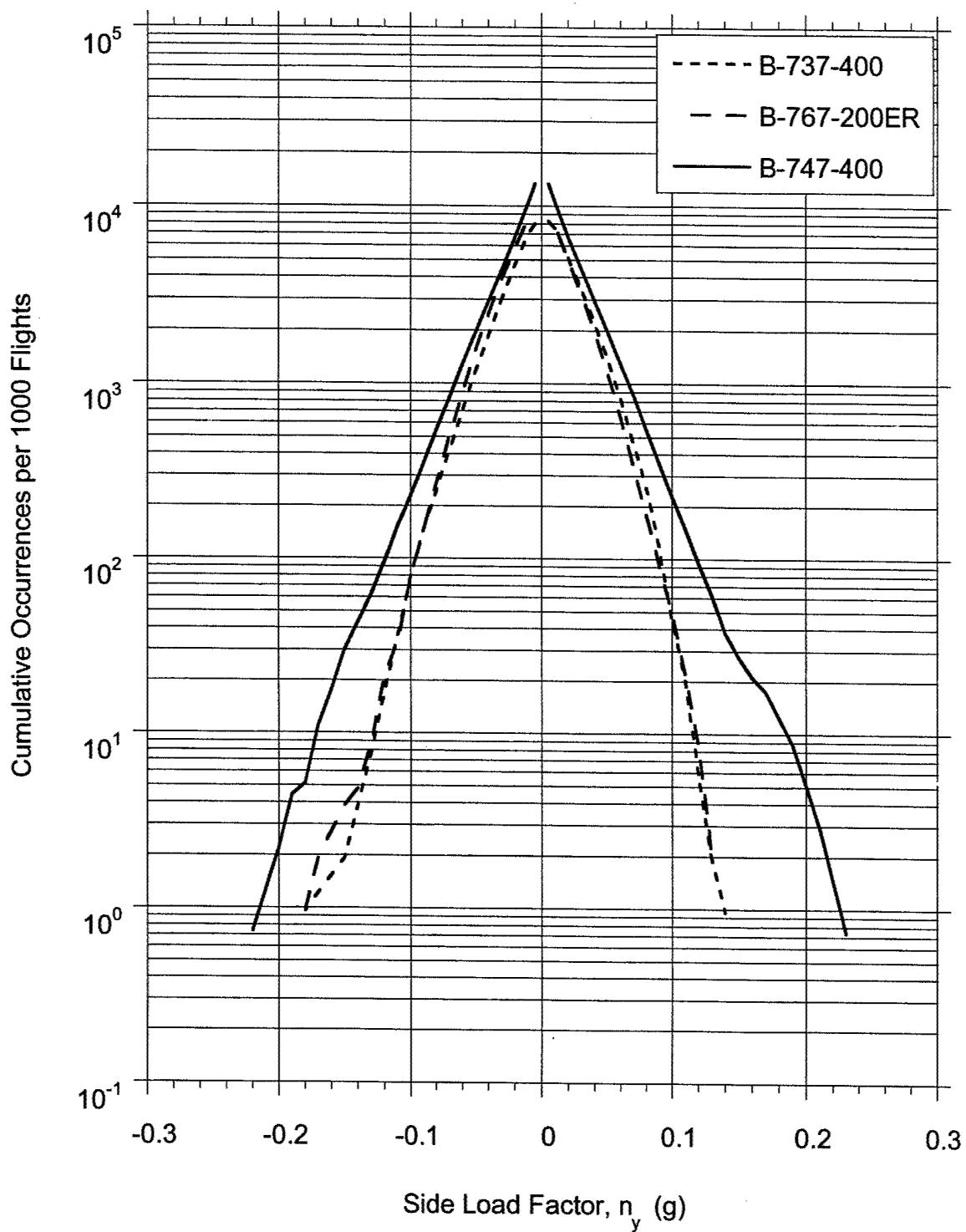
FIGURE D-7. COMPARISON OF CUMULATIVE FREQUENCY OF SIDE LOAD
FACTOR WHILE THRUST REVERSER IS DEPLOYED
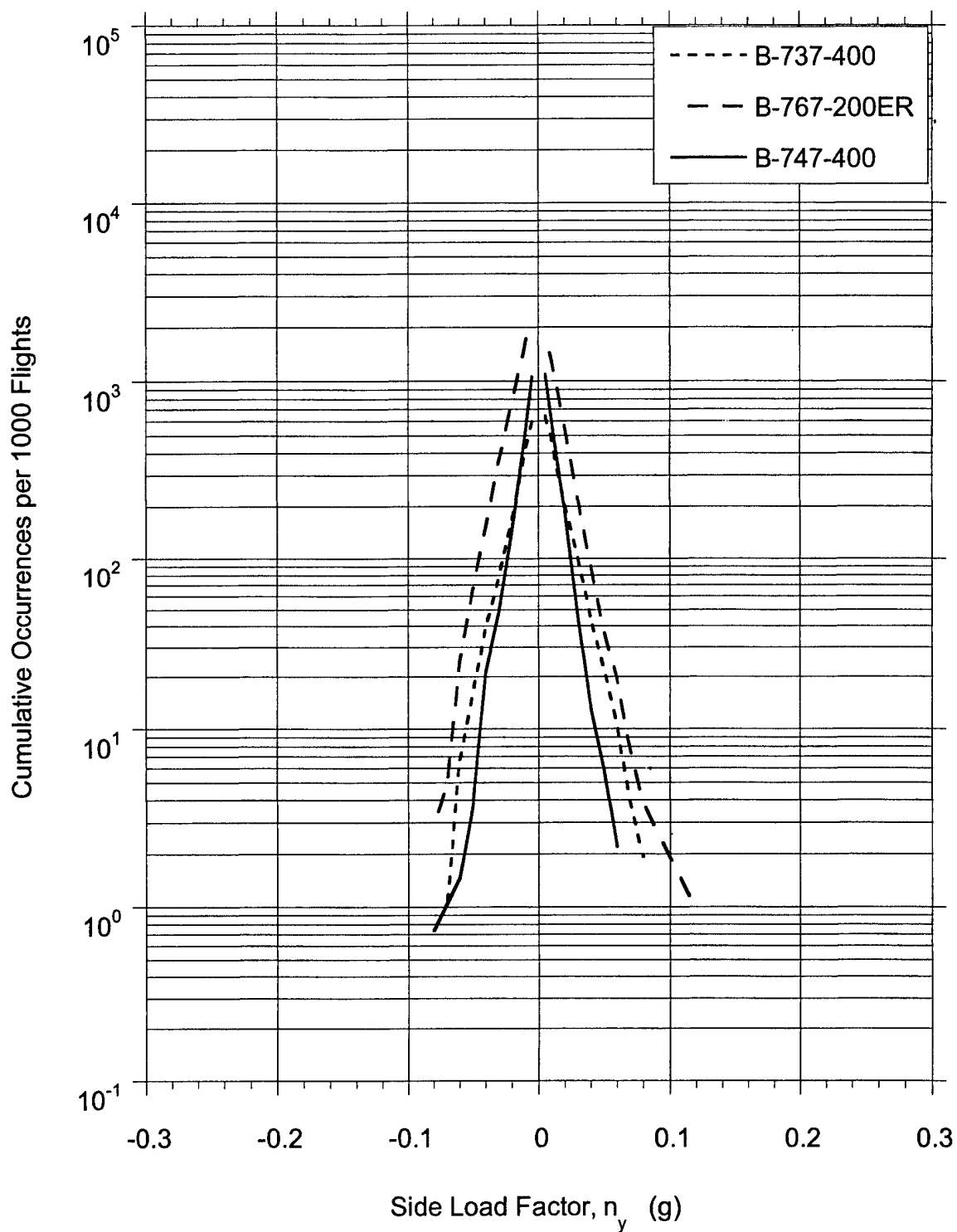
FIGURE D-8. COMPARISON OF CUMULATIVE FREQUENCY OF SIDE LOAD
FACTOR AFTER THRUST REVERSER STOWED DURING LANDING ROLL
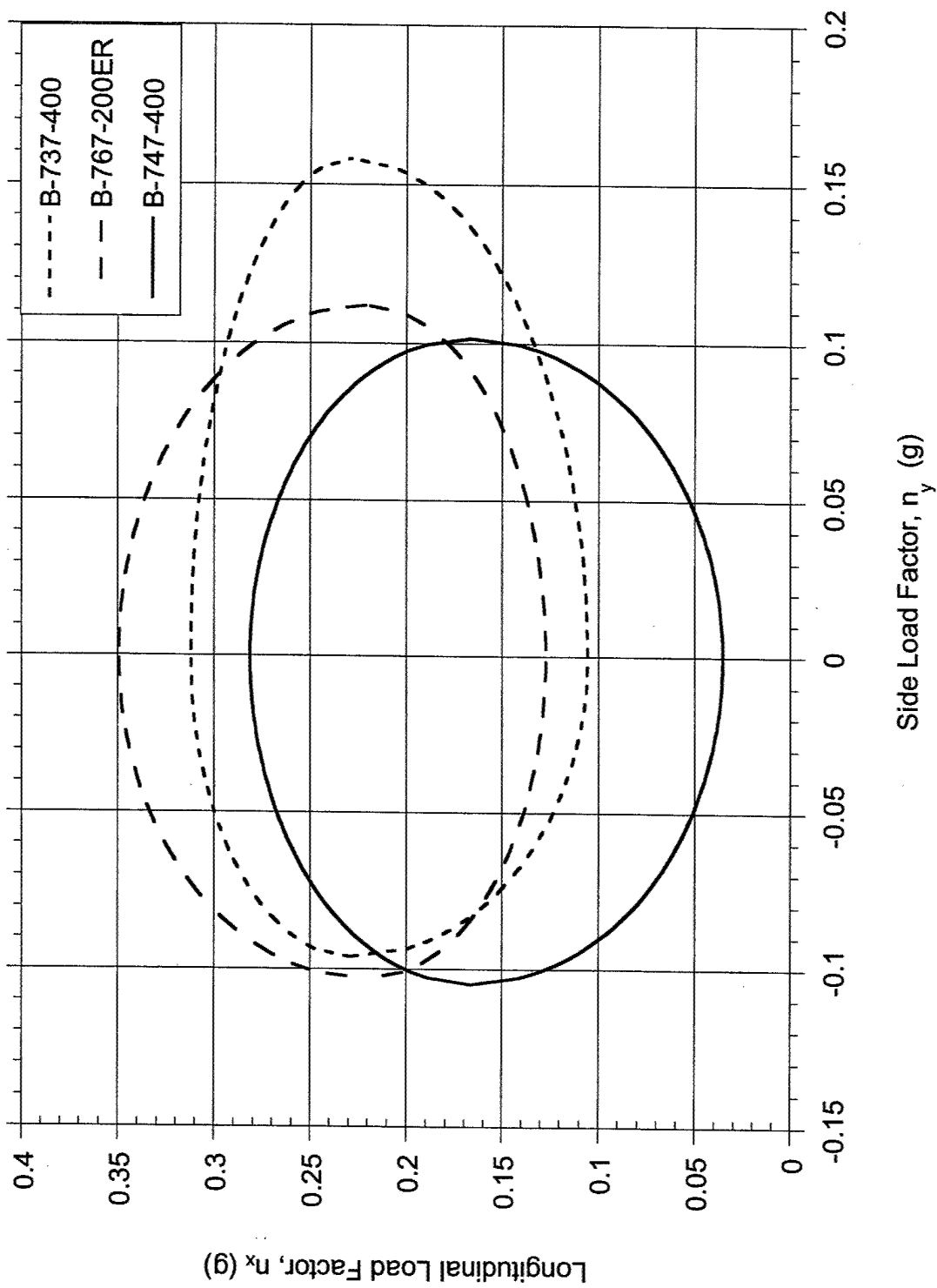
FIGURE D-9. COMPARISON OF 95 PERCENTILE OF COINCIDENT LONGITUDINAL LOAD FACTOR AT MAXIMUM SIDE LOAD FACTOR DURING TAKEOFF ROLL
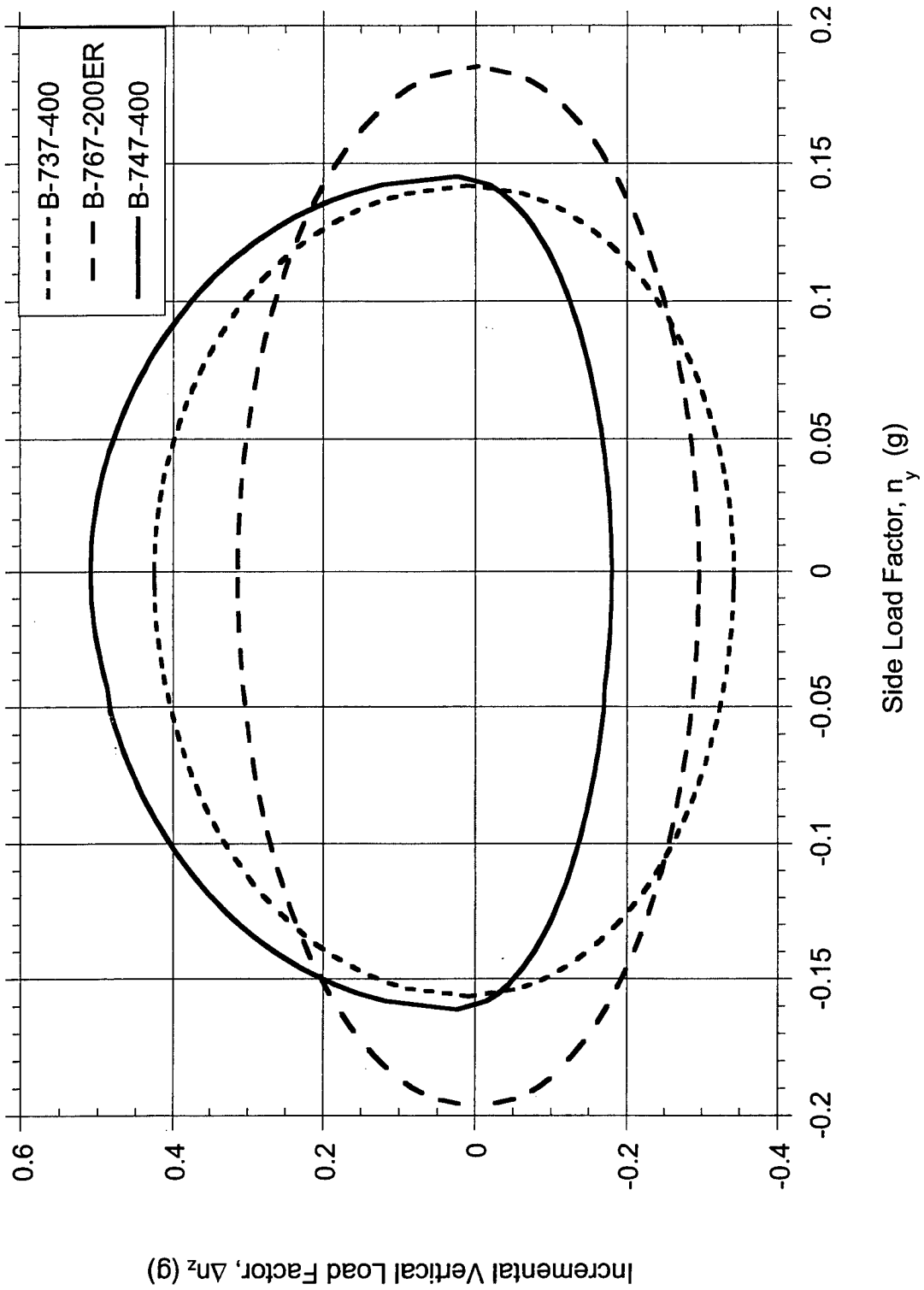
FIGURE D-10. COMPARISON OF 95 PERCENTILE OF COINCIDENT INCREMENTAL VERTICAL LOAD FACTOR AT MAXIMUM SIDE LOAD FACTOR AT TOUCHDOWN
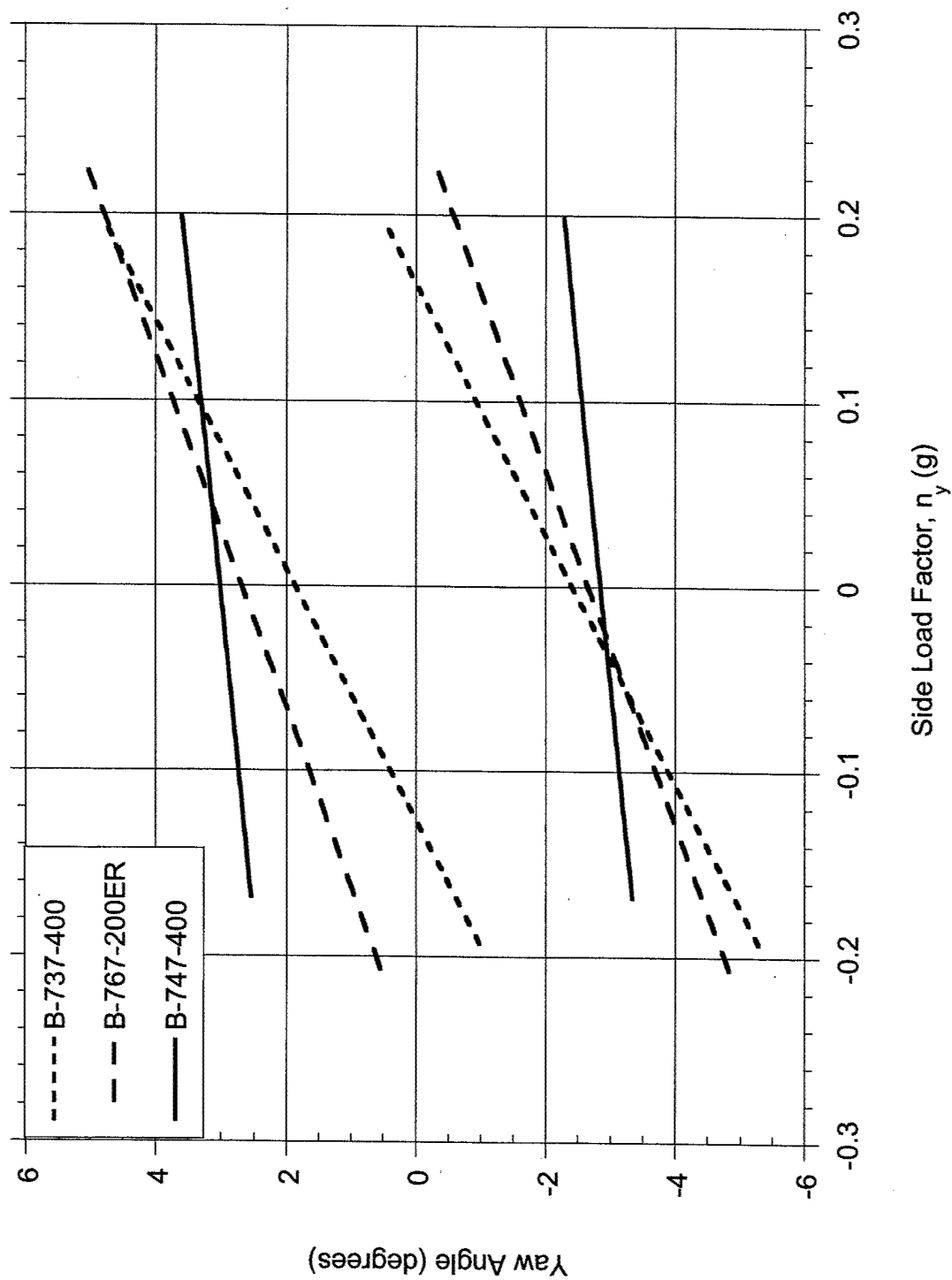
FIGURE D-11. COMPARISON OF 95 PERCENT BOUNDS OF YAW ANGLE AND MAXIMUM SIDE LOAD FACTOR AT TOUCHDOWN
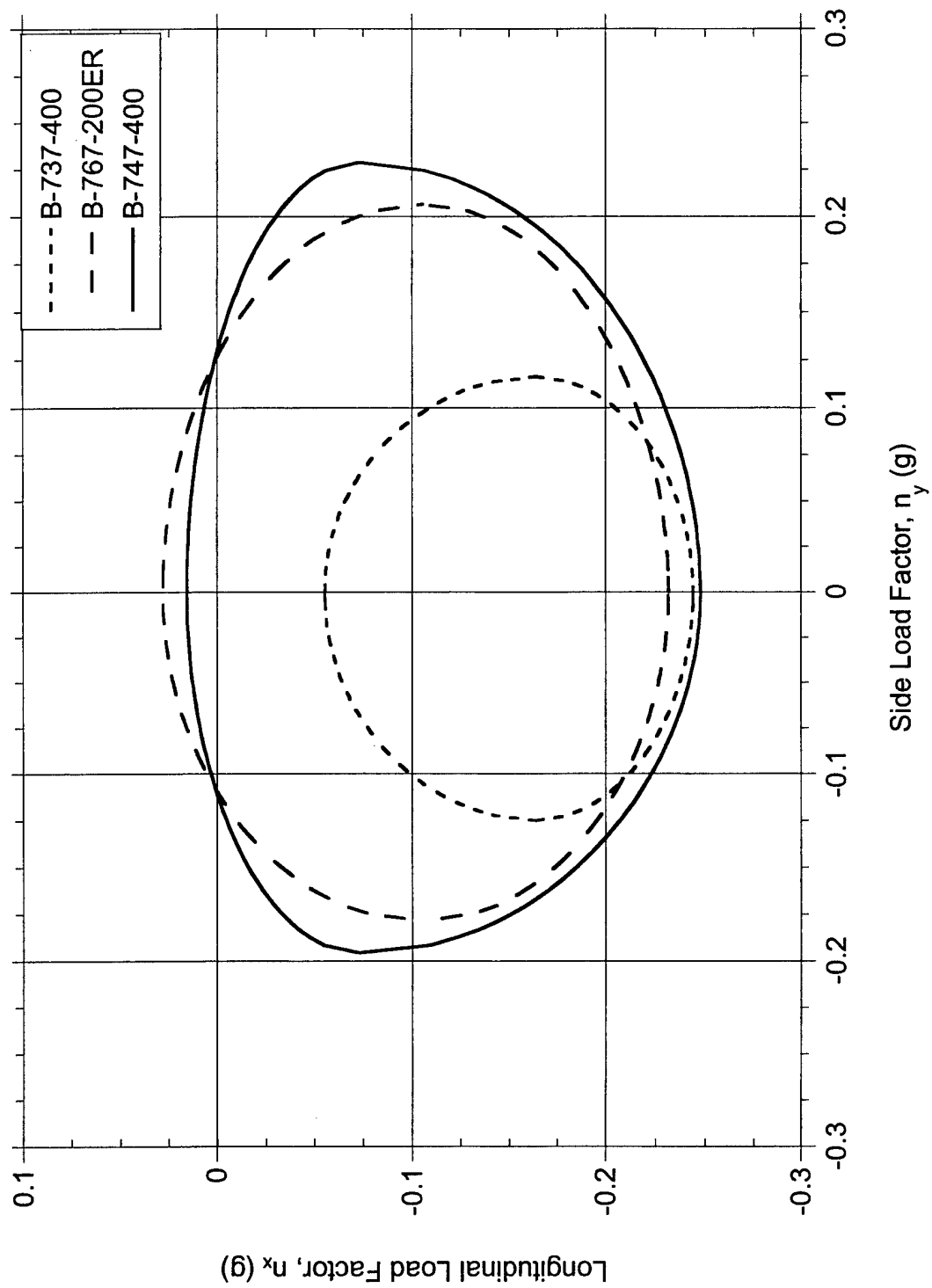
Side Load Factor, n_y (g)

Longitudinal Load Factor, n_x (g)

Legend:
- B-737-400
- B-767-200ER
- B-747-400

FIGURE D-12. COMPARISON OF 95 PERCENTILE OF COINCIDENT LONGITUDINAL LOAD FACTOR AT MAXIMUM SIDE LOAD FACTOR BEFORE THRUST REVERSER DEPLOYMENT
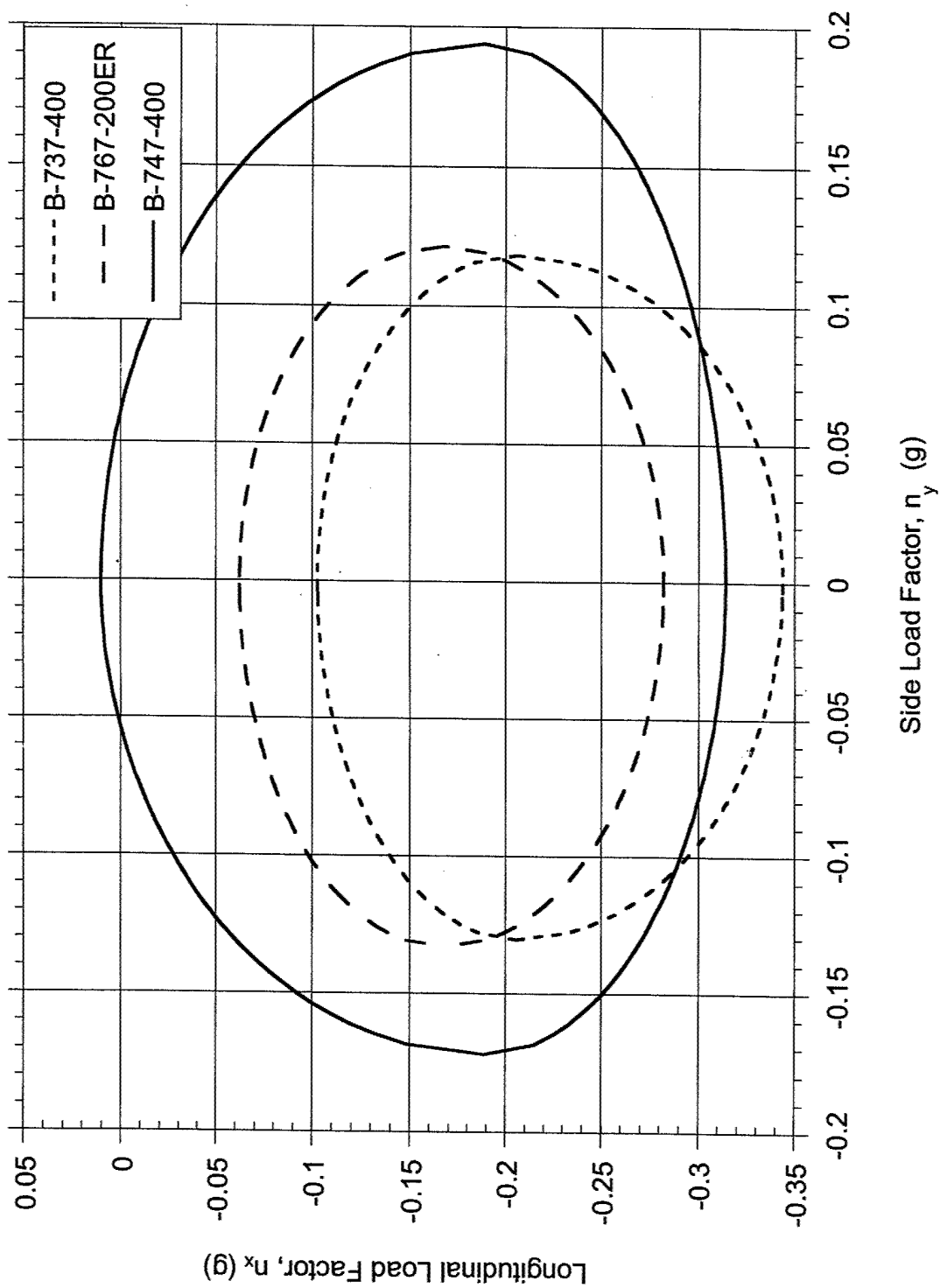
FIGURE D-13. COMPARISON OF 95 PERCENTILE OF COINCIDENT LONGITUDINAL LOAD FACTOR AT MAXIMUM SIDE LOAD FACTOR WHILE THRUST REVERSER IS DEPLOYED
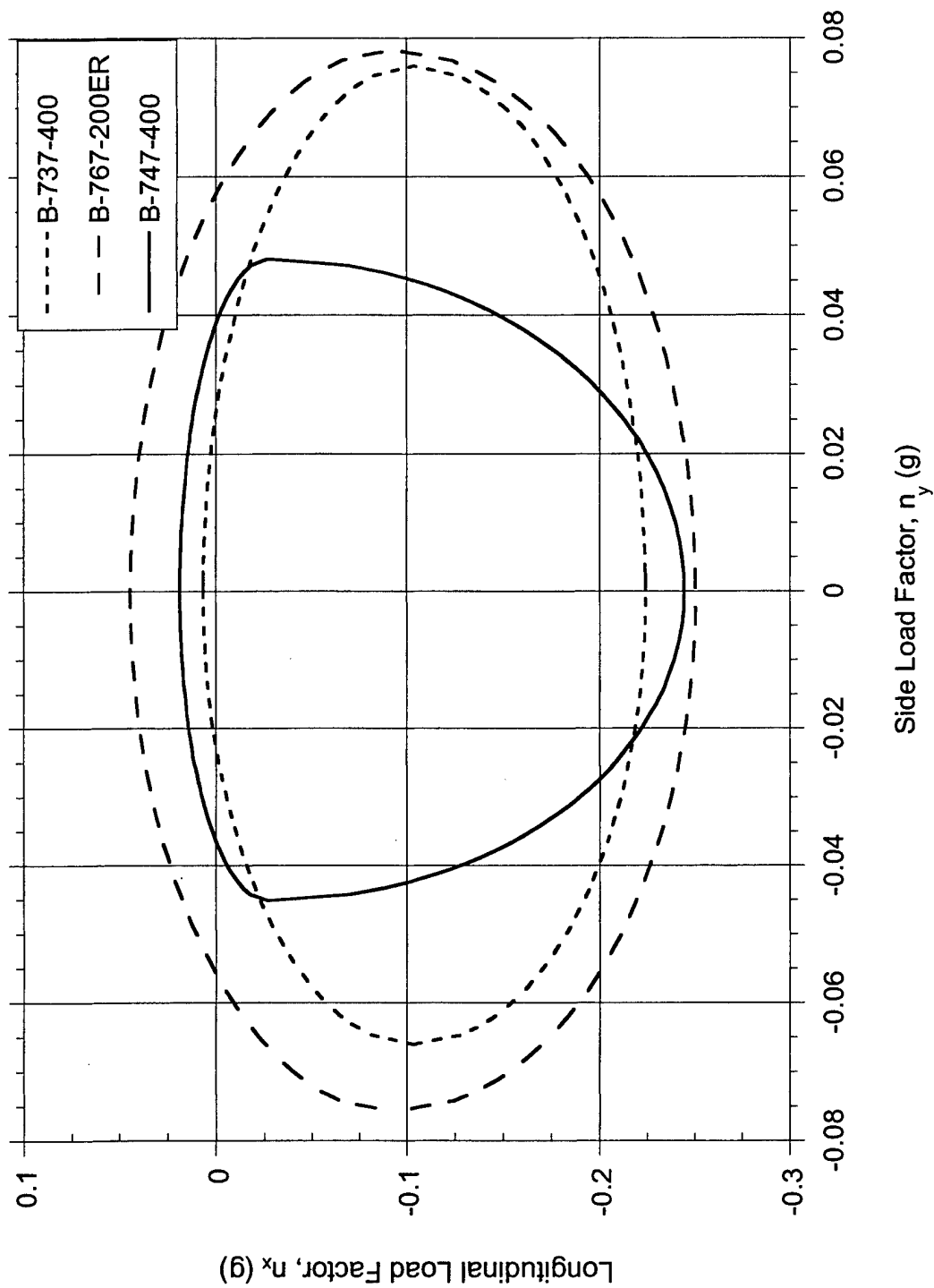
FIGURE D-14. COMPARISON OF 95 PERCENTILE OF COINCIDENT LONGITUDINAL LOAD FACTOR AT MAXIMUM SIDE LOAD FACTOR AFTER THRUST REVERSER STOWAGE DURING LANDING ROLL
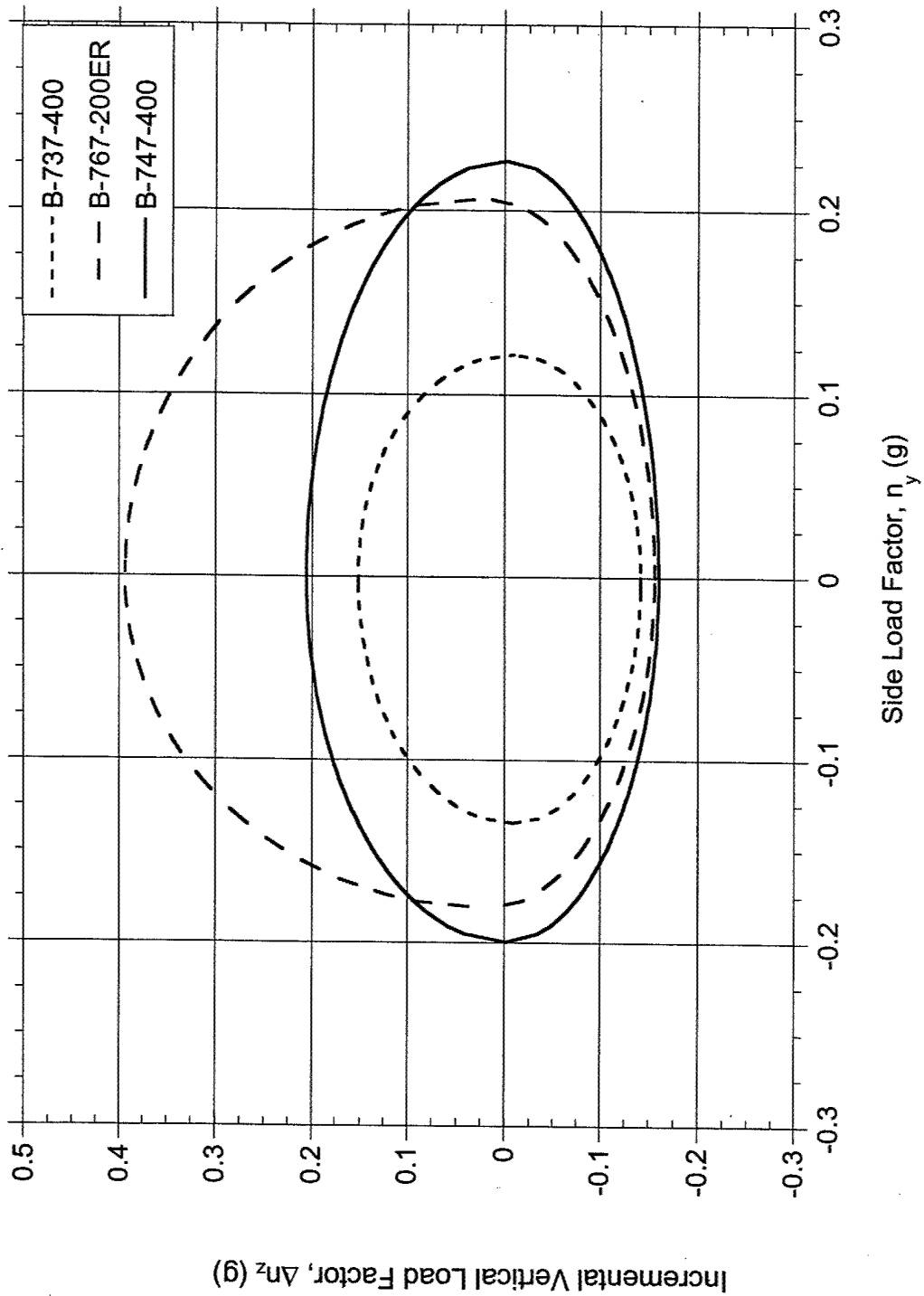
FIGURE D-15. COMPARISON OF 95 PERCENTILE OF COINCIDENT INCREMENTAL VERTICAL LOAD FACTOR AT MAXIMUM SIDE LOAD FACTOR DURING LANDING ROLL
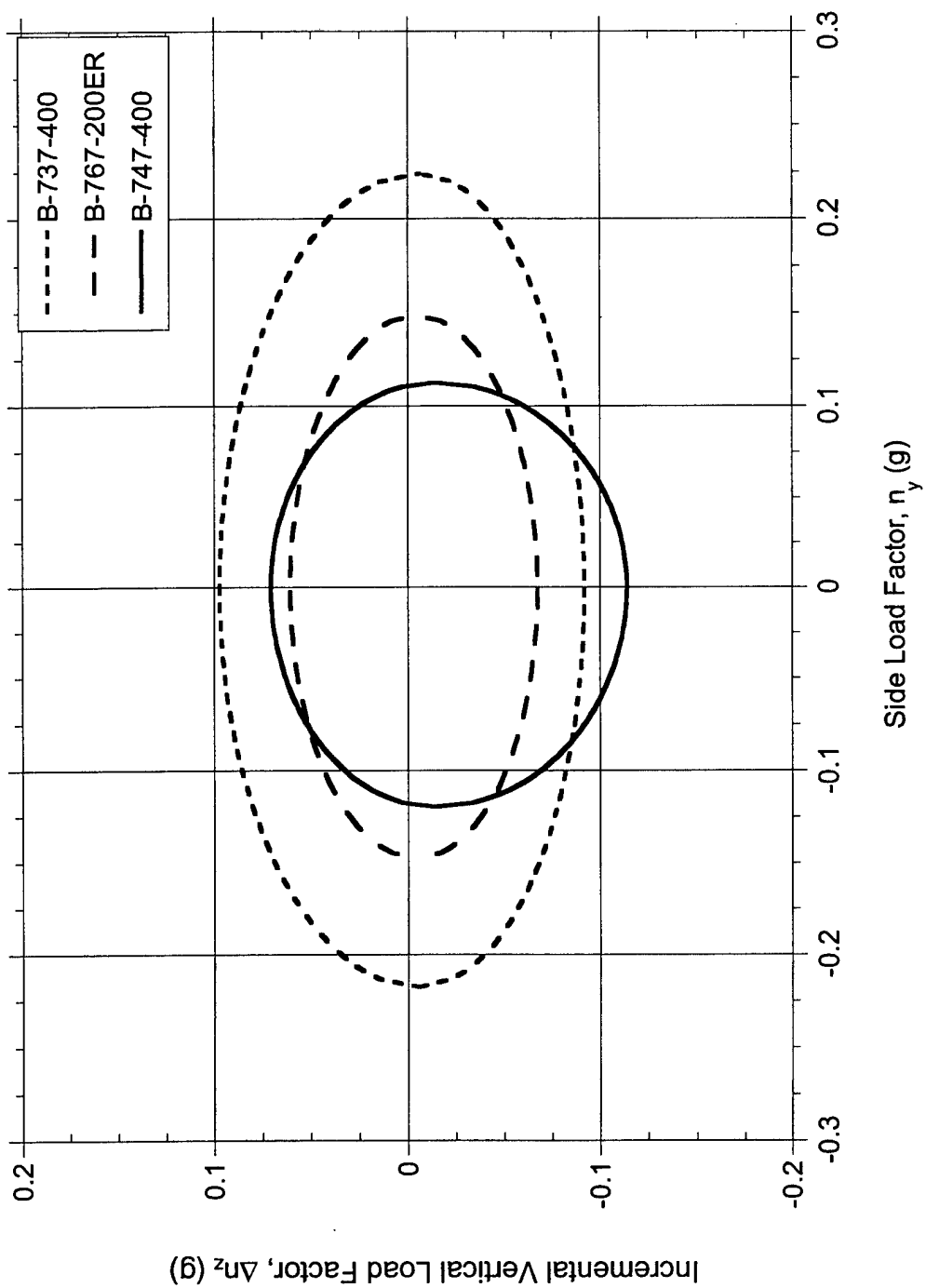
FIGURE D-16. COMPARISON OF 95 PERCENTILE OF COINCIDENT INCREMENTAL VERTICAL LOAD FACTOR AT MAXIMUM SIDE LOAD FACTOR DURING RUNWAY TURNOFF AFTER LANDING
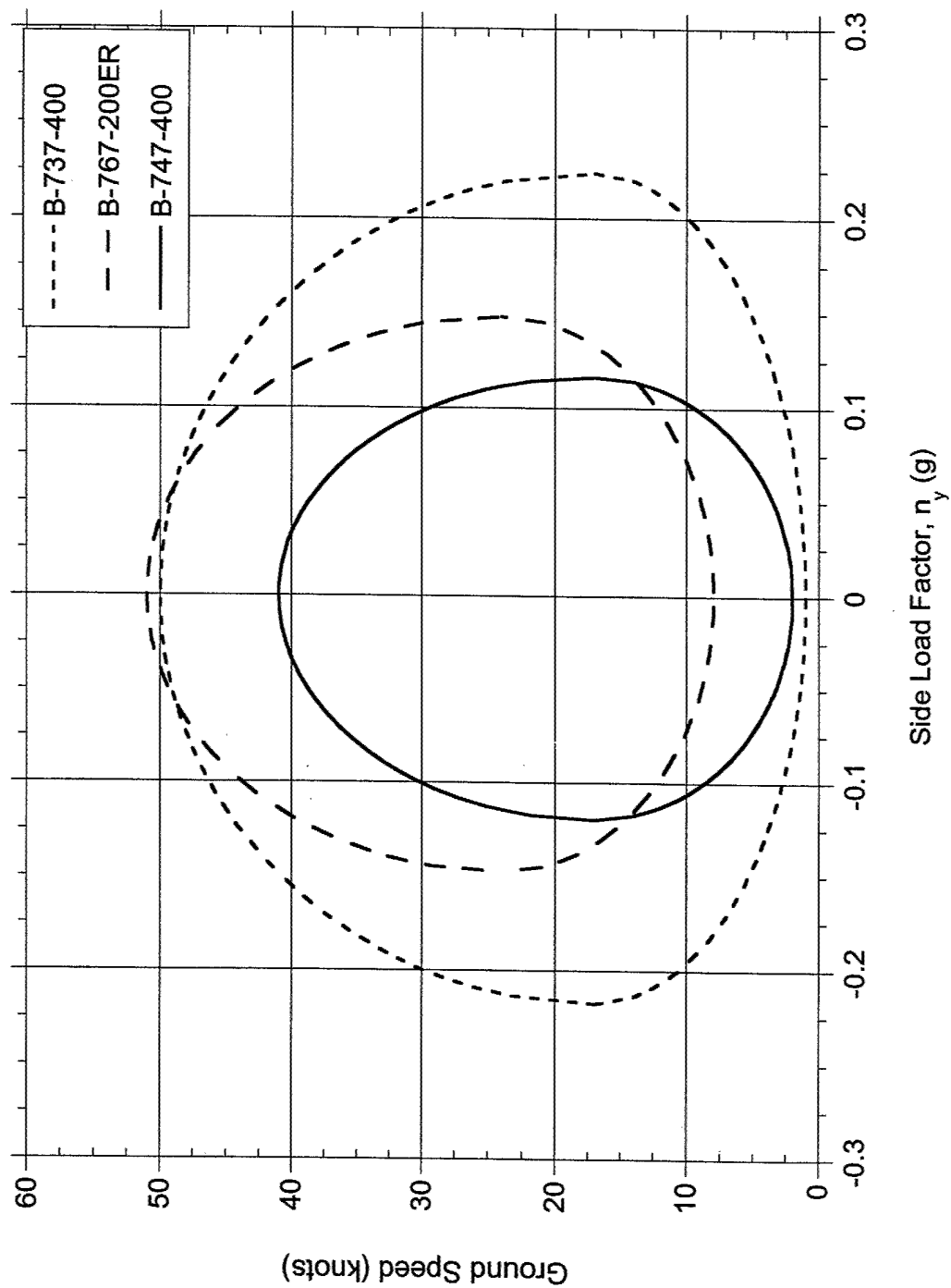
FIGURE D-17. COMPARISON OF 95 PERCENTILE OF COINCIDENT GROUND SPEED AT MAXIMUM SIDE LOAD
FACTOR DURING RUNWAY TURNOFF AFTER LANDING

APPENDIX E—DEVELOPMENT OF A NORMALIZATION PROCEDURE FOR LATERAL LOAD FACTORS DUE TO GROUND TURNING

E.1 INTRODUCTION.

Many variables influence the operational loads environment experienced by an aircraft. For this reason, the statistical loads data for commercial aircraft have been presented by aircraft type. These data from the individual aircraft types would normally be used to predict the loading environment for aircraft judged to be similar. Applying the data to aircraft that differed greatly from the aircraft for which statistical data had been obtained always entails some degree of uncertainty. If the data could be normalized or correlated through the use of fixed parameters that account for differences in aircraft, then a single loading spectrum could be derived that would apply to any aircraft for the prediction of loading spectra. As part of the ground loads data collection effort, statistical data for lateral load factors during ground turning maneuvers are available. The lateral load factors are presented as cumulative occurrences per 1000 flights. The data, when presented in this format, show differences between aircraft types. A data correlation approach has been developed that provides a means to consolidate the available ground turning data from different aircraft into a single relationship. This relationship can be used to estimate the ground turning side load spectra on any aircraft regardless of size.

E.2 DATA ANALYSIS.

Figures E-1 and E-2 present the ground turning side load factor spectra for taxi-out and taxi-in for five commercial aircraft displayed by increasing gross weight. As can be seen, differences exist between the spectra for the five aircraft as well as between the taxi-out and taxi-in operations. Acceleration data are recorded in three directions: normal (z), lateral (y), and longitudinal (x). As shown in figure E-3, the positive y direction is airplane starboard. Thus, the negative load factors represent left turns, and the positive load factors represent right turns. Figures E-4 to E-8 present the spectra from figures E-1 and E-2 in terms of absolute load factor values for each of the airplanes individually. This form of representation more clearly shows the differences in spectra due to left and right turns and taxi-out and taxi-in operations. Review of the spectra results in two useful observations: (1) the taxi-out and taxi-in spectra represent two distinct populations and (2) the spectra between left and right turns do show some asymmetry but are essentially symmetrical. Some of the asymmetry may be due to offsets in the acceleration measurements on specific aircraft. The symmetry is expected to improve as the size of the database increases from 1196 flights for the B-767, 3987 flights for the MD-82, 11,723 flights for the B-737 aircraft, 6226 flights for the A-320, and 1362 flights for the B-747-400.

For the purpose of defining repeated loads spectra, it is commonly assumed that there are differences between the number of occurrences for preflight and postflight operations. However, for left and right turns, or inboard and outboard load cycles, an equal number of occurrences are normally assumed in both directions. Therefore, for this study, the taxi-out and taxi-in spectra will be addressed separately, and the spectra for left and right turns will be considered symmetrical. A symmetrical spectrum of absolute load factor values representing the left and right turns can be obtained by calculating the arithmetic mean of corresponding positive and negative load factor magnitudes. However, the higher load factor levels of the left and right

spectra are based on a few widely spaced load factor measurements at different magnitudes for left and right. While these are actual measurements, inclusion in the arithmetic mean calculation will require interpolation and extrapolation of sparse data that would result in questionable accuracy of the resulting spectra at the higher load factor levels. Thus, these points were eliminated from the symmetrical spectra calculations. Figures E-9 and E-10 show the resulting frequency distributions for the five aircraft for the taxi-out and taxi-in operations, respectively.

E.3 DATA CORRELATION.

Figures E-9 and E-10 clearly show the differences between the spectra for the five airplanes. These cumulative frequency distributions can be approximated by a straight line when plotted in a semilog form as the cumulative occurrences versus the square of the load factor. Figures E-11 and E-12 present the cumulative occurrences in this format for taxi-out and taxi-in respectively. These differences in the slopes of the spectra cannot simply be attributed to any obvious difference in commercial airline ground turning operations at civil commercial airport facilities. A number of unknown and different variables may be contributing to this difference.

It is postulated that the differences in gear geometry, such as main gear track dimension and the distance between main and nose gears, could affect the pilot's turning input options relative to the fixed widths of runways or taxiways. If this were the case, it would account for the differences in the slopes of the spectra. The differences in the zero intercept of the spectra could be the result of operations into different airport types, such as international airports, large and small domestic airports, or airports with multiple or single runways. Differences in the size and the layout of these airports could account for the differences in the total number of turns in taxi-out and taxi-in operations.

Because it is not clear how the gear dimensions affect the ground turning operations, no simple theoretical formulation can be derived to account for these differences. Thus, the study proceeded on the basis that it might be possible to develop some form of empirical relationship that accounts for the effect of gear geometry differences on the side load factor experienced during ground turning. Such a correlation would allow consolidation of the different spectra into a single empirical relationship applicable to all aircraft. Since the spectra exhibit straight-line variations when plotted in semilog form, a general curve fit equation can be employed of the form:

$$N = N_0 e^{-\left(k n_y^2\right)} \tag{E-1}$$

where:

$N =$ the number of cumulative occurrences of any n_y
$N_0 =$ the number of cumulative occurrences at $n_y=0$
$n_y =$ the maximum lateral load factor measured in a ground turn
$k =$ constant reflecting the influence of the main and nose landing gear dimensional arrangement on the expected side load factor magnitude during a ground turn in comparison to other aircraft

Correlative analyses of the measured spectrum data and various aircraft gear dimensional combinations using a curve fit equation of the form defined by equation E-1 was conducted. The purpose was to determine the combination of the landing gear geometry dimensions and the associated values of N_0 and of k that would provide the best single representation of the measured values for all the aircraft when used in equation E-1. It was determined that the k constant that provided the best overall agreement was of the form $d^m t$, where d represents the landing gear base dimension and t represents the landing gear track dimension.

Figure E-13 shows the dimensional references of the landing gear arrangement, and table E-1 shows the dimensional values for the three aircraft of this study. Thus, the optimum curve fit equation that will account for the influence of gear geometry for different aircraft thus is represented by:

$$N = N_0 e^{-\left(d^m t n_y^2\right)} \tag{E-2}$$

A general curve fit equation of the form of equation E-2 was applied to the measured spectra to solve for the constants N_0 and m using the Levenberg-Marquardt algorithm. This algorithm uses an iteration procedure to produce a curve fit until the Chi-square does not change for a specified number of iterations or the percent change in the normalized Chi-square is less than a specified allowable error. The allowable error used in the curve fit was set at 1 percent. Discussion of the procedure is beyond the scope of this report, but can be found in reference E-1. Figures E-14 to E-23 show the curve fits obtained for the taxi-out and taxi-in cases for the five airplanes.

Table E-2 presents the values for the constants derived from the curve fits to the measured spectra. Average values shown for the constants represent the arithmetic means of the constants obtained for the individual aircraft.

The reliability of using the gear geometry dimensions in the form of $d^m t$ to account for differences in the measured spectra can now be tested by comparing the mean cumulative occurrences derived from the measured data with the cumulative occurrences calculated from the derived relationship expressed by equation E-2 using the average values shown in table E-2. Figures E-24 to E-28 present the comparisons of taxi-out and taxi-in side load factor spectra obtained from the measured data and as calculated. In these comparisons the calculated spectra are considered quite acceptable for determining repeated loads spectra. How far these results can be extrapolated to other aircraft with widely varying landing gear dimensional arrangements cannot be known until additional data from such aircraft becomes available. However, within the variations covered by the study aircraft, the present approach would be expected to provide acceptable results. Figure E-29 presents an envelope of the gear dimensions covered by the study aircraft.

E.4 DEFINITION OF DESIGN CONDITION.

Not only can the approach presented be used to determine the expected ground turning acceleration spectrum for a specific aircraft, but it can also be used to define a static design condition for ground turning. At present, an arbitrary value of 0.5 g is specified for the maximum required ground turning load condition. If it is agreed that an aircraft is operated in

accordance with its perceived capability, as determined by its landing gear dimensional arrangement, then a design condition can be specified for an airplane based on its landing gear geometry. All that is necessary is to specify a maximum acceptable exceedance level of the design loading condition, such as once per lifetime for limit load. Equation E-3 is used to determine the load factor level for a specific level of exceedances N.

$$n_y = \sqrt{\ln \frac{N_0}{N} \frac{1}{d^m t}}$$ (E-3)

where the values of N_0, and m are as defined in table 2 for taxi-out and taxi-in.

Establishment of an acceptable exceedance level of limit load is outside the scope of this study. Table E-3 shows the respective cumulative frequency per 1000 flights of a 0.5-g lateral load factor turn for each of the airplanes. The data show that the B-737-400 has the highest frequency of encountering a 0.5-g lateral load factor during ground turning. If this cumulative frequency is taken as establishing an acceptable design level, then the lateral load factor expected for the same frequency for other airplanes can be predicted. Figure E-30 shows the lateral load factor levels for the five airplanes in this study based on the cumulative frequency of the B-737-400 for a 0.5-g turn.

E.5 CONCLUSIONS.

The approach and the derived equation for mathematically predicting ground loads turning spectra are based on the average experiences of five quite different aircraft operated by different airlines at different airports. The mathematically determined ground turning load spectra will, therefore, never exactly duplicate the measured spectra. However, the approach presented does provide a very reasonable representation of the expected ground turning side load factors, as well as provide a better basis for predicting repeated side turning loads than has heretofore been available. It is always prudent to re-evaluate the approach as more data become available from additional aircraft and operators.

It appears that the maximum lateral load factor that can be expected during ground turning operations is influenced by the size of the airplane in terms of the landing gear base and track dimensions. Thus, the static design requirement of a fixed lateral load factor of 0.5 g for ground turning operations regardless of aircraft size will penalize the larger aircraft. A design lateral load factor based on a fixed level of occurrences or probability would provide a more consistent strength level.

E.6 REFERENCES.

E-1.   Press, William H., Flannery, Brian P., Teukolsky, Saul A., and Vetterling, William T., "Numerical Recipes in C, the Art of Scientific Computing," Cambridge University Press, 1992.
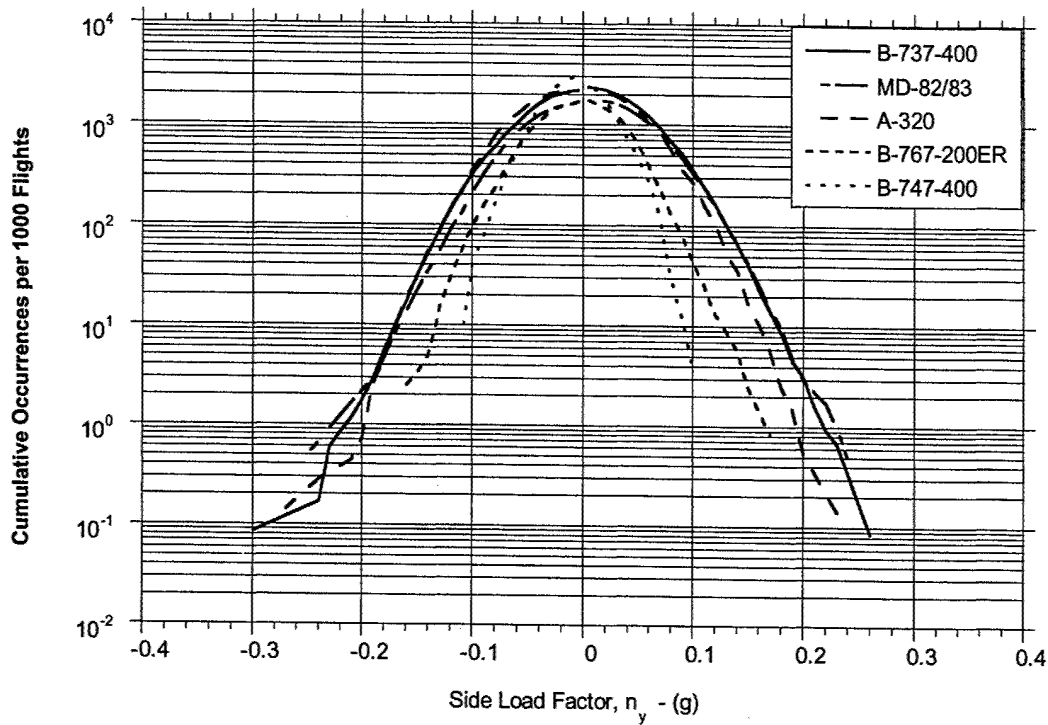
FIGURE E-1. CUMULATIVE FREQUENCY OF LATERAL LOAD FACTOR DURING GROUND TURNING, TAXI-OUT
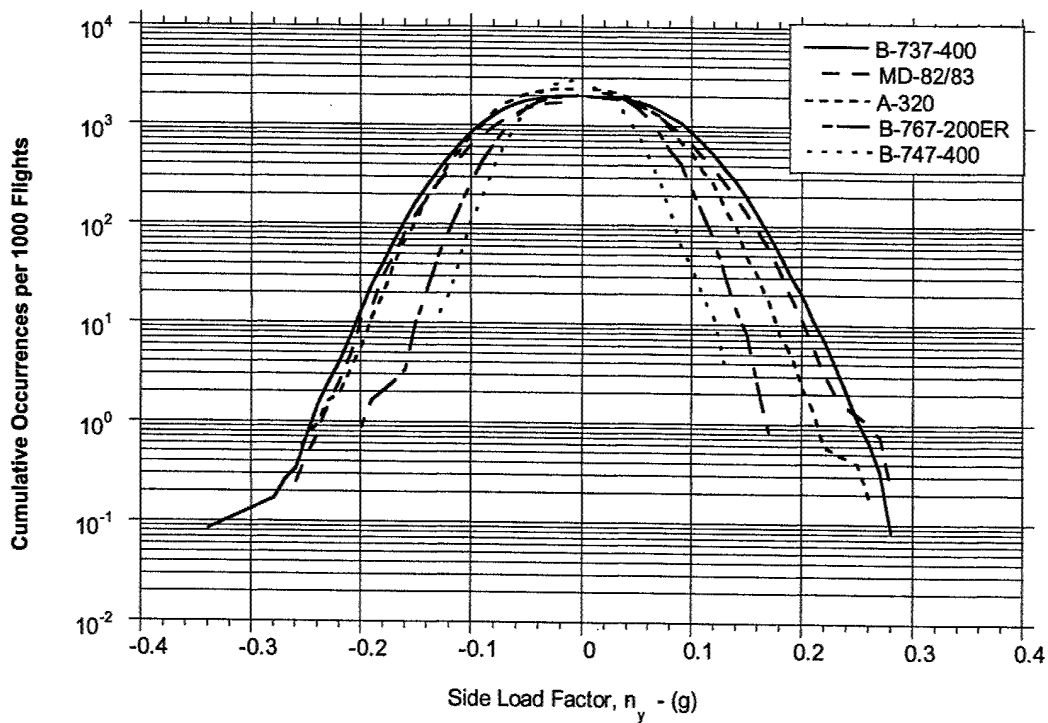

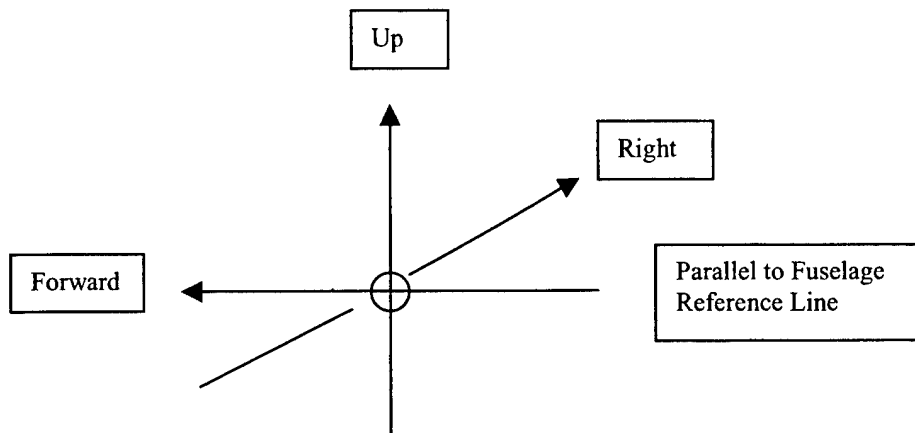FIGURE E-2. CUMULATIVE FREQUENCY OF LATERAL LOAD FACTOR DURING GROUND TURNING, TAXI-IN
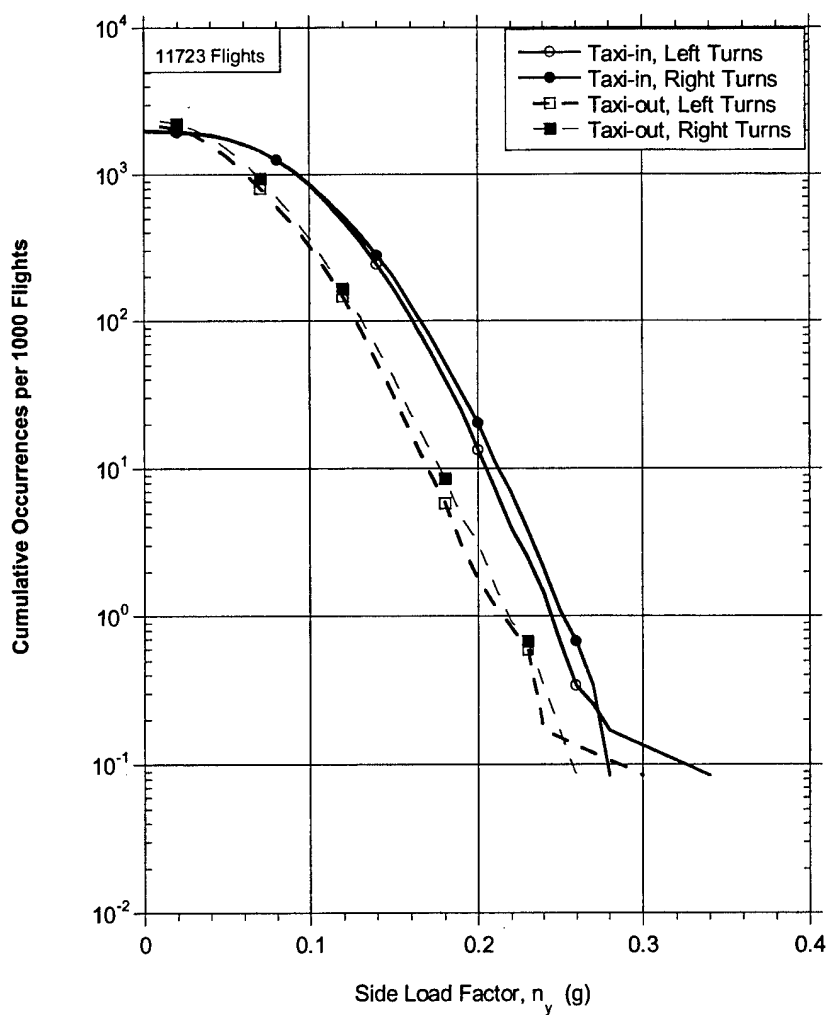
FIGURE E-3. SIGN CONVENTION

FIGURE E-4. CUMULATIVE FREQUENCY OF LATERAL LOAD FACTOR DURING
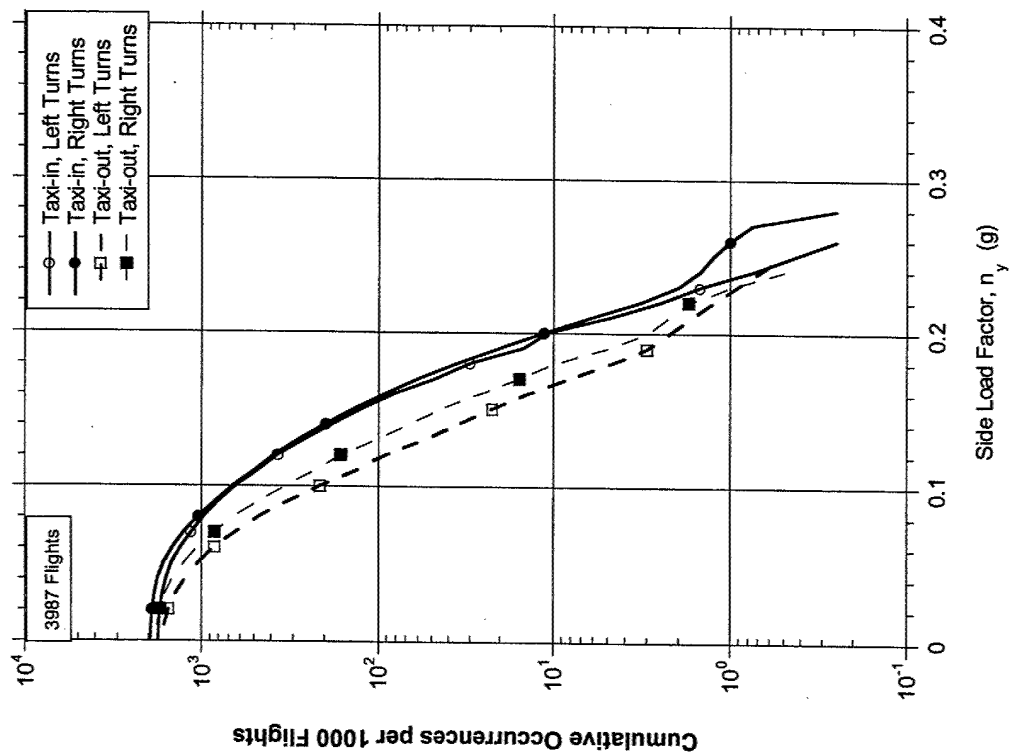GROUND TURNING, B-737-400

FIGURE E-5. CUMULATIVE FREQUENCY OF LATERAL
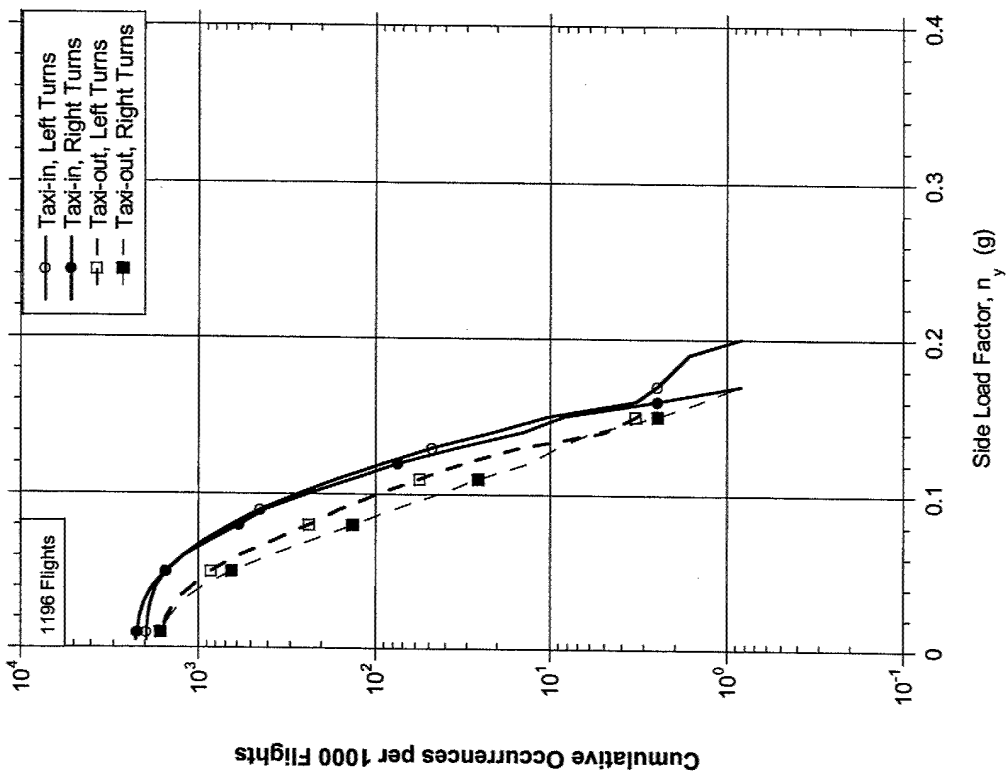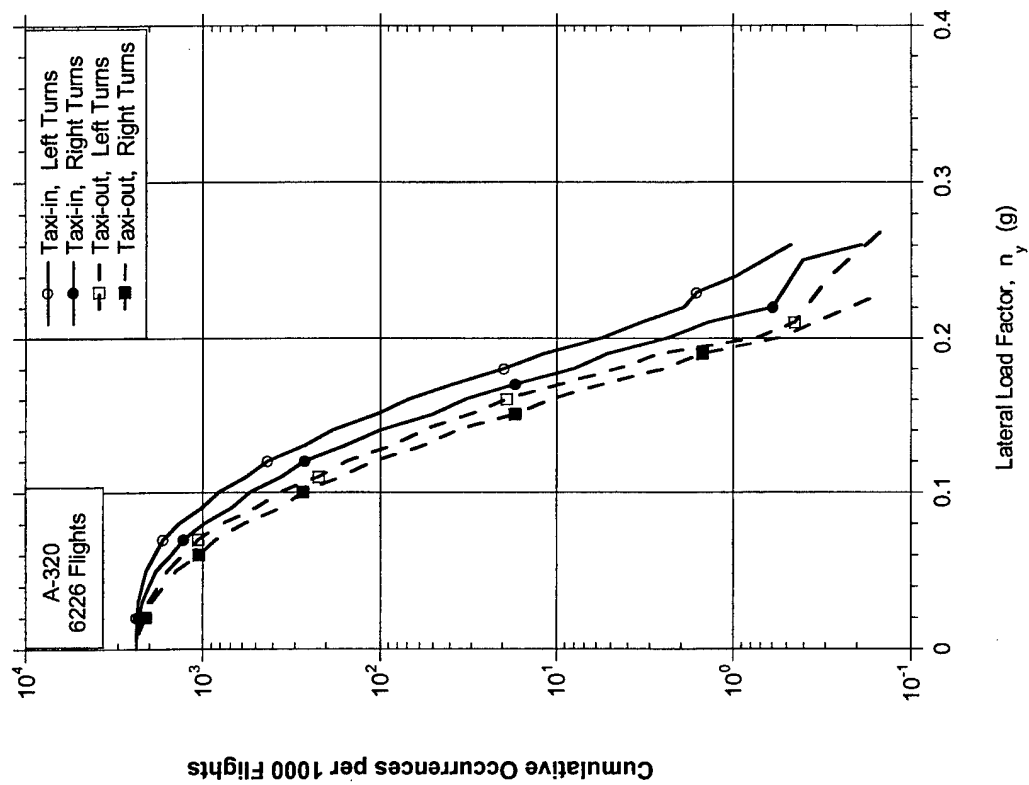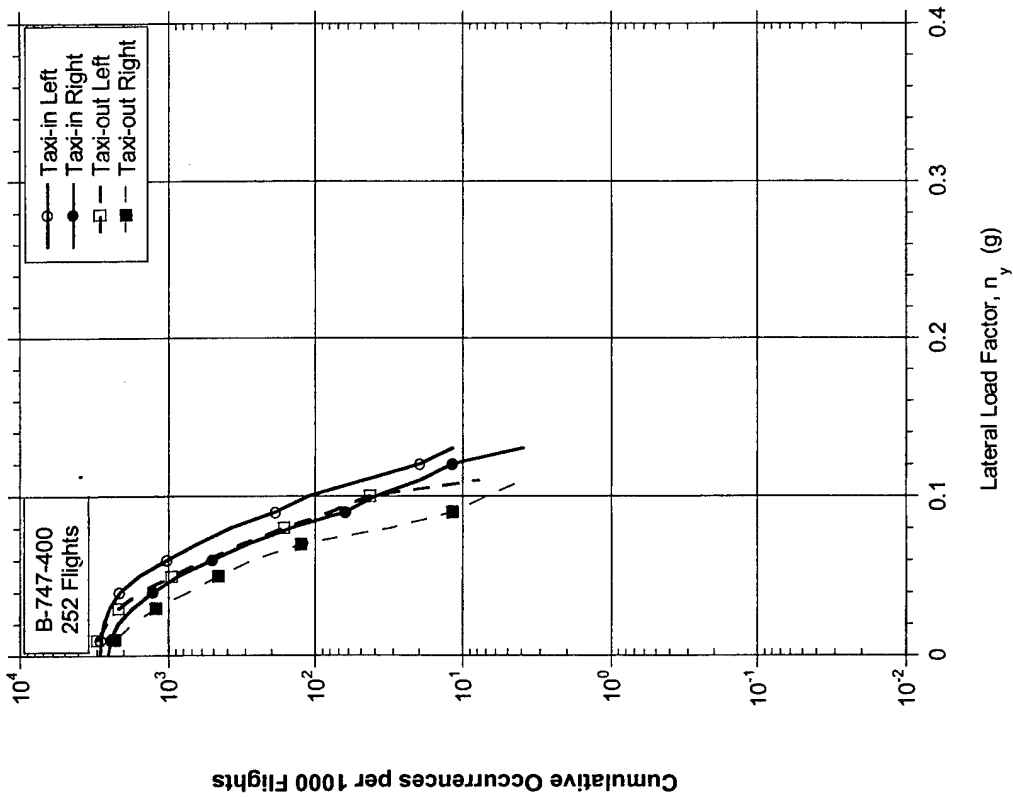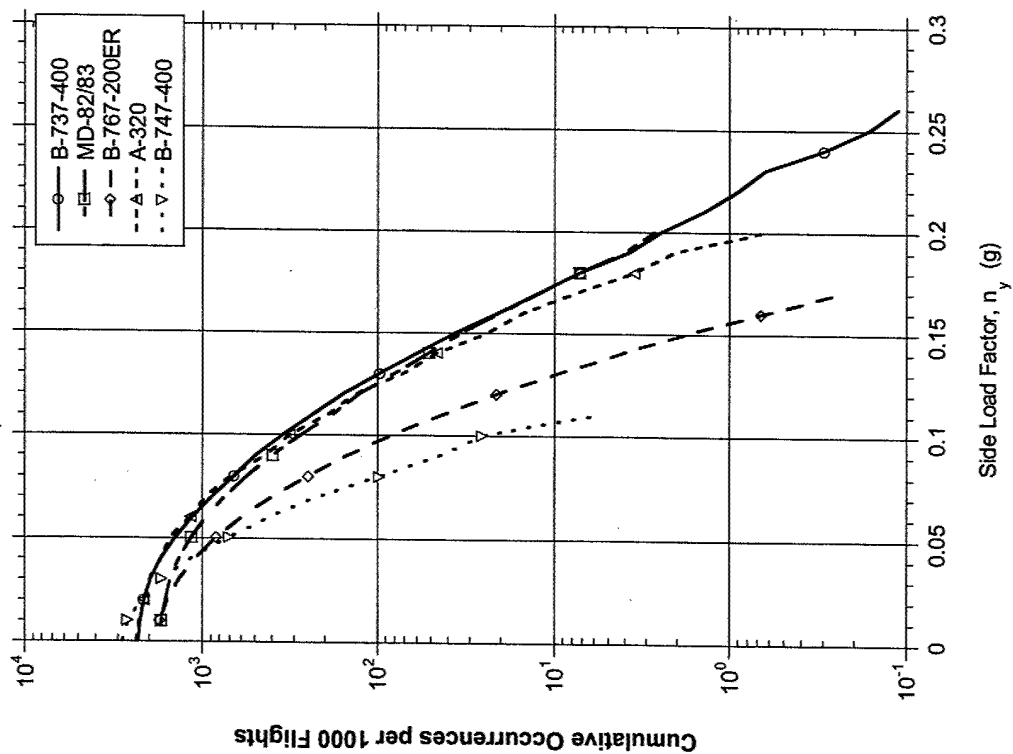LOAD FACTOR DURING GROUND TURNING, MD-82/83

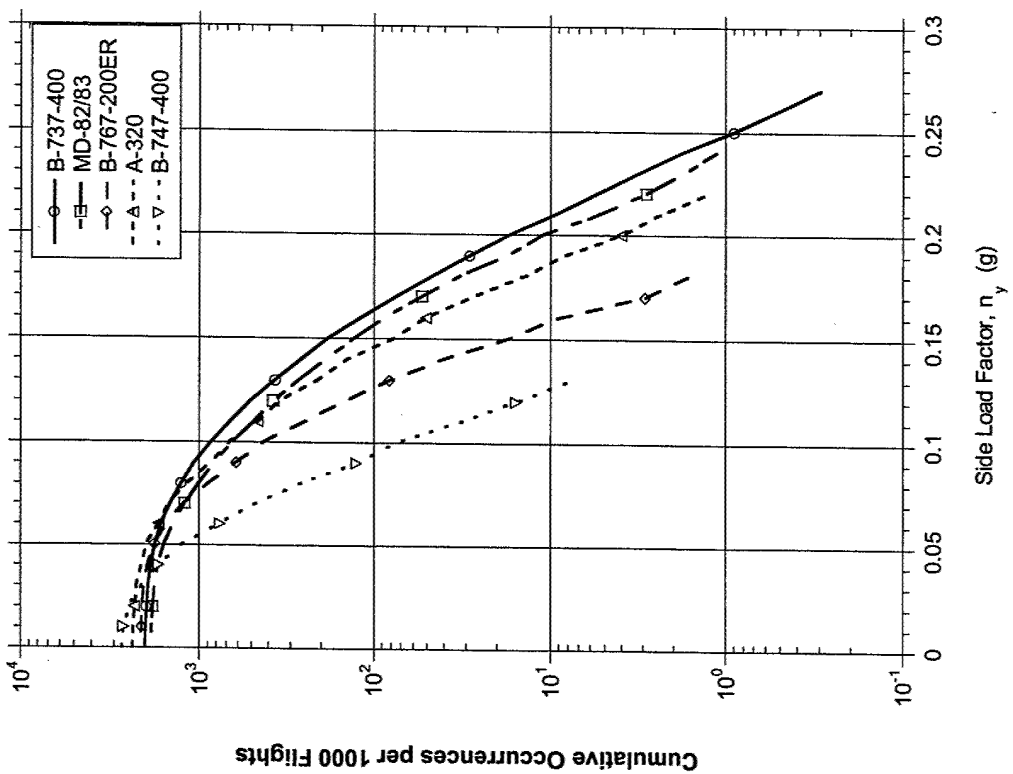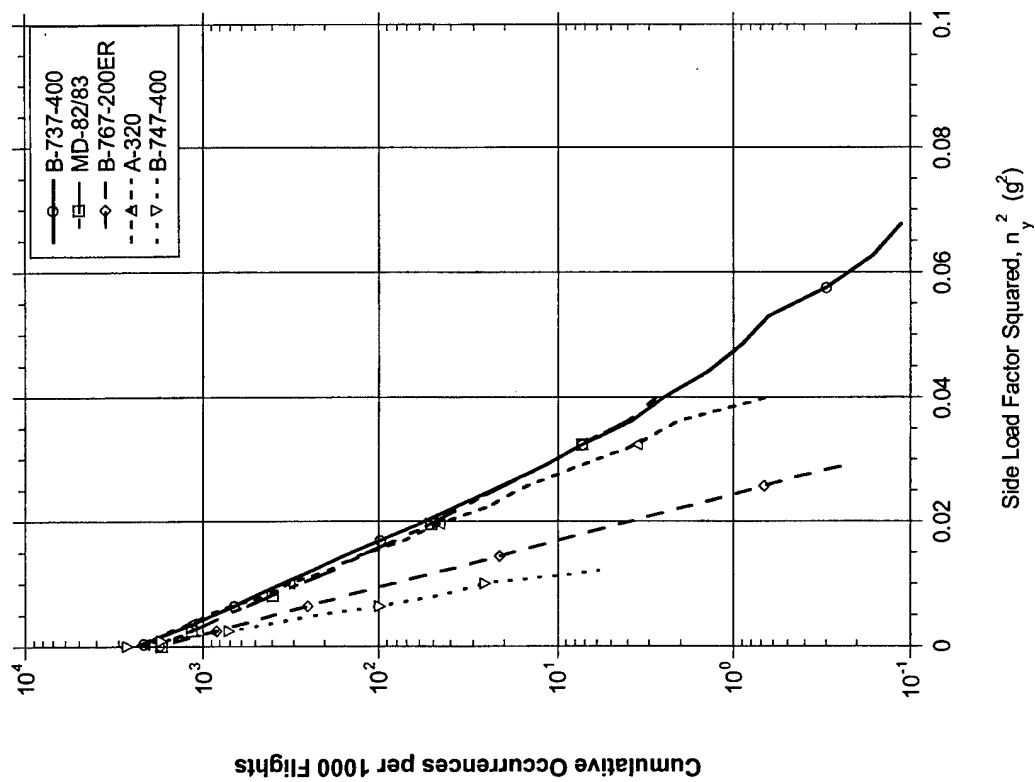FIGURE E-6. CUMULATIVE FREQUENCY OF LATERAL
LOAD FACTOR DURING GROUND TURNING, B-767-200ER

FIGURE E-8. CUMULATIVE FREQUENCY OF LATERAL LOAD FACTOR DURING GROUND TURNING, B-747-400

FIGURE E-7. CUMULATIVE FREQUENCY OF LATERAL LOAD FACTOR DURING GROUND TURNING, A-320

FIGURE E-10. CUMULATIVE FREQUENCY OF LATERAL
LOAD FACTOR DURING GROUND TURNING, TAXI-IN,
ALL AIRCRAFT

FIGURE E-9. CUMULATIVE FREQUENCY OF LATERAL
LOAD FACTOR DURING GROUND TURNING, TAXI-OUT
ALL AIRCRAFT

FIGURE E-12. CUMULATIVE OCCURRENCES OF
LATERAL LOAD FACTOR SQUARED DURING GROUND
TURNING, TAXI-IN, ALL AIRCRAFT

FIGURE E-11. CUMULATIVE OCCURRENCES OF
LATERAL LOAD FACTOR SQUARED DURING GROUND
TURNING, TAXI-OUT, ALL AIRCRAFT
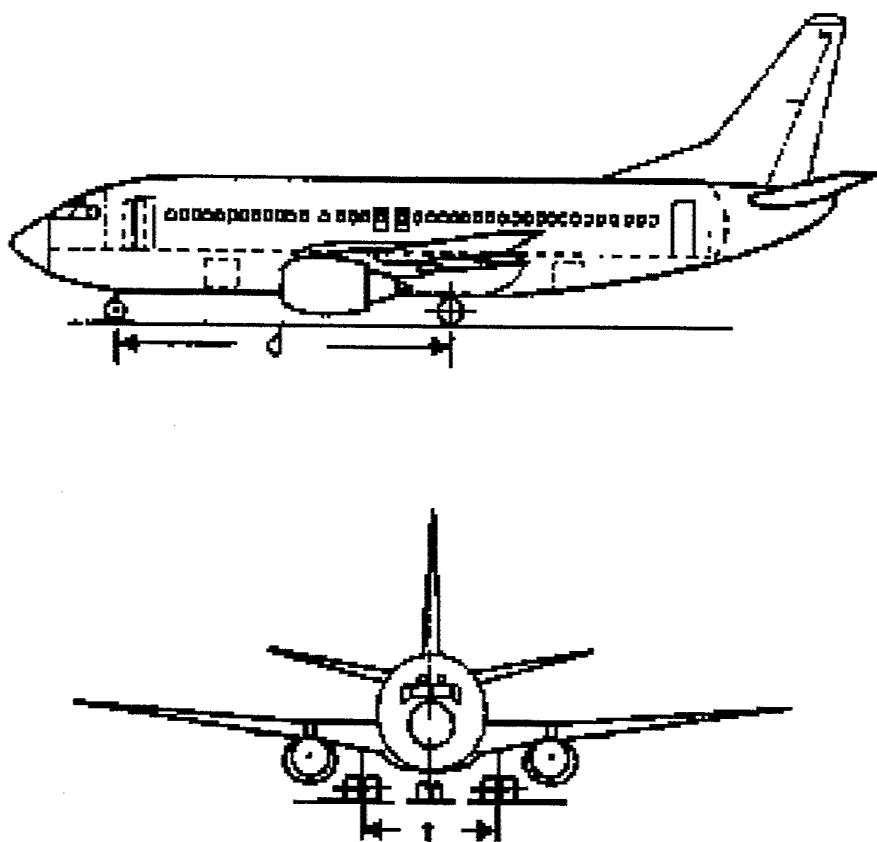
FIGURE E-13. GEAR BASE AND TRACK GEOMETRY

TABLE E-1. LANDING GEAR BASE AND TRACK DIMENSIONS

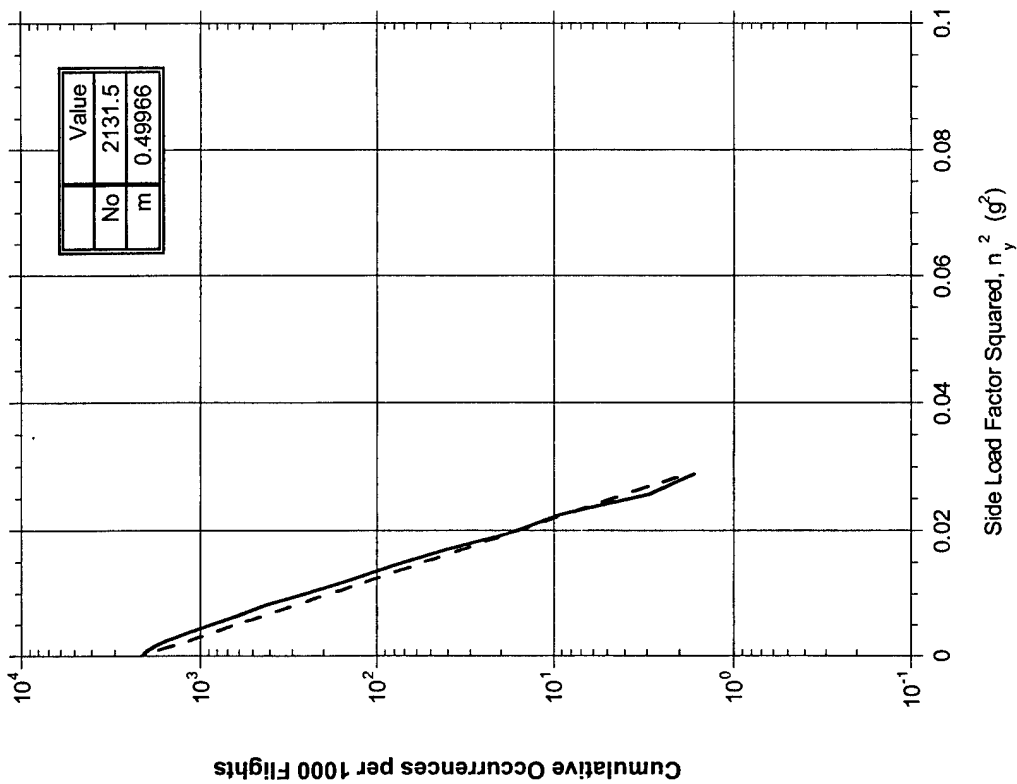| Airplane	Dimensions (feet)	
	d	t
B-737-400	46.83	17.17
MD-82/83	72.40	16.70
B-767-200ER	64.58	30.50
A-320	41.47	24.92
B-747-400	84.0	36.08

FIGURE E-15. CURVE FIT OF CUMULATIVE FREQUENCY OF LATERAL LOAD FACTOR SQUARED DURING GROUND TURNING, TAXI-IN, B-737-400
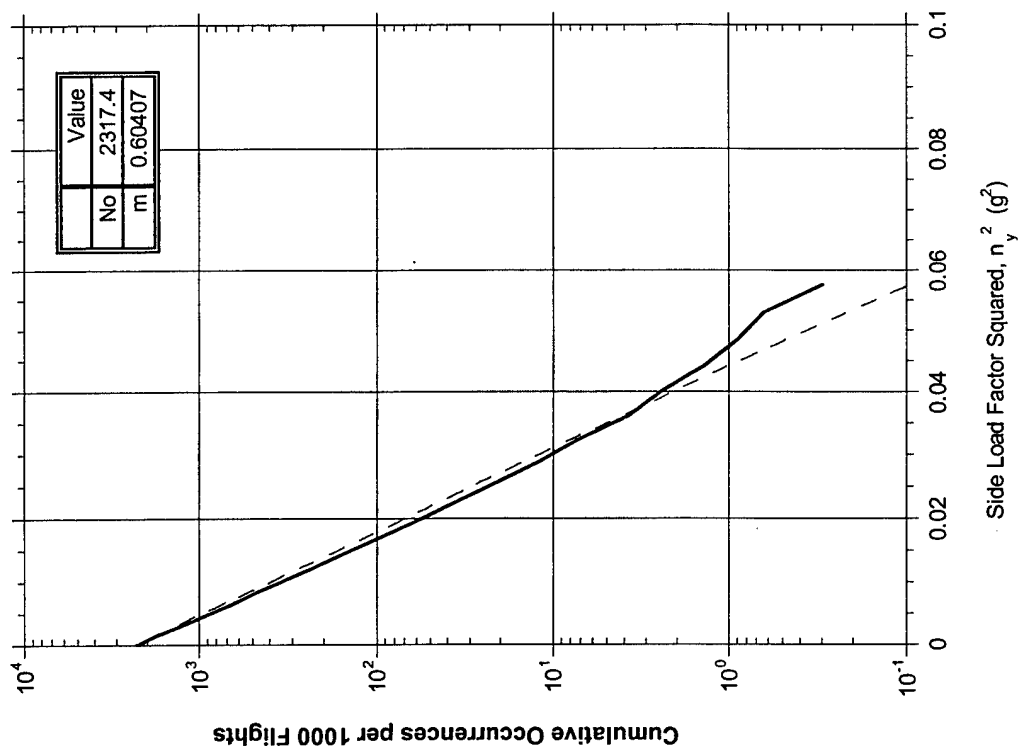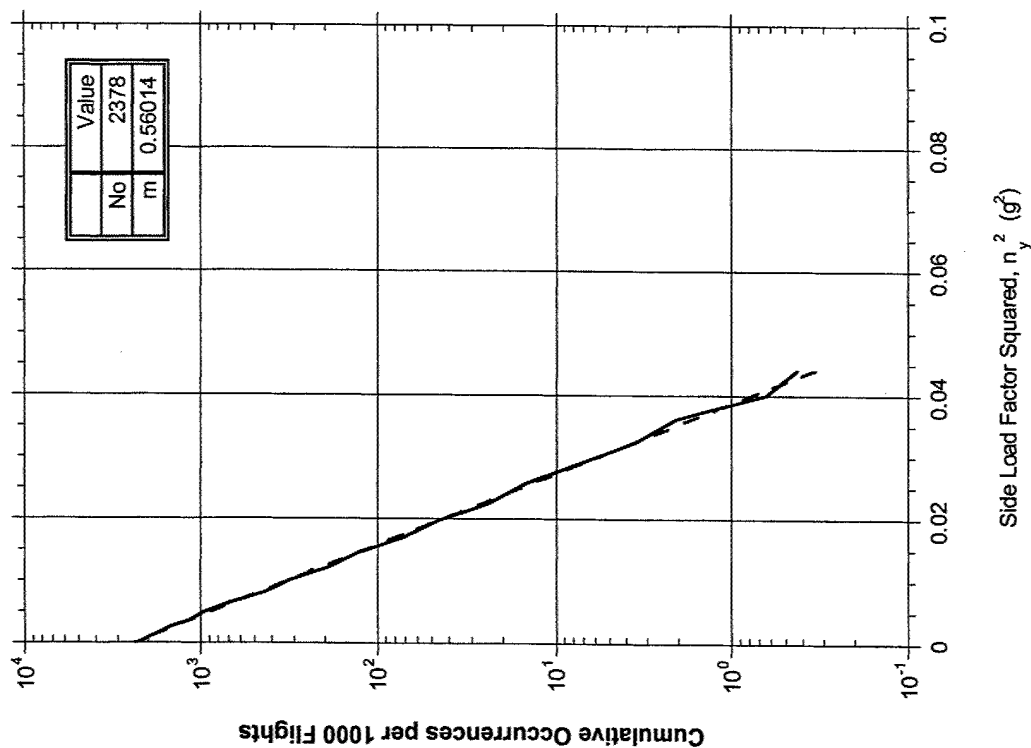
FIGURE E-14. CURVE FIT OF CUMULATIVE FREQUENCY OF LATERAL LOAD FACTOR SQUARED DURING GROUND TURNING, TAXI-OUT, B-737-400

FIGURE E-17. CURVE FIT OF CUMULATIVE FREQUENCY OF LATERAL LOAD FACTOR SQUARED DURING GROUND TURNING, TAXI-IN, MD-82/83
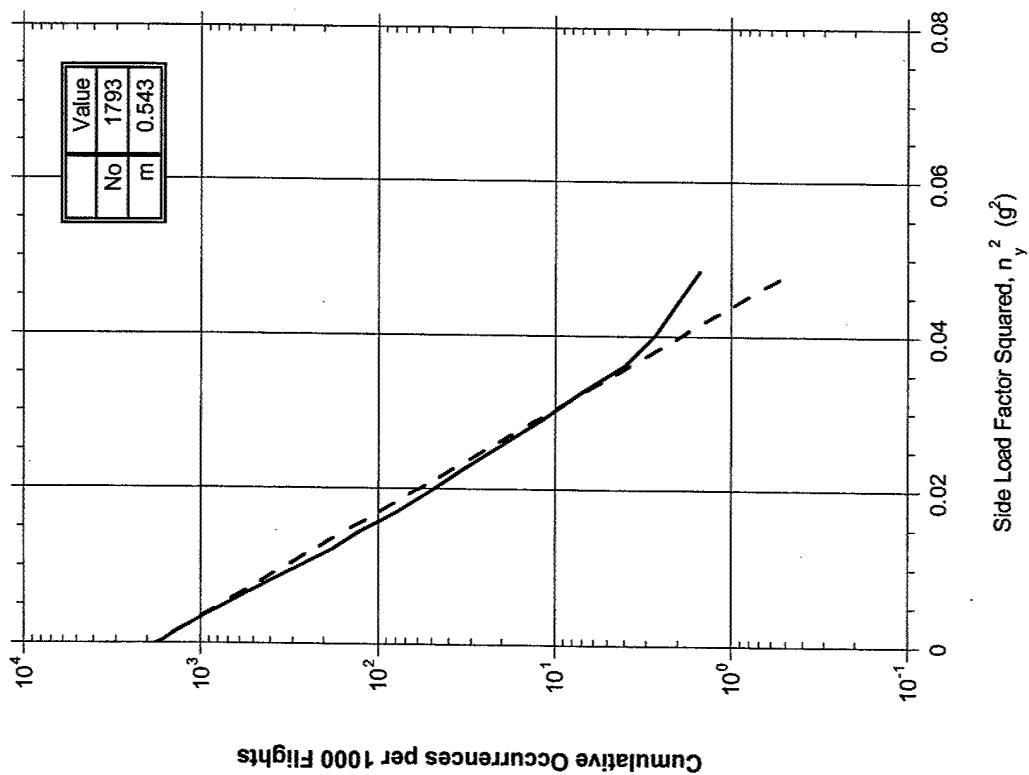
FIGURE E-16. CURVE FIT OF CUMULATIVE FREQUENCY OF LATERAL LOAD FACTOR SQUARED DURING GROUND TURNING, TAXI-OUT, B-MD-82/83

E-13

FIGURE E-19. CURVE FIT OF CUMULATIVE FREQUENCY
OF LATERAL LOAD FACTOR SQUARED DURING GROUND
TURNING, TAXI-IN, B-767-200ER
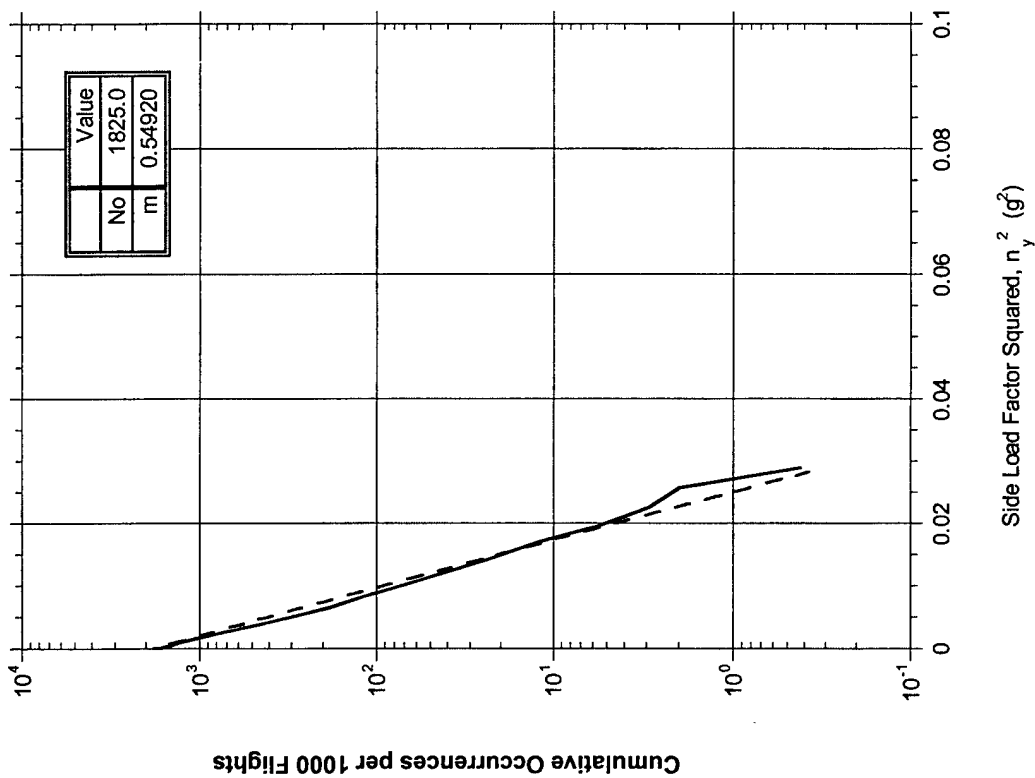
FIGURE E-18. CURVE FIT OF CUMULATIVE
FREQUENCY OF LATERAL LOAD FACTOR SQUARED
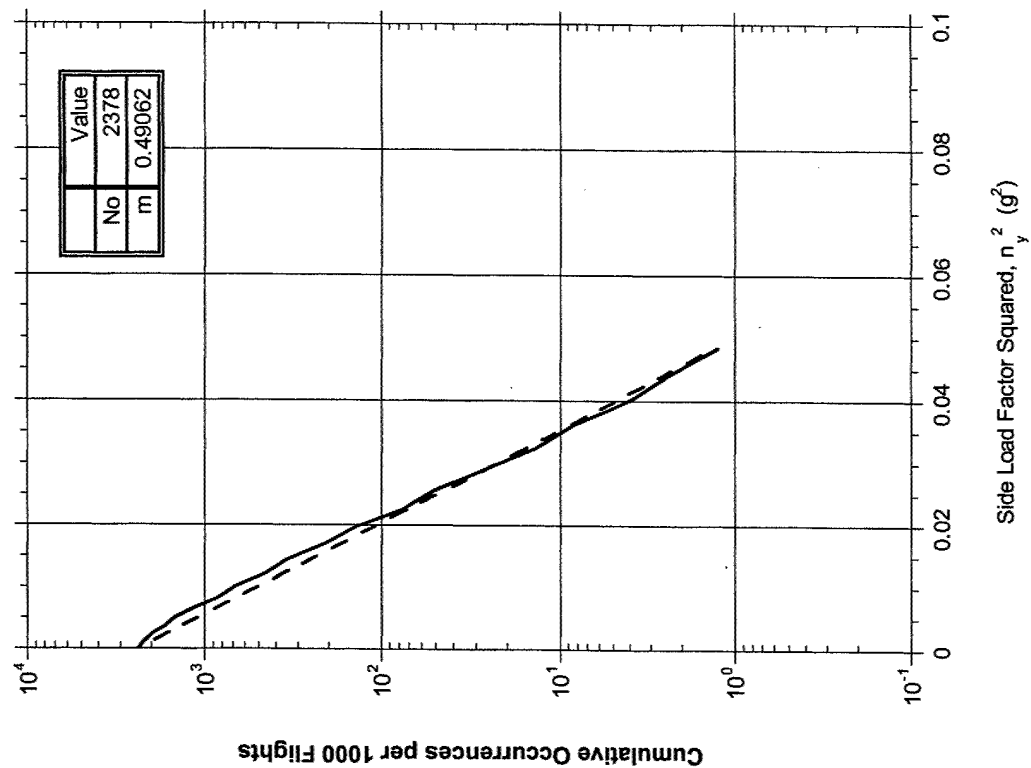DURING GROUND TURNING, TAXI-OUT, B-767-200ER

FIGURE E-21. CURVE FIT OF CUMULATIVE FREQUENCY OF LATERAL LOAD FACTOR SQUARED DURING GROUND TURNING, TAXI-IN, A-320

FIGURE E-20. CURVE FIT OF CUMULATIVE FREQUENCY OF LATERAL LOAD FACTOR SQUARED DURING GROUND TURNING, TAXI-OUT, A-320

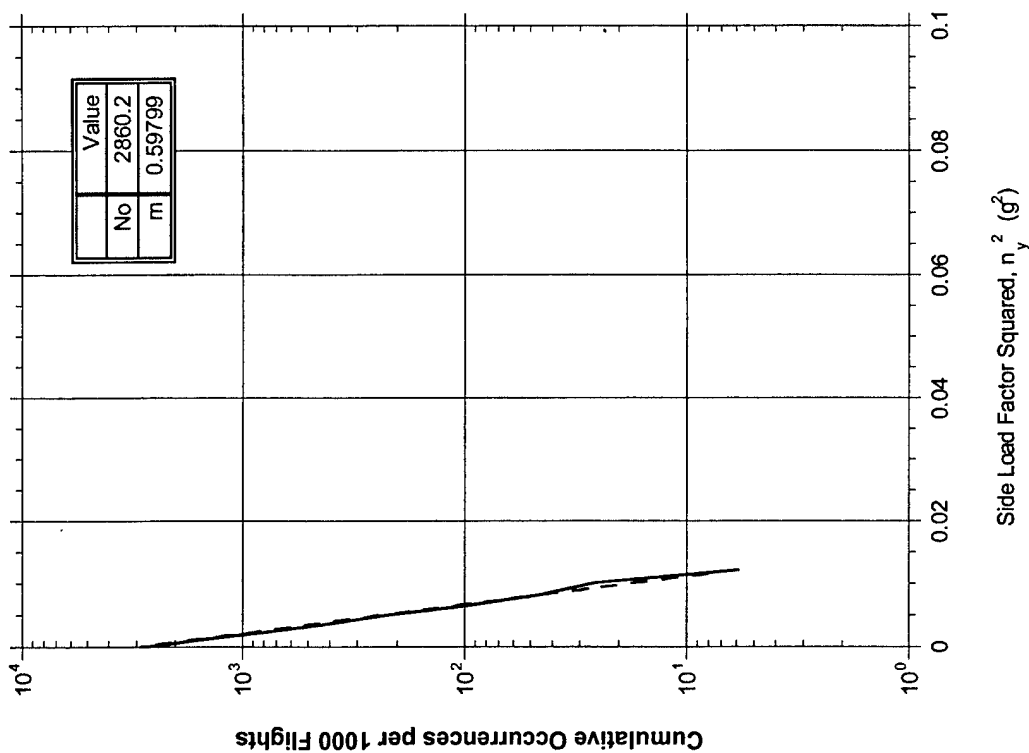FIGURE E-23. CURVE FIT OF CUMULATIVE FREQUENCY OF LATERAL LOAD FACTOR SQUARED DURING GROUND TURNING, TAXI-IN, B-747-400
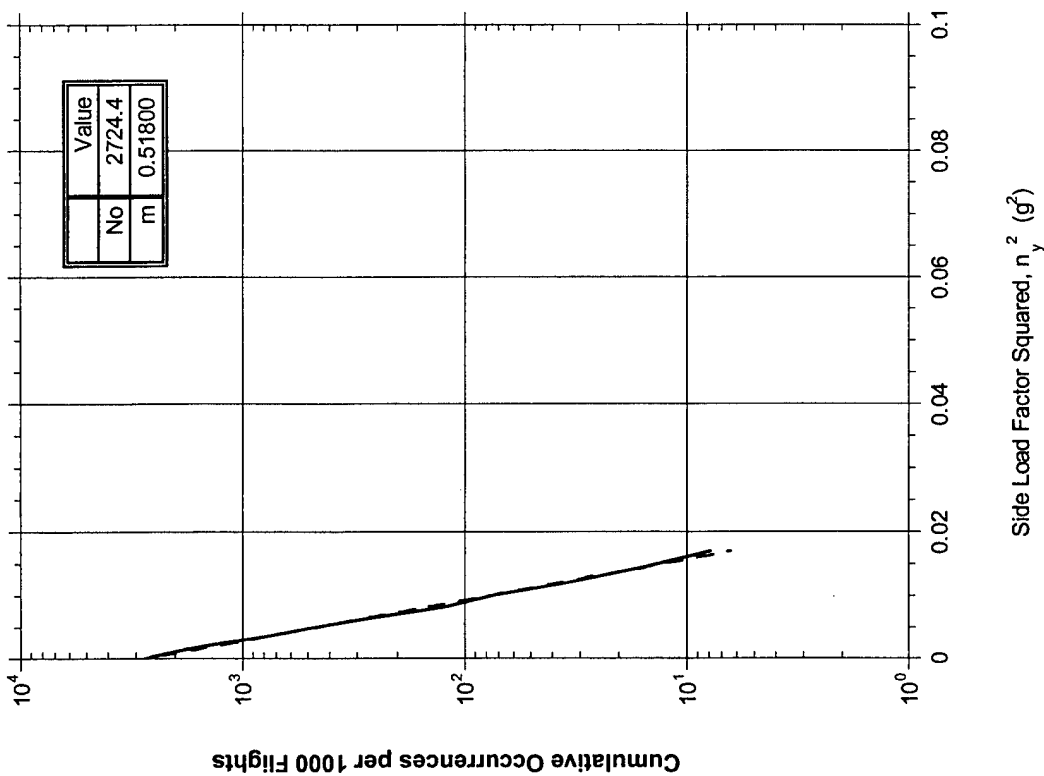
	Value
No	2724.4
m	0.51800

FIGURE E-22. CURVE FIT OF CUMULATIVE FREQUENCY OF LATERAL LOAD FACTOR SQUARED DURING GROUND TURNING, TAXI-OUT, B-747-400

	Value
No	2860.2
m	0.59799

E-16

TABLE E-2. EQUATION CONSTANTS

Aircraft	Taxi-Out		Taxi-In		Flights
	N_0	m	N_0	m	
B-737-400	2317.4	0.60407	2018.0	0.50799	11723
MD-82/83	1793	0.54300	1876.8	0.47459	3987
A-320	2378	0.56014	2378	0.49062	6226
B-767-200ER	1825	0.54920	2131.5	0.49966	1196
B-747-400	2860.2	0.59799	2724.4	0.5180	252
Average	2234.7	0.571	2225.7	0.498172	23384

$$N_{Taxi-out} = 2234.7 \times e^{-\left(d^{0.571} \times t \times n_y^2\right)}$$

$$N_{Taxi-in} = 2225.7 \times e^{-\left(d^{.498} \times t \times n_y^2\right)}$$

FIGURE E-25. COMPARSION OF MEASURED AND CALCULATED CUMULATIVE FREQUENCY OF GROUND TURNING, LATERAL LOAD FACTOR DURING TAXI-OUT AND TAXI-IN, MD-82/83
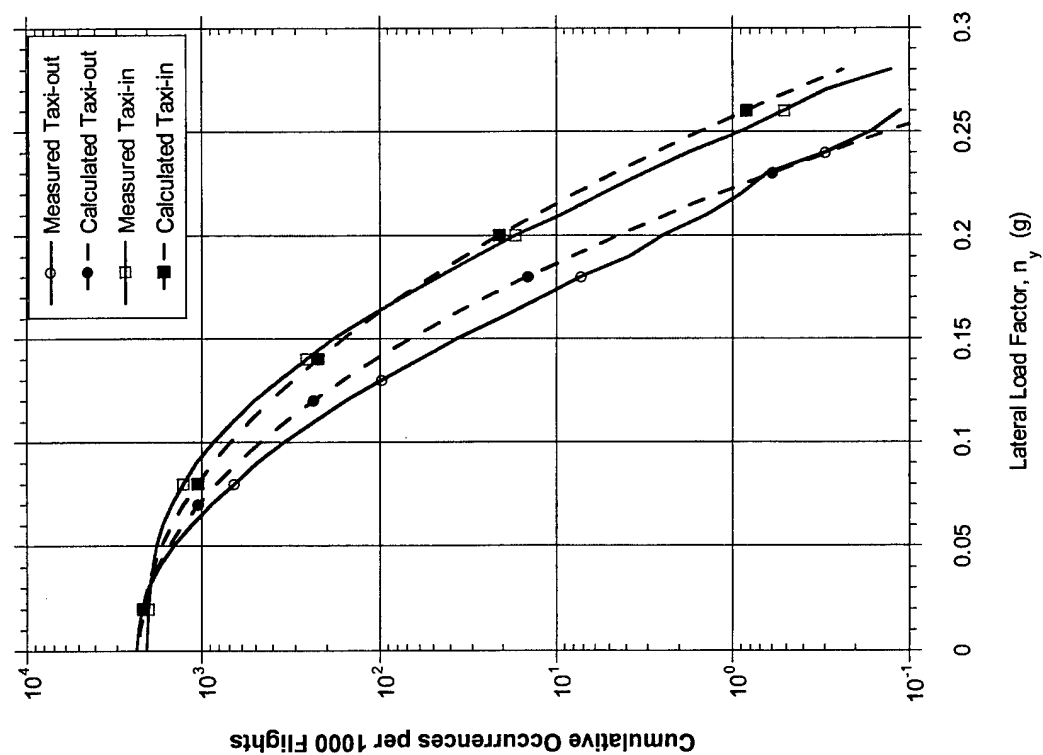

FIGURE E-24. COMPARISON OF MEASURED AND CALCULATED CUMULATIVE FREQUENCY OF GROUND TURNING, LATERAL LOAD FACTOR DURING TAXI-OUT AND TAXI-IN, B-737-400
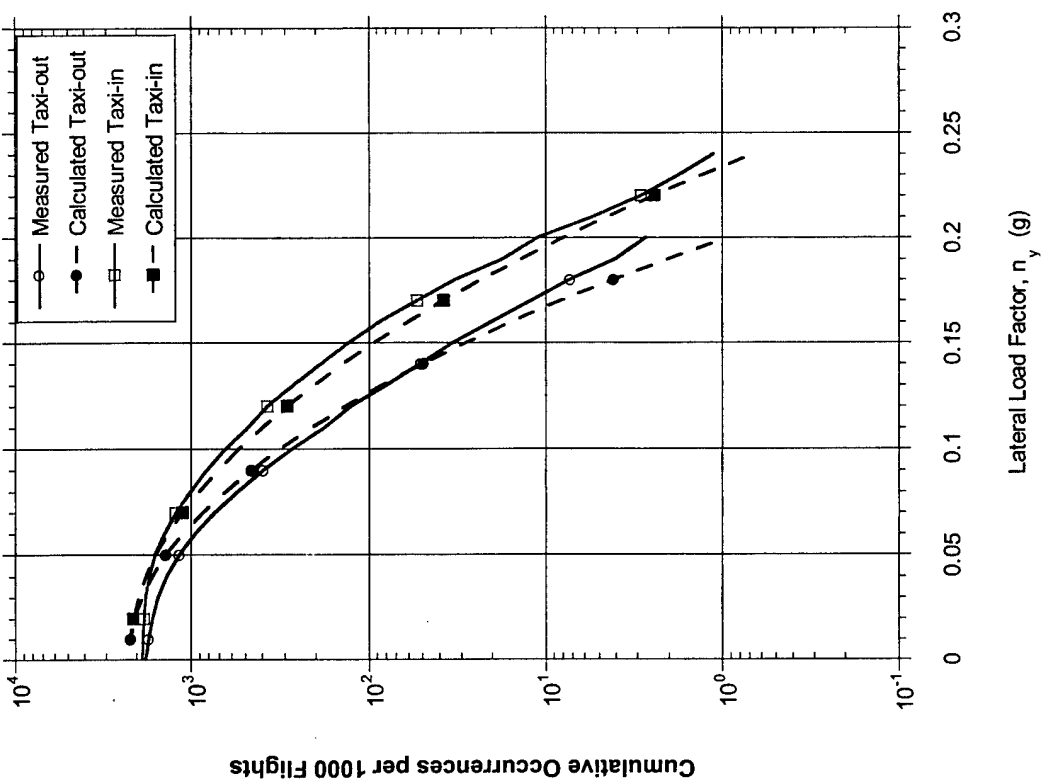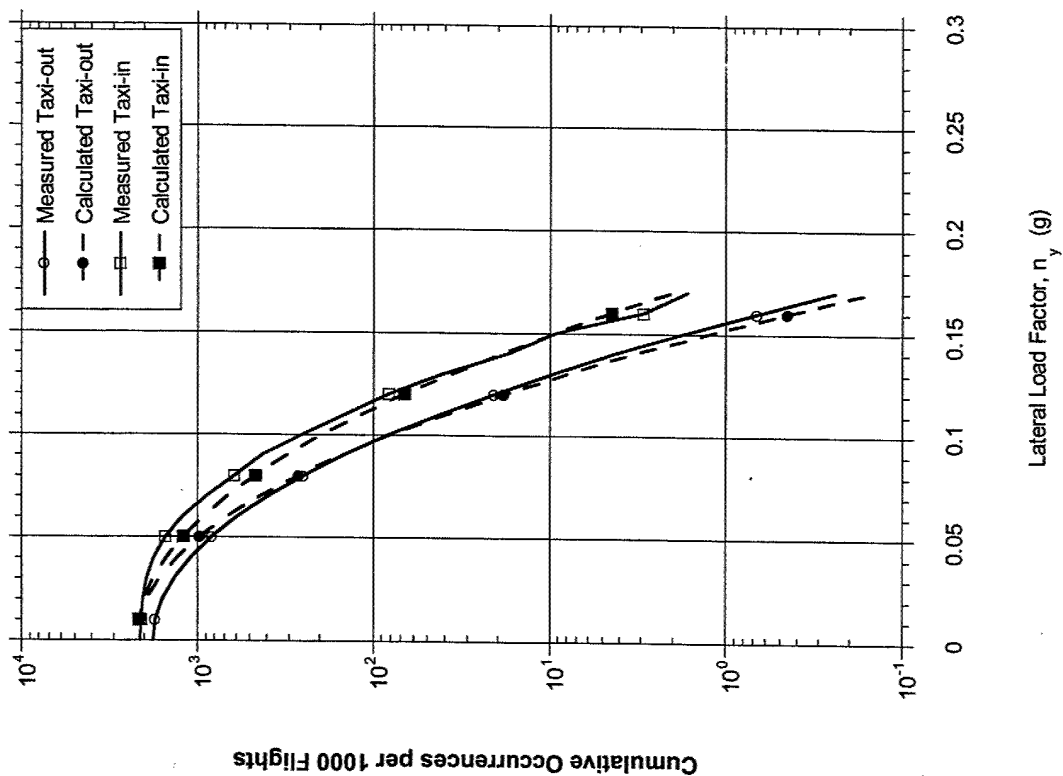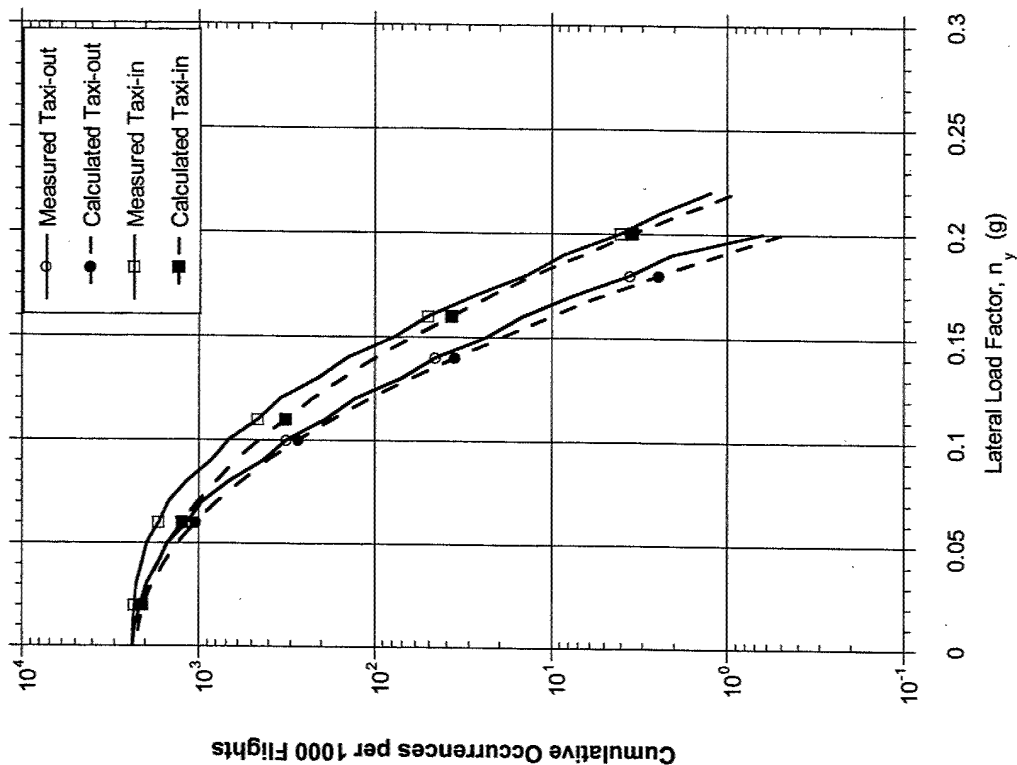
E-18

FIGURE E-27. COMPARSION OF MEASURED AND CALCULATED CUMULATIVE FREQUENCY OF GROUND TURNING, LATERAL LOAD FACTOR DURING TAXI-OUT AND TAXI-IN, A-320

FIGURE E-26. COMPARISON OF MEASURED AND CALCULATED CUMULATIVE FREQUENCY OF GROUND TURNING, LATERAL LOAD FACTOR DURING TAXI-OUT AND TAXI-IN, B-767-200ER

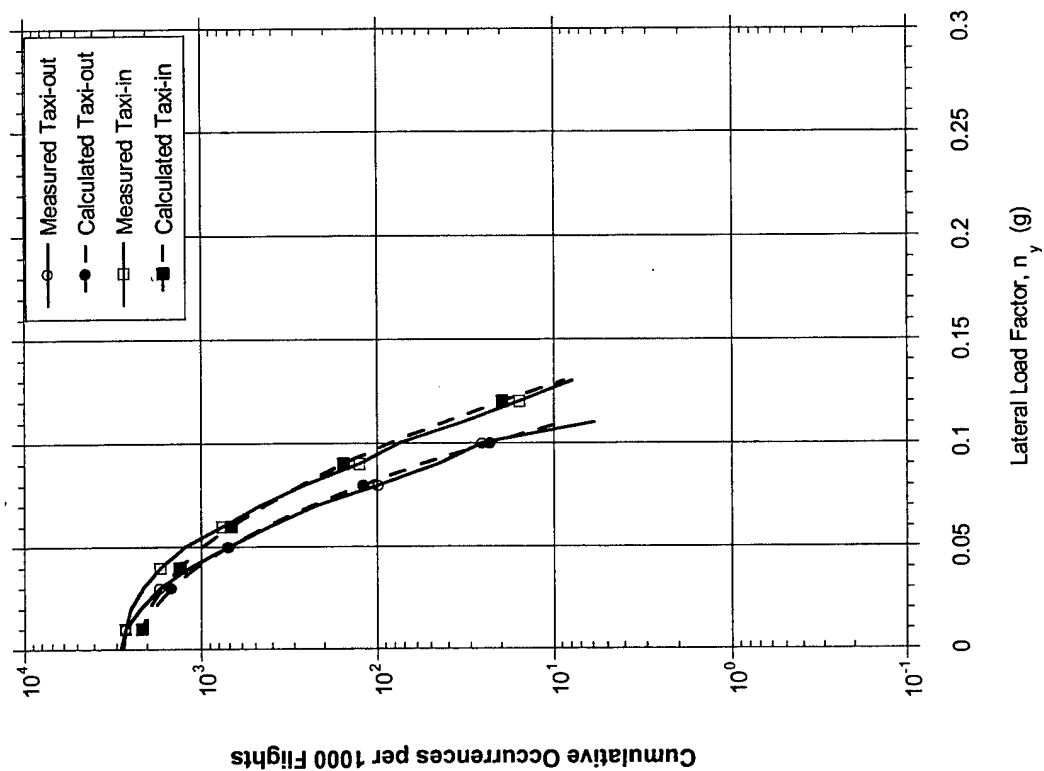FIGURE E-29. LANDING GEAR DIMENSIONAL ENVELOPE

FIGURE E-28. COMPARISON OF MEASURED AND CALCULATED CUMULATIVE FREQUENCY OF GROUND TURNING, LATERAL LOAD FACTOR DURING TAXI-OUT AND TAXI-IN, B-747-400
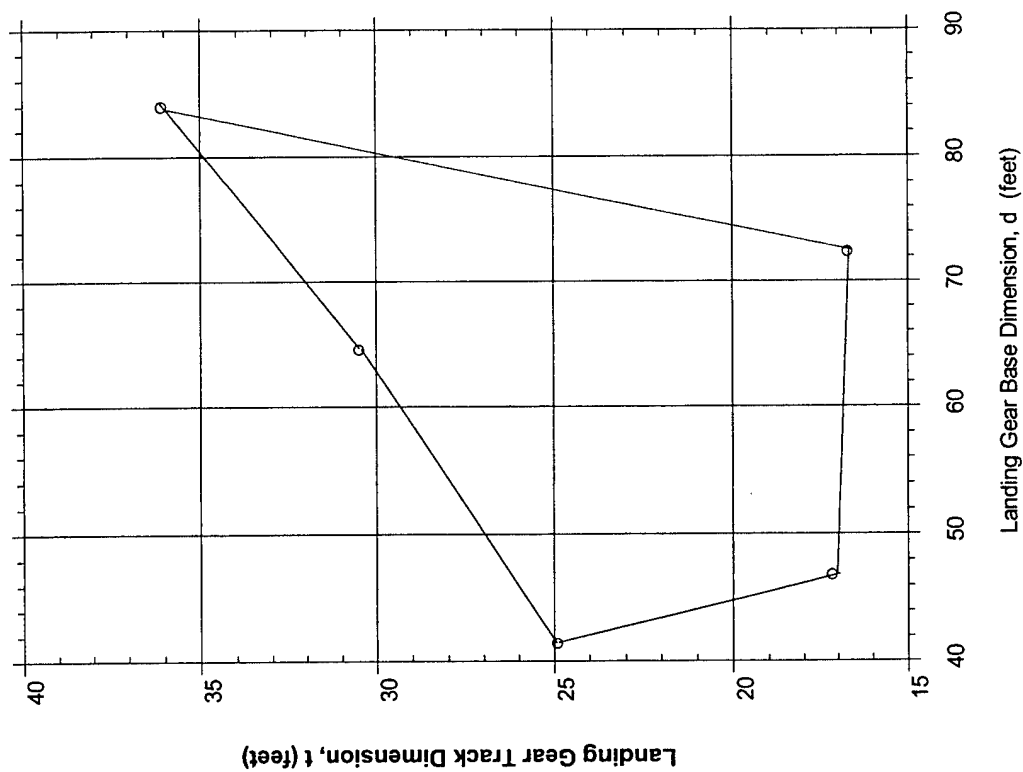
TABLE E-3. COMPARISON OF CUMULATIVE FREQUENCIES OF 0.5-g LATERAL LOAD FACTOR

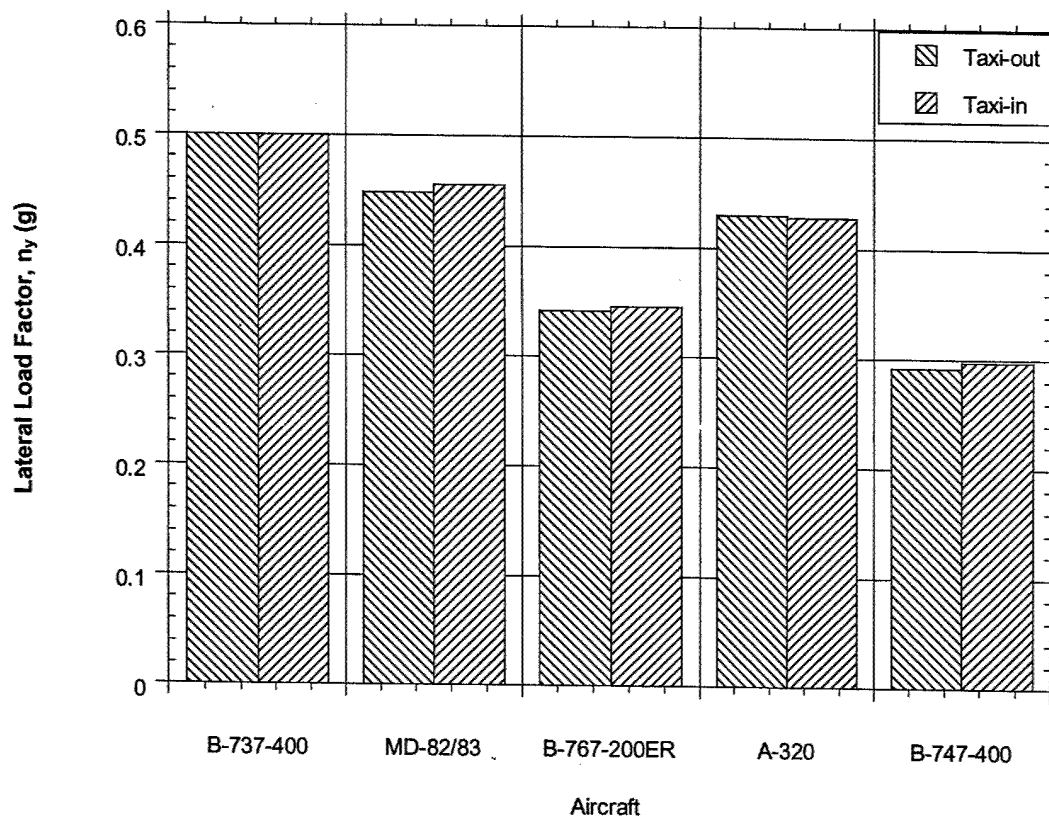| Aircraft	Lateral Load Factor	Cumulative Frequency, Taxi-Out	Cumulative Frequency, Taxi-In
B-737-400	0.5	4.00343E-14	4.78128E-10
MD-82/83	0.5	2.90091E-18	1.09566E-12
B-767-200ER	0.5	4.09287E-33	8.66253E-24
A-320	0.5	4.70488E-20	1.10148E-14
B-747-400	0.5	1.69683E-46	5.4205E-33

FIGURE E-30. COMPARISON OF EQUAL PROBABILITY LATERAL LOAD FACTORS DURING GROUND TURNING FOR FIVE AIRCRAFT